THE UNIVERSITY OF CALGARY

Quantification of Patellar Tendon Biomechanical Properties: In Vitro and In Situ

by

Dominic Young

A THESIS
SUBMITTED TO THE FACULTY OF GRADUATE STUDIES
IN PARTIAL FULFILMENT OF THE REQUIREMENTS FOR
THE DEGREE OF MASTER OF SCIENCE
IN BIOMEDICAL ENGINEERING

PROGRAM OF BIOMEDICAL ENGINEERING

CALGARY, ALBERTA
JANUARY, 1999

ABSTRACT

An investigation of the biomechanical properties of the cat patellar tendon (PT) is presented. Standard *in vitro* techniques were used to quantify stiffness, K, ultimate force, F_{UT}, and ultimate elongation, ΔL_{UT}, of matched pairs of PT specimens. Mean (±SD) values of 320 (±43) N mm^{-1}, 870 (±160) N and 4.8 (±1.6) mm were determined for K, F_{UT} and ΔL_{UT}, respectively. Mean left-right differences were not found to be significant ($P > 0.4$). Tissue stress and strain were quantified from failure tests. An elastic modulus, E, of 1335 (±221) MPa was observed in these tests. A new *in situ* non-contact technique for measuring the force-elongation behaviour of the intact PT in an animal model was developed. The technique was used to characterise the mechanical response of PT tissue in a controlled loading protocol. An *in situ* modulus, E, of 1509 (±229) MPa was estimated from a single experiment.

ACKNOWLEDGEMENTS

I would like to express my sincere thanks to:

Dr. Janet Ronsky, for her enthusiasm, encouragement, support and guidance.

Dr. Nigel Shrive and Dr. Ronald Zernicke, for serving on my committee and bringing their insight and expertise to this work.

Stan Ajemian, Steve Boyd, Brian Donnelly, Barbara Kralovic, Marilyn Powers, Craig Sutherland and Dan Magnusson, for their help with data collection and analysis.

Roni Fisher, Tim Leonard and Glenda McNeil at the Human Performance Lab in the Faculty of Kinesiology, for their technical assistance and patience. Paul Houle, Gail Leask, Kent Paulson and Greg Wohl in the Biomechanics Lab at the McCaig Centre, for Joint Injuries and Arthritis Research for their instruction and technical support. Greg East and Art Mohrle in the Department of Mechanical Engineering, for their work on developing and building experimental equipment.

My friends and fellow grad students at the HPL and the McCaig Centre, for assistance, support, fun and unlimited good humour throughout my M.Sc. career.

Natural Sciences, Engineering and Research Council of Canada and University of Calgary Research Services for the financial support of this study.

Janice Miller, for encouragement, humour and patience – and hugs!

My parents and my sister, for their love and support in all I've done. Thank you.

TABLE OF CONTENTS

LIST OF TABLES

LIST OF FIGURES

LIST OF ABBREVIATIONS

1D	one dimensional
2D	two dimensional
3D	three dimensional
CSA	cross sectional area (mm^2)
DAQS	data acquisition system
GCV	generalised cross-validatory
IHA	instantaneous helical axis
LED	light emitting diode
LVDT	linear voltage differential transducer
MAS	motion analysis system
PBS	phosphate buffered saline
PFJ	patellofemoral joint
PMMA	polymethyl methacrylate
PT	patellar tendon
PPTC	patella–patellar tendon–tibia complex
SD	standard deviation
TIFF	tagged image file format

LIST OF SYMBOLS

E	elastic modulus (MPa)
F	force (N)
H_a	alternate hypothesis
H_o	null hypothesis
K	stiffness (N mm^{-1})
L_0	initial length (mm)
P	mechanical or structural property
t	T-test statistic
U	loading energy
n	cycle number, specimen number
r	correlation coefficient
r	moment arm magnitude (mm)
ΔL	elongation (mm)
Σ	sum of
δ	difference between two measurements
ε	strain (%)
μ	mean value
σ	stress (MPa)

LIST OF SUBSCRIPTS

CYC	refers to a structural or mechanical property estimate derived from cyclic loading
FAIL	refers to a structural or mechanical property estimate derived from failure loading
L	refers to left PT specimens
LR	refers to a comparison, relative or absolute, between left and right PT specimens
R	refers to right PT specimens
UT	refers to the ultimate tensile value of a structural or mechanical property
i	index referring to a numbered sequence
n	cycle number
pl	proportional limit, refers to PT specimen behaviour in failure loading
t	toe region, refers to PT specimen behaviour in failure loading

1 INTRODUCTION

This thesis is focused on the biomechanical properties of the cat patellar tendon (PT). Previous studies have investigated the PT of several species including rabbit, dog and human (Butler, et al., 1984, Haut and Powlison, 1990; Haut et al., 1992; Yamamoto, et al., 1992; Danto and Woo, 1993). To date, there has been only one published study of the biomechanical properties of the cat PT (Archambault, 1995). Recently, an experimental model to investigate injury induced OA in the cat knee joint has been developed (Herzog, et al., 1993). The cat has also been used as an experimental model to study changes in gait and knee joint loading *in vivo* following surgical transection of the ACL (Hasler, et al., 1998). Experimental techniques have been developed to study the contact characteristics, joint surface geometry and kinematics of the PF joint of the cat (Ronsky, et al., 1995; Boyd, 1997; Boyd and Ronsky, 1998). A quantitative description of the biomechanical properties of the cat PT would be beneficial in numerous ways. Of primary interest to this research project, the biomechanical properties will provide one of the important parameters required to model the kinematic and dynamic behaviour of the cat knee joint. Additionally, these properties will provide information for understanding the mechanics of the cat patello-femoral (PF) joint.

Osteoarthritis (OA) of the knee is a condition that is characterised by degeneration of articular cartilage, pain and disability. An understanding of this phenomenon depends on the ability to quantify and explain the interactions between many biological and mechanical factors (Ronksy, 1994). In biomechanics, investigations motivated by the study of OA are often focused on the parameters that determine the kinematics and kinetics of the knee joint (Blankevoort, et al., 1990; Boyd, 1997 ; Hasler, et al.,1998). These parameters include the geometry of articulating surfaces, muscle forces and the properties of the soft connective tissue structures of the knee. Mathematical models offer an indirect approach to studying PF joint mechanics. They can be used to study the relative importance of and sensitivity to factors that influence joint mechanics. Constructing such a model is a complex problem that requires knowledge of these joint parameters as inputs. The mechanical properties of the PT are part of the tissue property inputs required.

Biomechanical properties are studied in association with factors such as maturation, ageing, activity and immobilisation, and healing of injured or transplanted tissues (Laros, et al., 1971; Frank, et al., 1983; Woo, et al., 1987; Bosch and Kasperczyk, 1992; Haut, et al., 1992). Quantification of tissue biomechanical properties may aid in the description of the response of tissues to these factors. These studies are most often based on comparisons between a treated or injured tissue and the unaffected structure of the contralateral limb. An important assumption used in many of these studies is that the properties of the experimental structure and the contralateral control are identical at the start of the experiment. Despite the importance of this assumption, few studies have concentrated on characterising the inter-limb variation between normal left-right pairs of tissue structures (e.g., Frank, et al., 1994). Further investigations in this area would be valuable in establishing the normal variability in contralateral tissue structures.

Interest in quantifying PT properties has also been motivated from the perspective of knee injury and treatment. After a trauma to the knee resulting in rupture of the ACL, the damaged tissue is often replaced with a tendon autograft. Often, the graft consists of the central third of the PT including sections of bone from the patella and tibia (Johnson, et al., 1992). Biomechanical studies of human PT and other soft connective tissues have been conducted by Butler and co-workers (Butler et al., 1984, 1986, and 1990). An important finding of these investigations was that specimen strain measured from tissue clamp displacement was significantly larger than strain measured in the mid-substance of tissue specimens. As a result, measures of tissue modulus and strength were significantly larger when derived from mid-substance strain measurements. Differences in strain estimates have generally been attributed to gripping artefacts or end effects at tissue insertions.

Longitudinal strain variation of tissue specimens *in vitro* is clearly important in terms of characterising tissue mechanical properties. Lateral variation in tissue mechanical behaviour may be important in the PT in the context of tendon autograft replacements or understanding the functional role the PT. A few studies have focused on quantifying variations in the stress-strain behaviour of the lateral, central and medial regions of the PT (Butler, et al., 1984; Yamamoto, et al., 1992; Archambault, 1995). None of these

investigation revealed significant lateral to medial variations in the mechanical response of PT specimens.

Tissue properties are derived from force-elongation data collected during *in vitro* mechanical tests. In addition to clinically motivated studies, investigations also seek to quantify tissue properties for the purpose of determining the functional behaviour of tissues and for use in predictive models of joint characteristics *in vivo*. In this case, *in vitro* properties may not accurately represent the *in vivo* behaviour of the tissue structure in the intact joint.

Recent studies have used implantable transducers to measure *in vivo* forces and strains in connective tissue. *In vivo* strains have been measured in the knee joint ligaments of the dog (Monahan, et al., 1984). Forces in the PT and *gastrocnemius* have been measured in cats walking on a treadmill (Hasler, et al., 1998). These types of transducers were capable of directly measuring either force or strain alone and not the whole structural or mechanical response of tissues. Furthermore, measurements were made in uncontrolled experiments where the force or strain *inputs* applied to the instrumented tissues could not be directly manipulated by the investigators.

The PT is an extra-articular structure which makes it relatively more accessible than other soft tissue structures of the knee. This gives rise to the opportunity to study the PT properties *in situ* using experimental models developed to quantify PF joint contact and kinematics. If the properties of the PT can be measured *in situ* then those measurements can be compared directly to *in vitro* results. If this is possible, then perhaps the results of this comparison can be used to gain a better understanding of PT behaviour *in vivo*.

1.1 HYPOTHESES AND OBJECTIVES

There were three hypotheses of the present study.

Hypothesis 1. Contralateral (left-right) differences in the structural properties of the cat *patella-patellar tendon-tibia complex* PPTC are not significant.

Hypothesis 2. The tendon mid-substance of PPTC specimens will exhibit a uniform strain distribution in the lateral-medial direction.

Hypothesis 3. The elastic modulus estimates based on mid-substance strain measurements are higher than estimates based on grip-to-grip strain measurements.

There were three main objectives in this study. The first two objectives relate to the hypotheses. The third objective relates to the development of a technique to measure the *in situ* mechanical behaviour of the PT.

Objective 1. Quantify the force-elongation behaviour of left-right pairs of PPTCs tested in an *in vitro* loading protocol. Determine the magnitude and significance of left-right differences in structural property estimates.

Objective 2. Quantify the lateral to medial variation in tissue strain in the elastic region of the structural response.

Objective 3. Develop and test a technique for measuring the *in situ* stress-strain behaviour of the cat PT.

1.2 OVERVIEW

There were three main components of the research conducted in this investigation. First, a study of the biomechanical properties of the cat *patella-patellar tendon-tibia complex* (PPTC) was carried out in order to meet the first objective. Established experimental techniques reported in the literature were applied. Second, a new tissue strain analysis technique was developed to study surface strain in the cat PT mid-substance. The technique was applied to high-speed video recordings of specimen failure tests. Finally, in the third part of the study, a new technique was developed to quantify the force-elongation response in the PT of the intact knee joint of the cat. This "*in situ*" technique combined an established protocol for quantifying *in situ* PF joint kinematics and contact characteristics with the strain analysis technique developed in the second part of the study. A single experiment was conducted to assess the technique and the results were used to quantify the stress-strain behaviour of the PT *in situ*.

2 REVIEW OF LITERATURE

2.1 TENDON

2.1.1 Composition and structure

Tendon is a complex tissue. For the purpose of providing a summary of important aspects of the tissue related to this investigation, a brief discussion of tendon structure and composition is presented. A detailed description of the biology, structure and material composition may be found in several reviews (e.g. Butler, et al., 1978; Viidik, 1990; Herzog and Loitz, 1994; Woo, et al., 1997).

Tendons are dense, soft connective tissue structures that attach muscle to bone and transmit tensile forces produced by contracting muscles. Tendon tissue is a structurally complex arrangement of collagen, elastin, ground substance and water. Approximately 80 % of the dry weight of tendon is Type I collagen (Curwin and Stanish, 1984). Collagen is produced by fibrocytes and aligned in parallel fibre bundles in the tissue. Ground substance and water produce a lubricating gel that permeates the fibrous matrix. The ground substance is composed of cells (fibrocytes), proteoglycans (PGs), glycolipids and water. Ground substance makes up a much smaller portion of the dry weight of tendon compared to collagen.

Collagen in tendon tissue is arranged in a hierarchical series of substructures (Butler, et al., 1978). The most fundamental of these is the tropocollagen molecule. Five tropocollagen molecules are banded together in a staggered arrangement to form a microfibril. Several microfibrils group together to make up a subfibril (or fibril). In mature tissue, collagen fibrils are attached to each other with strong inter- and intramolecular crosslinks. The crosslinks give tendon tissue its high tensile strength. When viewed under a polarized light microscope, fibrils of tendon fascicles exhibit a waveform appearance parallel to the fibre direction. This microstructural pattern is known as fibre "crimp." Crimp is thought to have an important influence on the biomechanical properties of soft tissues (Betsch and Baer, 1980; Stouffer, et al., 1985). Fibrils are grouped together into bundles and are surrounded by a collagen sheath or membrane, the *epitenon*. This is the largest substructure of tendon tissue and is called a fascicle. Fasicles are unattached and can slide

independently with respect to each other, aided by the lubricating action of the tendon ground substance. Tendons are composed of groups of fasicles enclosed in a membrane called the paratenon. The mechanical behaviour of tendon tissue structures is thought to be closely related to the architecture of these fibrous substructures. Elastin fibres are also present in the extracellular matrix of tendons but their function is not clear.

Water makes up 60 to 80 % of the wet weight of tendons (Curwin and Stanish, 1984). The mechanical behaviour of collagenous tissues such as the human intervertebral disc and the rabbit MCL has been shown to be strongly influenced by tissue water content (Panagiotacopulos, et al., 1979, 1987; Chimich, et al., 1992). The presence of water in the extracellular matrix of tendon has also been shown to influence its mechanical behaviour (Haut and Powlison, 1990). The mechanisms governing the inter-action between the matrix and water components are not understood. PGs are known to be hydrophilic molecules which trap water within the tissue matrix. It is speculated that water and PGs together form a lubricating substance that allows the interwoven and twisted fibres of the tissue (fasicles and fibres) to slide freely with respect to one another in response to loads (Woo, et al., 1997).

There are two types of attachments or junctions by which a tendon connects to bone: a *direct* or *indirect* insertion. Woo, et al. (1988) present a detailed decription of these osteotendinous junctions. Tendons inserting into epiphyseal bone do so through a direct insertion in which the tissue gradually changes from fibrous tendon, to fibrocartilage, followed by calcified fibrocartilage and finally bone. Tendons that insert at an acute angle to the bone do so through an indirect insertion. Superficial fibres of the tendon run parallel to the bone surface and insert into the periosteum. The deeper fibres insert obliquely into the bone. Muscle and tendon are joined in the myotendinous junction (Garrett and Tidball, 1988). In the myotendinous junction, muscle myofibrils and collagen of the tendon meet and form a region of longitudinal infoldings. The structure of the junction serves to increase the surface area and strength of the attachment.

2.1.2 Relevant anatomy

The patellar tendon (PT) is part of the *quadriceps femoris* muscle group. It runs distally from the *quadriceps*, attaches to and covers the patella and inserts into the tibial

tuberosity of the tibia. The PT transfers force between the *quadriceps* and the tibia, producing an extension moment at the knee (Hay and Reid, 1988).

The patella is a sesamoid bone that develops within the tendon of the *quadriceps* muscle group of the thigh. It has a rough convex anterior surface that serves as the attachment site of the *quadriceps* tendon and PT. The patella has a wide *base* (proximal end) and narrows to the *apex* at the distal end. The posterior surface of the patella has two concave *facets* (medial and lateral) for articulation with the medial and lateral *condyles* of the femur. The PT connects the apex of the patella to the tibial tuberosity at the anterior surface of the tibia near the condyles (Martini and Welch, 1998).

The detailed morphology of the *tendon insertion* has been investigated in the canine PT (Cooper and Misol, 1970). Superficial PT fibres run distally into the *periosteum* of the tibial tubercle. At the patella, superficial PT fibres run proximally into the *periosteum* that covers the anterior patellar surface. The deep fibres of the PT insertions at both the tibia and patella exhibit the four zones typical of a *direct insertion*. The PT, patella and PT insertion at the tibia form a knee joint tissue structure that will be referred to as the *patella-patellar tendon-tibia complex* (PPTC).

2.2 THE BIOMECHANICS OF TENDONS AND LIGAMENTS

2.2.1 Mechanics of materials concepts

The architecture of collagenous tissue structures is complex and varies depending on the location and function of the structure in the musculoskeletal system. Tendon and ligament (tissue) structures are composed of parallel fibre bundle arrangements which are well suited for the transmission of tensile force (Frank and Shrive, 1994; Herzog and Loitz, 1994). Physical properties of tissues are determined from mechanical tests in materials testing machines using principles analogous to those used in the study of engineering materials such as steels or plastics. The following section contains a review of basic principles of the mechanics of materials. A complete discussion of these concepts may be found in a mechanics of materials textbook (e.g., Beer and Johnston, 1985). The purpose of this review is to introduce basic concepts and establish definitions that will be used in the following sections and chapters.

Given a sample of a material, how are the physical properties of the material quantified? When the specimen is deformed (stretched or elongated) a force develops in the material. The elongation may be measured in millimetres (mm) and the force in Newtons (N). The larger the applied deformation, the greater the force. Another way to state this is that the material *responds* to a deformation by developing a force. Alternately, if a tensile force is applied to the material, the *response* is a deformation.

1. A structural *response* is the change in the physical state (e.g., length) due to the change in an input variable (e.g., force).
2. The structural *behaviour* of a material is characterised by the relation between force and deformation.

An ideal linear elastic material is one for which there is a direct linear relation between the force response and the applied deformation, i.e.,

$$F = K \cdot \Delta L, \qquad [1]$$

where K is the *stiffness* of the material in $N \cdot mm^{-1}$. The stiffness depends on aspects of the specimen's *structure* including its initial length, L_0, and cross-sectional area, *CSA*. A shorter, thicker specimen will have a higher stiffness than a longer, thinner specimen. Therefore K is referred to as a *structural property*. Initial length and cross-sectional area, are the key geometric aspects that influence the structural behaviour of an ideal linear elastic material.

Characterising the structural behaviour of a sample of a material is important. It is often more useful to describe and understand the physical properties of a material itself. *Stress* and *strain* are variables that can be used to quantify the physical behaviour of materials. Stress, σ, quantifies how force is distributed through a material specimen and is defined as:

$$\sigma = F \cdot CSA^{-1} \qquad [2]$$

Strain, ε, relates the elongation, ΔL, of a specimen to its initial length, or gauge length, L_0. Strain is defined as:

$$\varepsilon = \Delta L \cdot L_0^{-1}. \qquad [3]$$

Stress and strain are analogous to force and elongation, respectively. When a strain input is applied, stress develops in the material. Strain is a non-dimensional ratio of lengths,

expressed as a ratio in decimal form or as percent strain. Stress may be measured in $N \cdot mm^{-2}$ or in Megapascals (MPa). In an ideal linear elastic material subject ot uniaxial stress, stress and strain are directly related such that,

$$\sigma = E \cdot \varepsilon, \qquad [4]$$

where, E is the linear elastic modulus in MPa. E is referred to as a *material* or *mechanical property*, independent of the structural characteristics of a particular sample of the material. In this study, the term *structural* will be used to designate the properties and behaviour of a material structure or specimen. The term *mechanical* will be used to designate the properties and behaviour of the material itself. In the context of mechanical properties, the terms *response* and *behaviour* will be used in the same sense as in 1 and 2 above:

3. A mechanical *response* is the change in the physical state (e.g., strain) due to the change in an applied input variable (e.g., stress).
4. The mechanical *behaviour* of a material is characterised by the relation between stress and strain.

The distinction between *structural* and *mechanical* behaviour is important as the two terms apply to different aspects of the physical properties of tissues. In describing the properties of tissues, it may by convenient to refer to both their structural and mechanical properties collectively. The term *biomechanical* will be used to describe both the structural and mechanical aspects of the behaviour of the tissues.

2.2.2 Biomechanical properties of tissues

The basis for determining the biomechanical properties of tissues is explained by Woo, et al. (1997): "Because the main function of tendons and ligaments is to transmit tensile loading, experimental studies of the biomechanical properties of these tissues are generally performed in tension. The goal of these tests is to acquire the stress-strain curves of the tendon or ligament substance (from which the mechanical properties are determined) and the load-elongation [behaviour] for the bone-ligament-bone complex (from which structural properties are obtained)."

The load (or force) –elongation behaviour of tissue may be obtained from tensile tests of specimens mounted in a materials testing machine. Force data are recorded directly from load cell output. Elongation data are recorded from displacement transducer output.

Specimens are mounted in a material testing machine with some type of mechanical grips or clamps. The precise method of clamping used depends on the type of tissue. Mounted tissue specimens are generally classified as either grip-tissue-grip or bone-tissue-bone preparations.

Longer tendon structures have been tested as grip-tissue-grip preparations. In order to prevent slipping of tissue specimens at high loads specially designed serrated grips have been used to clamp tissues. The gripping surfaces may have sharp or rounded teeth (Figure 2–1). Butler, et al. (1984) used grips with sinusiodally-shaped teeth to clamp isolated *gracilis* or *semitendinosus* tendons. Lateral expansion of the free edges of tissue specimens occured when the specimens were compressed between the grips. Failure of the tissue specimens was initiated near or within the tissue grips. Based on a comparison of grip-to-grip versus mid-substance strains, the authors concluded that the clamping technique used was only partially successful in preventing the tissues from slipping (Butler, et al., 1984). It is thought that the direct clamping of specimens in mechanical grips may pinch or cut the tissue and cause stress concentrations at the grip-tissue interface. "Cryo-grips," that freeze the tissue where it is clamped have been used to minimise the effect of mechanically gripping soft tissues. Jansen and Savelberg (1994) tested equine flexor tendons between the origin and bony insertion of the tissues using a "cryo jaw clamp" to fix the tendon. In this study the insertion site was left intact with the hoof fixed to a movable clamp connected to the load cell of the materials testing machine. The authors did not provide details on modes of failure or the effects of clamping on test results.

Knee joint ligaments, for example the ACL (anterior cruciate ligament) and MCL (medial collateral ligament), of various species have been studied extensively (e.g., Figgie, et al., 1986; Butler, et al., 1990; Danto and Woo, 1992; Frank, et al., 1994). A standard approach is to set (or "pot") the tibia and femur in moulds with an acrylic cement (PMMA). Mounting pots include plastic or steel tubes or specially designed two piece molds (Danto and Woo, 1993; Haut, et al., 1992; Yamamoto, et al., 1992). The tissue is gripped indirectly, by clamping the bones containing the ligament insertion sites. These ACL and MCL preparations may be described as the femur-ACL-tibia complex (FATC) or the femur-MCL-tibia complex (FMTC), respectively (Woo et al., 1997).

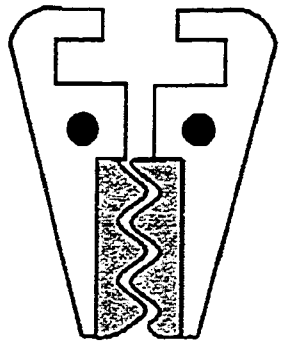

Figure 2–1 Sketch of tissue grips. A similar design was used by Butler and co-workers (1984) for clamping isolated tissue specimens in a grip-to-grip configuration. Note the rounded teeth on the inserts (shown in grey).

The biomechanical properties of the PT have been investigated for many species including human, dog, rabbit and goat (Haut, et al., 1992; Yamamoto, et al., 1992; Johnson, et al., 1994; Ng, et al., 1995). The PT is unique among tendon tissue structures in presenting two sites of bony attachment: the patella and the tibia. In tests of the PT, the tendon is held indirectly by fixing the tibia and the patella. The tibia may be potted in acrylic and clamped as described above. This potting technique may also be used to fix the patella (Yamamoto, et al., 1992). Another possibility is to clamp the *quadriceps* tendon, at the base of the patella in some variation of tissue grips (Danto and Woo, 1992). A variation of the cryo-grip technique has been used in tests of the dog PT (Ma, et al., 1996). The tibial component of specimens was fixed in a metal cylinder with pins and Cerro-Bend alloy. The *quadriceps* were held in a specially designed clamping device. Following fixation of the tibia and clamping of the *quadriceps*, the whole assembly was frozen. Prior to testing, both the distal PT and tibial insertion were selectively thawed.

Structural properties are determined by quantifying the force-elongation behaviour of specimens. Elongation is typically quantified by the displacement between the grips/insertion sites measured by an LVDT (linear differential voltage transducer) on the materials testing machine. Structural properties include stiffness, energy absorbed, ultimate load and ultimate elongation. In bone-tissue-bone preparations, structural properties depend

on the size of the tissue specimens and the strengths of the insertion sites. The same holds true for the tissue-clamp interface in a grip-tissue-grip preparation, i.e., the structural properties depend on the behaviour of the tissue in the clamps.

Mechanical properties are determined from the stress-strain behaviour of the tissue. Mechanical properties include: elastic modulus, ultimate stress and strain, and strain energy density. Stress is quantified by dividing the force measurements (load cell output) by tissue *CSA*. As described in section 2.3.1, tensile strain, ε, in a material is the ratio of the elongation, ΔL, and the initial length, L_0 of the specimen. There are two possibilities for determining the strain in a specimen: grip-to-grip strain or mid-substance strain. In determining grip-to-grip strain, specimen L_0 is measured between insertion sites in a bone-tissue-bone preparation or between clamps in a grip-tissue-grip preparation. ΔL is taken as the displacement between the grips or insertion sites, assumed to be equivalent to the motion of the actuator of the materials testing device. Mid-substance strain is quantified by measuring the deformation, ΔL, of a length, L_0, defined on the tissue mid-substance, between the grips or insertion sites. In this case the initial length is sometimes referred to as *gauge* length. Values of strain are only meaningful if the bases for L_0 and ΔL measurements are reported. Depending on the strain measurement technique that is used, mechanical properties are described as grip-to-grip or mid-substance based. It is generally accepted that in order to characterise the mechanical properties of the tissue itself, the mid-substance strain must be quantified (Shrive, 1994; Woo, et al., 1997).

2.2.3 Failure properties

2.2.3.1 Force-elongation response

The failure test has been used by many investigators to quantify the structural and mechanical behaviour of joint connective tissues. Clayton and Weir (1951) tested canine femur-MCL-tibia preparations by hanging an empty bucket from the tibia and filling the bucket with water until the specimens ruptured. The ultimate tensile strength of the specimens was determined by the weight of the water in the bucket. Today, tests are carried out on more sophisticated material testing devices. Loading rates are precisely controlled and force-elongation data may be acquired at high sampling frequencies. The general

principle remains the same, that is to elongate tissue specimens until they rupture. The failure response of soft connective tissue specimens is non-linear and is described by Butler et al. (1978) as having four regions (Figure 2–2).

The first region of the failure response, called the *toe-region*, is characterised by a relatively small change in force compared to elongation. At higher elongations, tissues demonstrate a stiffer response and an approximately linear force-elongation behaviour. This is the *elastic-region* of the failure response. Following the elastic-region, there is a decrease in the slope of the failure response associated with extensive elongation. This region is the *inelastic-region*. The change from the elastic to inelastic region may not be marked by a sharp boundary. The inelastic region is followed by the *failure-region*, in which there is an abrupt decrease in the force.

Two mechanisms have been suggested to explain the non-linear response of tissues in failure: straightening out or *flattening* of fibre crimp and *progressive recruitment* of fibres. First, toe-region (region 1) behaviour may be related to the straightening of crimped fibres. Tissue stiffness increases when the crimp pattern "flattens out." Second, the transition from the toe-region to the elastic region may be related to the progressive recruitment of tissue fibre bundles with varying degrees of crimp and different lengths (Frank and Shrive, 1994). High stiffness in the linear-region (region 2) may be due to the majority of the tissue fibres supporting tension. The change from region 2 to region 3 is thought to begin as individual tissue fibres, stretched to their ultimate lengths, begin to fail. Once this microscopic failure of individual fibres has begun, remaining fibres must support more tension and the stiffness of the tissue decreases as the failure of remaing fibres accelerates (region 3). Complete failure of the whole specimen (region 4) occurs rapidly after this decrease in stiffness (Butler, et al., 1978; Frank and Shrive, 1994).

2.2.3.2 Biomechanical properties in failure

Failure tests are used to determine tissue structural properties. Structural properties of interest include: stiffness (K), ultimate tensile force (F_{UT}), ultimate elongation (ΔL_{UT}) and failure energy. Stiffness is the slope of the force-elongation curve. Values of K reported for tissue structures are often determined by calculating the average slope between two points in the linear elastic region of a force-elongation curve (e.g., Haut, et al., 1992). The

ultimate tensile force and elongation are the highest value of force and elongation attained prior to total failure (Figure 2–2). Specimen failure energy is an additional means of quantifying and comparing the response of tissue structures (e.g., Woo, et al., 1987a and Haut, et al., 1992). Failure energy is defined as the area under the force-elongation curve up to the point of ultimate force and elongation.

The mechanical property analogs of these structural properties are: (elastic) modulus (E), ultimate tensile stress (σ_{UT}), ultimate tensile strain (ε_{UT}) and strain energy density. The ultimate stress and ultimate strain are the highest values of stress and strain attained prior to total failure. Strain energy density is defined as the area under the stress-strain curve up to the failure point. Modulus values may be obtained from the slope of the linear portion of the stress-strain curve (Butler, et al., 1978; Yamamoto, et al., 1993). Another possibility is to fit a function to the stress-strain data and calculate the modulus as the derivative of this function (Danto and Woo, 1993).

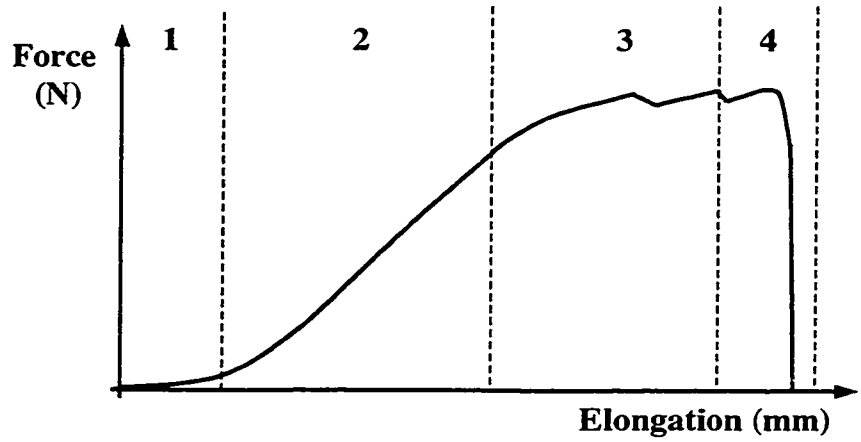

Figure 2–2 Force-elongation curve for a tissue specimen. The regions are indicated between the dashed lines: toe region (1); elastic region (2); inelastic region (3); failure region (4). Adapted from Frank and Shrive (1995).

2.2.3.3 Failure modes

A bone-tissue-bone preparation can fail in one of several modes or mechanisms: a *mid-substance failure*, in which the specimen fails in the tissue mid-substance, away from the bony insertion sites; an *avulsion failure*, whereby pieces of the bone are torn away with the tissue; and an *insertion failure*, in which the tissue seperates from the bone leaving the insertion site intact (Woo, et al., 1997). The mode of failure (failure mechanism) indicates the weakest part of the specimen. Ultimate tensile force and elongation may be used to represent characteristics of the structural response of a specimen if a mid-substance avulsion or insertion failure occurs. The mechanical response of the tissue can only be decribed by the ultimate tensile stress and strain if the specimen fails in the mid-substance (Woo, et al., 1997).

2.2.4 Viscoelastic behaviour

2.2.4.1 Relaxation

Relaxation is a reduction in the force (stress) in a specimen in response to a constant elongation (strain). Relaxation behaviour reflects the viscous component of a specimen's force (stress) response (Figure 2–3). In terms of the structural behaviour of a tissue specimen, when an elongation is applied, the force peaks and immediately decreases. The decay in force is non-linear until a steady-state is reached. The difference between the initial force and the steady state value is the *total relaxation*. A cyclic relaxation test is also possible, in which the specimen is stretched repeatedly to the same elongation. The peak force in each cycle follows a non-linear pattern, decreasing until a steady state value is achieved.

2.2.4.2 Creep

Creep is an increase in the elongation (strain) in a specimen in response to a constant force (stress). Creep behaviour reflects the viscous component of a specimen's length (strain) response (Figure 2–4). In terms of the structural behaviour of a tissue specimen, when an force is applied, the elongation increases rapidly to an initial value and continues to increase over time until a steady state value is reached. The elongation response is non-linear. The difference between the initial elongation and the steady state

value is the *total creep*. A cyclic creep test is also possible, in which the specimen is subjected repeatedly to the same elongation. The peak elongation in each cycle follows the same pattern as the elongation in the static experiment.

2.2.4.3 Hysteresis

The energy absorbed by a tissue specimen that deforms under the action of an applied force can be determined from the area under the force-elongation curve. If the specimen is unloaded to its original length the difference in areas under the loading and unloading curves is the *hysteresis* (Figure 2–5). Hysteresis represents the energy dissipated by the specimen in the loading-unloading cycle. It has been established that repeated cycling reduces the area of the hysteresis loop and therefore the energy dissipated with each cycle (Butler, et al., 1978).

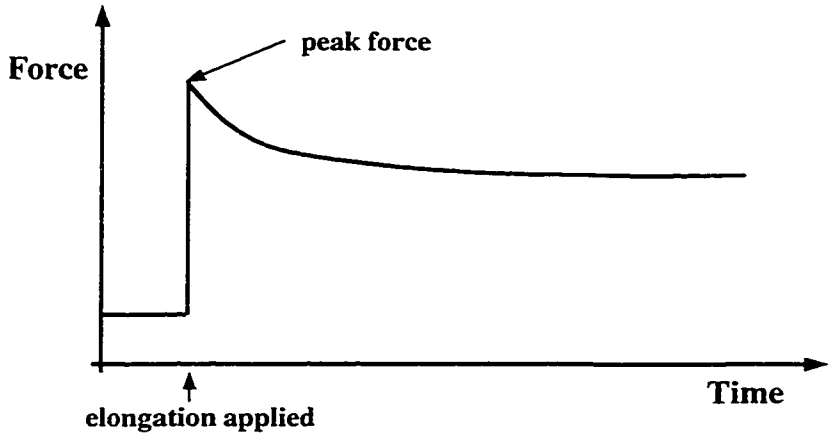

Figure 2–3 Force relaxation curve for a tissue specimen. The force decreases non-linearly at a constant elongation. Adapted from Frank and Shrive (1995).

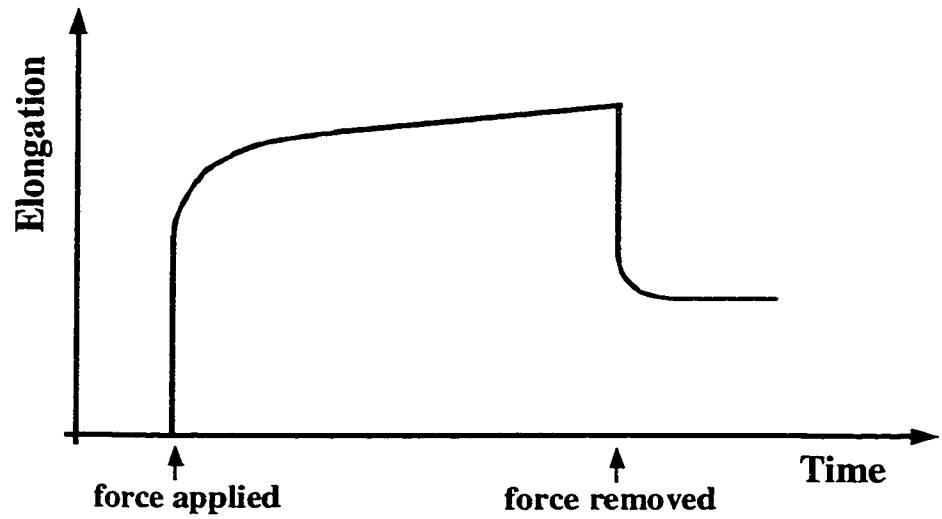

Figure 2–4 Creep response of a tissue specimen. The length increases non-linearly at a constant elongation. Adapted from Frank and Shrive (1995).

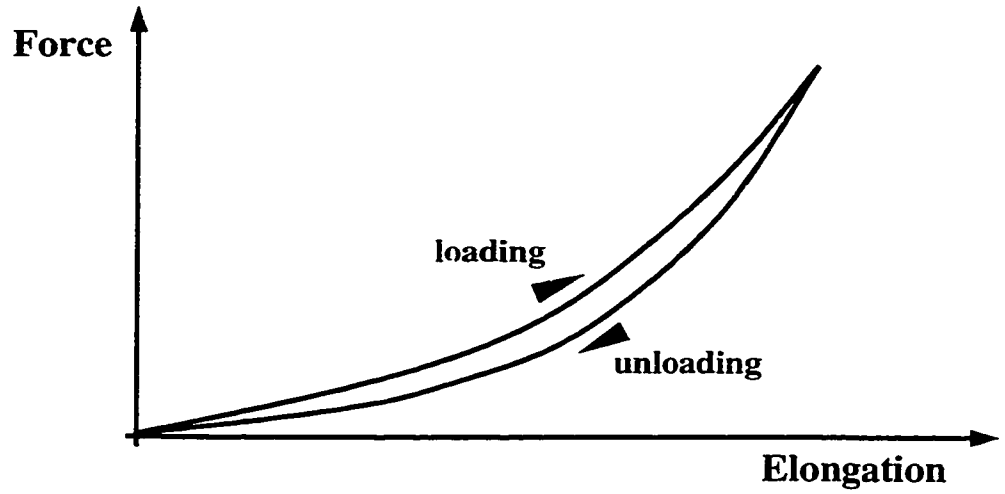

Figure 2–5 Hysteresis curve for a tissue specimen. Loading and unloading follows different paths on the curve. The grey area represents the energy dissipated in the loading cycle. Adapted from Frank and Shrive (1995).

2.3 *CSA* MEASUREMENT

The measurement of tissue *CSA* presents a difficult technical challenge in biomechanics. The *CSA* of knee joint tissue structures varies considerably depending on species and location (Table 2–1). Tissue structures are very pliable and the geometry of their cross-sections may feature many small irregularities. In addition, the cross-section of a tissue may vary along its length (Iaconis, et al., 1987). Measurements of tissue *CSA* are typically performed with the specimen under a small pre-tension. As the specimen elongates under the action of an applied load it will contract in the tranverse plane reducing the *CSA*. Characterisation of tissue stress response is based on the initial *CSA* and does not represent the "true stress" in the tissue.

Tissue	Species	CSA (mm^2)	Study
PT (n = 7)	human	50.5±2.8	Butler. et al.. 1984
ACL (n = 1)	cow	105	Iaconis, et al., 1987
ACL (n = 8)	pig	51.56±9.98	Lee and Woo, 1988
MCL (n = 8)	rabbit	2.63±0.48	Shrive, et al., 1988
PT (n = 27)	dog	24±7	Haut, et al., 1992
PT (n =14)	rabbit	14.0±0.3	Yamamoto, et al., 1992
PT (n = 9)	cat	13.5±0.8	Archambault, 1995

Table 2–1 Comparisons of *CSA* measurements across several species. *From central 1/3 of the tissue.

Techniques for measuring the *CSA* of tissues have been divided into two categories: contact and non-contact methods. Contact measurement techniques include, vernier callipers, area micrometer and tissue area callipers. Non-contact measurement techniques include the "shadow amplitude," profile, laser micrometer and laser reflectance system.

The vernier callipers method is a simple approach for determining tissue *CSA*. The tissue width and thickness are measured. Then the *CSA* is estimated from an assumed tissue cross-section, either rectangular or elliptical (Haut and Little, 1969; Woo et al, 1983a). There are two important sources of error associated with this method. First, pressure from

the callipers may deform the tissue producing inconsistent measurements of the tissue dimensions. Second, the simplistic assumption about the shape of the tissue cross-section may be inaccurate and lead to errors in the *CSA* measurements. For example, if the tissue is roughly elliptical, measurements made based on a rectangular assumption will tend to overestimate the *CSA*. Another method, known as the area micrometer system produces measurements of *CSA* by compressing the tissue into a precisely machined slot of known dimensions with a micrometer (Walker, et al., 1964). The *CSA* is calculated from the width of the slot and the depth/height of the micrometer. This method is also limited by the errors that may be induced by deforming and compressing the tissue. Control of the applied pressure is important with this method, as the measured *CSA* is dependent on the applied pressure (Allard, et al., 1979; Butler, et al., 1986). Butler and co-workers (1984, 1986) used an adapted area micrometer system to measure the *CSA* of human knee ligaments, PT and fascia lata using an applied pressure of 0.12 MPa to the tissue. The exact pressure used is arbitrary, but low and controlled pressures have been established as a standard with this method (Ellis, 1969). Another technique, the *tissue area* callipers, was introduced by Shrive et al. (1988) for measuring the *CSA* of rabbit MCL and similar smaller tissues. The profile of a tissue is determined from instrumented callipers that measure the specimen's thickness as a function of width. Estimates of MCL *CSA* produced by the technique were shown to be sensitive to the pre-load on the tissue and the alignment of the instrument. The most consistent measurements were obtained with the specimen under a pre-load of 5 N. The pressure on the tissue applied by the calliper arms was estimated at 0.1 MPa. If the cross-section of the tissue is known to be approximately elliptical, or has a large width to thickness ratio, the tissue area callipers can provide accurate (5%) estimates of *CSA* (Shrive, et al., 1988).

Investigators have employed techniques that rely on numerical reconstruction of specimen cross-section from optical measurements of tissue profiles. Briefly, the approach of these non-contact methods is to make measurements of tissue profile width from multiple viewpoints. The *CSA* of a tissue specimen is estimated using a reconstructed cross-section from the profile width measurements. The shadow amplitude method determines the *CSA* of specimens from the radius of specimen profiles (Ellis, 1969). An

alternate technique, the profile method, measures the width of a tissue imaged with a video camera that is rotated around the specimen (Njus and Njus, 1986). Both of these techniques work on the basis of fitting the profile measurements to an assumed cross-sectional shape function. Iaconis, et al. (1987) introduced a technique that produced radius measurements by focussing two light beams on a tissue specimen mounted on rotating bearings. The radius measurements were plotted in polar co-ordinates to reconstruct the cross-section of the tissue. The accuracy of the radius measurements was found to be ±0.1 mm. The *CSA*s of bovine knee ligaments were measured with the optical technique and compared to measurements from frozen sections. Measurements differed by 1% to 7% for cruciate ligaments and 5% to 10% for collateral ligaments (Iaconis, et al., 1987).

The laser micrometer system of Lee and Woo (1988) operated on a similar principle as the shadow and profile techniques. A collimated scanning laser casts a precisely measured shadow of a rotating specimen. Profile data collected as the specimen is rotated through 180° are used to reconstruct the cross-sectional shape. The reconstruction algorithm used makes no assumptions about the shape of the specimen cross-section, which gives this technique an advantage over the earlier profile methods. The laser micrometer system produced accurate results and was capable of reproducing the geometry of known objects to within 5%.

The common limitation of all of these non-contact techniques is the inability to detect concavities in the surface of tissue structures. In an effort to overcome this limitation and produce very accurate representations of tissue cross-sections, a laser-reflectance system was used by Chan et al. (1995) to measure the *CSA* of pig ACL. The system measures distance to the specimen from reflected laser radiation together with angular position as it is rotated 360° around the specimen. The laser-reflectance system produced accurate results and was capable of reproducing the geometry of known objects with an accuracy of 2.5 %. The tissue area callipers have been compared to the use of vernier callipers in measuring the *CSA* of rabbit MCL (Shrive, et al., 1988). Measurement based on a rectangular and elliptical cross-section were found to over estimate tissue *CSA* by 43 % and 13 %, respectively (Table 2–2). The laser micrometer was compared to the area micrometer in measurements of the *CSA* of pig ACL (Lee and Woo, 1988). The area

micrometer underestimated the *CSA* by 18% compared to the laser micrometer (Table 2–2). A further study comparing the laser reflectance system and the laser micrometer was conducted using the ACL of pigs (Chan, et al., 1995). It was found that the laser micrometer overestimated the *CSA* of specimens by 10 % compared to the laser-reflectance system. No studies have been conducted to compare tissue area callipers with a laser reflectance system. However, both of these approaches offer two distinct advantages over the other techniques. First, they are not based on assumptions of tissue cross-sectional geometry. Second, the tissue area callipers and the laser reflectance system are capable of distinguishing concavities in the surface of irregularly shaped tissues, which is not possible with the other methods.

Tissue	**Rabbit MCL**	**Rabbit MCL**	**Rabbit MCL**	**Pig ACL**	**Pig ACL**
Method	Tissue area callipers*	V. callipers (rectangular assumption)*	V. callipers (elliptical assumption)*	Laser micrometer**	Area micrometer**
CSA (mm^2)	2.63±0.48	3.77±0.64	2.96±0.50	51.56±9.98	42.39±5.96

Table 2–2 Tissue *CSA* measurements from contact and non-contact methods. Comparative measurements of rabbit MCL and pig ACL(*Shrive, et al., 1988; **Lee and Woo, 1988).

2.4 STRAIN MEASUREMENT

2.4.1 Measurement of tissue strain

Shrive (1994) describes three approaches for measuring strain. The first approach is to measure an equivalent strain that is output by a strain transducer. An example of this is the voltage signal from a liquid metal strain gauge (Monahan, et al., 1984). Strain is determined directly by converting the voltage signal to strain with a calibration factor. The second approach is to measure the change in length, ΔL, of the specimen. This principle is employed with the extensometer technique of Shrive, et al., 1992. The third approach is to measure the deformed length of a specimen and calculate ΔL with respect to a measured

gauge length. Photographic techniques and video dimension analysis, described in the following sections, are based on this approach. If E and E_0 represent errors in the measurements of L and L_0, respectively, then the change in length, ΔL, can be expressed as:

$$\Delta L = L - L_0 \pm (E + E_0). \qquad [5]$$

Errors in strain measurement using this approach will be large if ΔL is close to the value of $E + E_0$ (Shrive, et al., 1994).

Techniques developed to measure strain may be described as *contact* and *non-contact* techniques. Contact based techniques include the use of devices such as the liquid metal strain gauge (Monahan, et al., 1984) or the Hall effect transducer (Arms et al., 1983) to measure tissue deformation. These devices are physically attached to a region of tissue and produce a voltage signal that corresponds to the displacement of the tissue region. These devices may alter the mechanical response of tissues to which they are attached. Carefully designed to minimise its effect on tissue response, the LMSG has been used recently to quantify the strain response in the structurally complex cruciate ligaments of the knee joint (Bach, et al, 1997). A recently developed device, the extensometer, may be suitable for the measurement of very small strains but is limited in its ability to produce reliable measurements (Shrive, et al., 1992).

The concern that measurement artifacts may arise due to direct contact with tissue specimens has motivated the development of a number of non-contact methods (Woo and Sites, 1988). Non-contact techniques are based on optical measurements of tissue deformation. A variety of approaches have been developed to measure strain. The following sections present an overview of techniques that have been used to measure strain in the soft connective tissues of the knee joint: photographic analysis, video dimension analysis (VDA) and digital image analysis.

2.4.2 Photographic analysis

This technique uses film or flash-photography to record the motion of markers on the tissue surface during mechanical tests. Surface fibres of the tissue are marked with black ink or tissue stain during specimen preparation. As an alternative to staining the tissue, beads or sutures are sewn or adhered to the surface. The specimen is then filmed during mechanical testing. After the experiment, photographic images of the specimen are

projected onto a digitising board, and the locations of surface markers in sequential images are recorded. An initial image provides the gauge length (L_o) between marker coordinates. Coordinate data from subsequent points in time are used to calculate strain. The exact type of photographic technique may vary. At high strain rates, high-speed film-photography (400 fps) has been used (Butler et al., 1984; Zernicke et al., 1984). These studies found large differences between the surface strains in the tissue mid-substance and the grip-to-grip strains. Mid-substance strains were found to be 25% to 30 % of the grip-to-grip strains for gracilis, semitendinosus and PT specimens. Elastic modulus estimates based on mid-substance strain measurements were determined to be two to three times higher based on mid-substance strain compared to grip-to-grip strains. Studies of tissue specimens tested at low strain rates have also used conventional flash-photography (Jansen and Savelberg, 1994). Butler et al. (1990) used microphotography to study strain in PT and ACL fascicles. Photographs were taken at 0.1 Hz during low rate loading of specimens marked with silk sutures.

Photographic analyses of tissue strain have been shown to produce both reproducible and accurate measurements. Butler et al. (1984) reported an error of 0.1 mm in the location of repeatedly digitised points. This is equivalent to an error of 4 % strain over a gauge length of 10 mm. A study of low rate failure tests of equine tendons reported errors in repeatability of 0.1 times the failure strain over gauge lengths of 2 to 22 cm (Jansen and Savelberg, 1994). The micro-photographic system of Butler, et al. (1990) yielded results with a strain accuracy of 0.4 %. The low frequency response of some systems places limitations on the strain rates applied in mechanical testing. Photographic techniques are very labour intensive because strain measurements rely on marker displacement data from hand-digitised images.

2.4.3 Video dimension analysis

Video dimension analysis (VDA) applies video technology to the study of strain in soft connective tissues. VDA is based on the same principle as photographic analyses: strain measurement from images of marked tissue specimens. The technique was first introduced by Yin et al. (1972) to measure dimension in video images. First, the surface of the specimen is marked with black ink or tissue stain. The stain is typically applied in lines

or bands across the tissue, perpendicular to the axis of loading. The output signal from a video camera (image of the tissue specimen) is transmitted through a "video dimension analyser" microprocessor to a monitor. Two "windows" are projected on the image in the monitor by the dimension analyser. The windows are positioned over two stain lines on the tissue surface, delineating the portion of the video signal that is analysed. A detector in the dimension analyser, scans the video signal for changes in brightness as the signal passes across the edge of a stain line. A timer starts when the video signal crosses the first stain line and stops when the second stain line is crossed. The scan time between the two stain line edges is converted to a voltage. When the specimen is loaded, the output voltage increases as distance between the stain line edges increases. Tissue strain can be quickly calculated from the voltage outputs as:

$$\varepsilon = \frac{V_1 - V_0}{V_0}, \qquad [6]$$

where ε is the strain, V_0 is the initial voltage corresponding to the known gauge length and V_1 is the output voltage (Lam, et al., 1992). The camera signal can be recorded and analysed from playback on a VCR.

Woo, et al. (1982; 1983) made extensive use of this technique to study strain in the rabbit MCL. More recently, VDA has been used to measure strain in mechanical tests of rabbit patellar tendon (Yamamoto, et al., 1992; 1993; 1996) and human patellar tendon (Johnson, et al., 1994). Studies using VDA have reported differences between grip-to-grip strain and mid-substance strain. In tests of rabbit PT, mid-substance strains were 38 % of grip-to-grip strains. This resulted in modulus estimates for the PT mid-substance that were 2.5 times the corresponding grip-to-grip estimates (Yamamoto, et al., 1992).

The accuracy of VDA systems has been reported at 0.5 % (Woo, et al., 1982). VDA systems have been shown to be more accurate at higher strain levels. Calibration (quantification of voltage versus change in specimen length) of a VDA system has been shown to be influenced by object distance, the medium through which the specimen is viewed and the orientation of the specimen and the camera (Lam, et al., 1992). The same study found that the strongest influence on the system's calibration was found to be object distance, with a 70 % change in calibration factor when the object distance was changed

from 175 mm to 300 mm. More importantly, it was demonstrated that errors in strain measurements would be larger for lower nominal strains. For example, the error at 10 % strain was 10% while the error at 1 % strain was roughly 40% (Lam, et al., 1992).

The key limitations of VDA are frequency response and lack of precision in measurements of crooked or diffuse stain lines. Conventional video technology operates at 60 Hz. High speed failure tests cannot be monitored at this rate. For example, movement in 0.1 mm increments can only be captured up to a displacement rate of 6 $mm \cdot s^{-1}$. Stain line edges (providing the light-dark contrast) must remain in the windows. If the motion is slow enough the operator can maintain the relative position of the edges and the window. As the strain increases in a tissue marked with a contrast stain, the stain lines become "wavy and diffuse." This results in less precise measurements of the distance between two edges.

2.4.4 A digital image analysis technique

New techniques combine the approach of video-monitoring of tissue specimens with the application of digital image technology to measure tissue deformations (Soslowsky, et al., 1993; Derwin, et al., 1994). This technique relies on the same basic approach as previously described optical techniques. Tissue specimens are marked with a black contrast medium and monitored with a video camera during mechanical testing. The video signal is sent to a VCR and a video controller is used to write a time code on the audio channel of the video signal. The VCR record/play back frequency is 30 frames per second. After an experiment, the video record is processed in a series of steps. Frames from the video record are captured as digital images. These images "show a section of tissue with stain lines approximately parallel to the direction of uniaxial stretching" (Derwin, et al., 1994). The operator manually selects the region of interest in the images and a strain analysis algorithm is applied to the image data in the frames of interest. Strain measurements are based on detection of stain line edges in images from the video recording. The edge detection relies on an analysis of image intensity gradients on rows of pixels that are assumed to be parallel to the direction of strain. Strain is determined from the distance between stain line edges in sequential frames. The accuracy was determined to be ±0.23 % strain at 11.74 % strain and from ±0.07 to ±0.28 % strain at 3.52 % based on a gauge length of 25.55 mm.

With the system described by Derwin and co-workers (1994), it was possible to track the motion of the region of interest as it moved in the camera's field of view. The strain measurement software determined the edge location at 200 to 300 discrete points along the edge of each stain line and then produced an average position of the line. This is more precise than VDA systems that automatically average the position of the stain line edge in the entire window. The technique was capable of precise measurement of strains across a region that has small irregularities and waviness in the stain lines. Once the region of interest has been manually identified, repeated and varied analyses of the strain variation in the region of interest were possible. The selection of the region of interest in each frame was done manually and was labour intensive. This step in the analysis was reported as a possible source of error. Irregularities in the shape of the stain lines may result in apparent deformation being measured if the region of interest was not repeatably selected in sequential frames. Finally, the standard 30 Hz playback and record of the system limits the speed of tissue tests to slower strain rates (Derwin , et al., 1994).

2.4.5 Common sources of error and limitations

The optical techniques described above share two sources of error: lens distortion and rigid body movement. Consider a specimen oriented in an orthogonal coordinate system (Figure 2–6) with the x,y-plane as the plane of measurement, where strain is being measured in the y-direction (Derwin, et al., 1994). The first type of error, lens distortion, is due to surface errors on a lens that distort the recorded image (film or video) of the specimen. Movement of the specimen in the x,y-plane may give rise to apparent deformation due to lens distortions. Derwin et al. (1994) reported an apparent strain of 0.6% in displacing a 25.4 mm gauge length by 6.35 mm. The amount and direction of distortion is unique to a lens but tends of be larger at the edges of the field of view (Nigg and Cole, 1994). The second type of error, rigid body movement, refers to translation and rotation of the specimen with respect to the plane of measurement. Translation of the specimen is movement out of the plane of measurement ($\pm$ z-direction). Derwin et al. (1994) reported an apparent strain of 0.6% on a gauge length of 25.40 mm, for a z-displacement of 10 cm (towards the camera). This magnitude of relative motion between the camera and specimen is not typical. Based on this finding, apparent strain due to

translation is not a significant source of error. The investigators also studied the apparent strain arising from rotation of the specimen (Figure 2–6 and Table 2–3). Rotations about the *y*-axis (the direction of strain) produced no apparent strain. Apparent strain measurements were found to be most sensitive to rotations about the *x*-axis (perpendicular to the direction of strain). For a gauge length of 25.40 mm, at +5° the apparent strain was –0.6 % and +10° the apparent strain was –2 %.

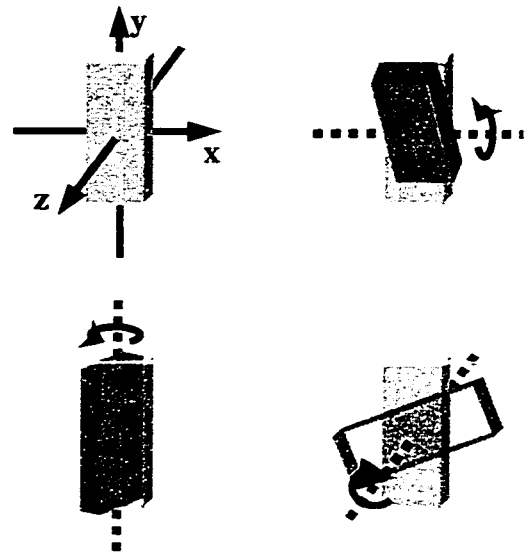

Figure 2–6 Sources of error in 2D strain measurements. Specimen in a coordinate system. Elongation is in the *y*-direction (top left); rotations about the *x*-axis (top right); rotations about the *y*-axis (bottom left); rotations about the *z*-axis (bottom right). The *z*-axis is parallel to the optical (viewing) axis.

Axis of rotation	**Apparent strain (%) at *n*°of rotation**						
	–20°	–10°	–5°	0°	5°	10°	20°
***x*-axis**	-	–1.1	–0.2	0	–0.5	–2.0	-
***y*-axis**	0	0	0	0	0	0	0
***z*-axis**	–0.2	–0.0	0	0	0	–0.0	–0.2

Table 2–3 Apparent strain measured due to gauge block rotation (Derwin, 1994).

2.4.6 Summary

Photographic techniques and VDA have been used to demonstrate important aspects of tissue behaviour, including variation in specimen surface strain and the influence of strain measurement technique on the quantification of tissue mechanical properties. Photographic analyses have been found to be labour intensive and, without the use of high-speed film photography, limited in frequency response. A more convenient technique, VDA may also be limited in its frequency response unless high speed video is used to record tissue deformation during testing. Strain measurements using VDA may also be affected by a lack of precision in measurements of crooked or diffuse stain lines.

A digital image analysis technique developed by Derwin et al. (1994) was capable of precisely determining the location stain line edges even over regions of irregularity and waviness in the stain lines. Application of the technique may be more labour intensive than VDA but offers the possibility of rapid, repeated and more flexible analysis of tissue strain.

These approaches avoid the problem of artefacts arising from direct contact with the tissue specimen. However, there are four important limitations affecting 2D optical measurements of tissues strain:

1. Strain is quantified by measurements of a deformed length relative to an initial, undeformed, gauge length. Therefore, strain measurements may have large errors.
2. Strain measurements should be qualified as being *surface strain measurements* (Butler, et al., 1984). Quantification of tissue mechanical behaviour is based on the assumption that the strain response of the surface fibres represents the behaviour of the deep fibres of tissue specimens.
3. Strain measurements may be affected by errors associated with lens distortion or motion of the specimen with respect to a 2D plane of measurement.
4. Media used to mark the surface of tissue specimens (e.g., ink, histological stain) may react with and alter the mechanical properties of the collagenous substructures of the tissue (Shrive, 1994).

2.5 FACTORS INFLUENCING TISSUE BIOMECHANICAL PROPERTIES

There are a variety of factors which can influence the measured biomechanical properties of tissues. Woo et al. (1997) classified these factors into three categories:

experimental, external and biological. Experimental factors are associated with aspects of mechanical testing that are (to some degree) controlled by the investigator. Experimental factors include but are not limited to alignment, hydration, strain rate and temperature. External factors originate outside of the immediate environment of the *in vitro* test. The two important external factors identified by Woo et al. (1997) are storage by freezing and irradiation. For the purpose of the present study, freezing will be included in this discussion as an experimental factor. Biological factors include maturity, injury, activity levels and immobilisation. These factors are functions of the development, growth and biological response of tissues. These factors are "controlled" to some degree by selection of the population of the donor organism or may be manipulated by the investigator.

The following sections outline details of the experimental factors that are relevant to the present study: alignment, hydration, strain rate, temperature and storage by freezing.

2.5.1 Alignment

Specimen alignment or orientation has been shown to be a critical factor which influences the structural and mechanical response of bone-tissue-bone preparations. Studies have examined the effect of alignment on the femur-ACL-tibia complex (FATC) of dog, rabbit and human (Figgie, et al., 1986; Woo, et al., 1987; Woo, et al., 1991). In the case of this type of preparation, the alignment may be described by: i) the relative orientation of the tissue structure and the direction of loading; and ii) the relative orientation of the tibia and the femur (knee flexion angle). All three studies found that specimens were strongest when the direction of loading was parallel to a line joining the insertion sites on the femur and the tibia. In the studies of dog and rabbit FATCs, it was also reported that the mode of failure was sensitive to the direction of loading. Insertion failures occurred when the direction of loading was aligned to the ligament while midsubstance failures occurred when the direction of loading was perpendicular to the ligament (Figgie, et al., 1986; Woo, et al., 1987; Woo, et al., 1991). Figgie, et al. (1986) observed decreases in the structural properties of specimens with increasing knee flexion when the direction of loading was aligned with the tibial axis. Structural properties were not sensitive to knee flexion when the direction of loading was parallel to the ligament axis. Woo et al. (1991), reported

significantly higher ultimate load, stiffness, and failure energy for human FAT specimens tested in an anatomic orientation, with the ligament aligned in the direction of loading.

These studies demonstrate the strong influence of specimen alignment on both the structural properties and mode of failure. The speculated mechanism for the difference between the two directions of loading is that fibre bundles are loaded at the same time when the direction of loading is parallel to the ligament. When the direction of loading is "off axis," fibre bundles are loaded unevenly and fail progressively across the ligament cross section (Woo, et al., 1987).

A recent study presented by Ma, et al. (1996) demonstrated the effect of loading angle on the stiffness, strength and failure mode of the canine patellar tendon-tibia unit. Specimens were tested with the direction of loading aligned with the tendon. However, the angle between the tendon and the insertion site was varied. PT insertion sites at the tibia were prepared for histological examination and the orientation of the calcified fibrocartilage with respect to the insertion tide mark was quantified. Additional specimens were tested at five loading angles, -45°, -15°, 0°, 15° and 30° with 0° being aligned with the calcified fibrocartilage. Negative angles corresponded to loading in the posterior direction. Negative loading angles resulted in tendon substance failures while positive loading angles resulted in bony avulsion failures. Specimens loaded in negative angles were significantly stronger than those loaded in positive angles. The authors speculated that the negative angle tests loaded the insertion in shear and compression and the calcified fibrocartilage of the insertion is strongest in this load configuration.

2.5.2 Hydration

Tissues contain a large amount of water but will become dehydrated when exposed to dry air. Most *in vitro* testing protocols incorporate some method of tissue hydration to maintain the water content. Saline drip or saline bath environments have been used. The method of tissue hydration has been shown to influence the failure properties of specific tendon and ligament tissues. The rabbit ACL was observed to exhibit larger elongation at failure and higher failure energies following immersion in a saline bath compared to testing in air (Viidik and Lewin, 1966). Rat tail tendon which has been dehydrated in air is stronger and stiffer than tissue hydrated by means of a saline bath (Betsch and Baer, 1980).

Haut and Powlison (1990) found that human PTs tested in a saline bath had a 60 % higher modulus and were 40 % stronger compared to PTs hydrated with a saline drip. Tissue hydration has also been shown to effect the viscoelastic behaviour of specific tissues. Chimich, et al. (1992) demonstrated that rabbit MCL specimens with higher water content demonstrated higher cyclic load relaxation. A recent study (Haut and Haut, 1997) suggests that the sensitivity of tissue biomechanical properties to strain rate depends on water content. The stiffness and load relaxation of human PT specimens were observed to increase with higher water content.

The mechanisms that relate tissue hydration with biomechanical properties remain unexplained. Chimich et al. (1992) speculated that load relaxation behaviour depends on relative movement between the structural components of the rabbit MCL and higher water content increases this relative movement.

2.5.3 Strain rate

As viscoelastic materials, ligaments and tendons exhibit time dependent behaviour including strain rate sensitivity. A number of studies have focussed on the effect of strain rate on the biomechanical properties of tendon and ligament tissues (e.g., Noyes, et al., 1974; Haut, 1983; Peterson, et al., 1987; Danto and Woo, 1993). These studies are based primarily on *in vitro* failure testing of specimens and have also focussed on the strain dependent behaviour of failure modes in bone-tissue-bone preparations. Noyes et al. (1974) tested left-right pairs of FATCs from rhesus monkeys at fast and slow strain rates (66 %/s and 0.6 %/s). Specimens tested with the higher extension rate had significantly higher maximum loads, failure strains and higher failure energies. Specimens tested at the higher rate showed an increased tendency to fail in the ligament substance. Haut (1983) describes three failure parameters used to quantify the age-dependent strain rate sensitivity of rat tail tendon: tensile strength, failure strain, and failure energy density. Two strain rates were used, 720 %/s and 3.6 %/s. Each of the three failure parameters increased with strain rate (and the sensitivity to strain decreased with rat growth and maturation).

Danto and Woo (1993) carried out a comparative study of the mechanical properties of the rabbit PT (central third) and ACL (medial half) from mature animals. Three failure parameters were used to quantify tissue response: initial modulus, rate of

change of modulus (from the toe region), and the linear elastic modulus. Both types of tissue structures demonstrated a sensitivity to strain rate over a range of three extension rates, 0.003. 0.3 and 113 mm/s. However, not all of the mechanical properties showed a monotonic increase with increasing strain rate. The authors suggest that monotonic increases in mechanical properties will be observed over large changes in strain rate (eg. four orders of magnitude) and that this effect may be related to species. It is also of interest in this study that 90% of the specimens failed by avulsion. Peterson and colleagues' study (1987) obtained strictly substance failures for mature FMTCs. This suggests that the failure mode of tissue structures also depends on the type of tissue.

2.5.4 Temperature

In *Collagen*, Woo and Sites (1988) briefly review a number of studies in which the temperature dependency of structural and mechanical properties of tendon and ligament tissues were investigated (Hunter and Williams, 1951; Rigby et al., 1958; Apter, 1972; Kuie et al., 1979). The general observation of these studies was that tissues and tissue structures are stiffer with colder temperatures. Changes in tissue properties may be small over a reasonable range of temperatures. In their review, the authors cite a well controlled study of temperature dependence of cyclic load relaxation response of canine MCL. FMTCs were tested in a 0.9% saline bath over a range of temperatures from 2°C to 37°C (Woo, et al., 1984). A linear relationship between the normalised peak load and temperature was observed such that the peak load increased for decreasing temperatures. The normalised peak load was 30% larger at 2°C compared to 22°C and 20% less at 37°C compared to 22°C. The study supported the earlier observations that tissues are stiffer at colder temperatures.

These studies highlight some important indications for the testing of tissue structures. Tissues that are frozen prior to testing should be allowed to have their temperatures equalised with the ambient temperature of the testing environment. Furthermore, steps should be taken to ensure that the temperature of the tissue does not vary greatly during testing.

2.5.5 Storage by freezing

The biomechanical properties of bone-ligament-bone preparations do not appear to exhibit dramatic changes when tissues are stored frozen prior to mechanical testing however the findings of studies are not conclusive. Studies have obtained conflicting results, with some investigators reporting no differences and others observing statistically significant differences between fresh and frozen tissues. Noyes and Grood, (1976) found no differences in the structural properties between bone-ligament-bone preparations tested fresh or stored for four weeks at –15°C. Barad, et al. (1982) observed no changes in the stuctural and mechanical properties between pairs of specimens stored at 4°C overnight and those stored at –80°C for three to five weeks.

Woo, et al. (1986) studied the effect of storage by freezing on the biomechanical properties of the rabbit FMTC. Paired specimens were tested fresh or following storage at -20°C for 45 days. No statistically significant differences in the structural (load-deformation characteristics of the FMTCs) or mechanical response (stress-strain characteristics of the MCL substance) were noted between the fresh and stored samples. No differences were observed in the failure energy between fresh and stored samples but the area of hysteresis of the stored samples was significantly reduced in the first few cycles. A later study by Turner, et al. (1988) examined the effect of cold storage on the structural properties of the canine ACL bone-ligament-bone preparations. Paired specimens were tested fresh or following storage at -70°C for eight to twelve weeks. No difference in ultimate tensile strength was observed between the fresh or frozen specimens. A significant decrease in stiffness and increase in elongation at failure was noted in the test specimens.

The elastic modulus of cat tendons was found to decrease after two weeks of storage at -10°C (Matthews and Ellis, 1968). Recently, the effect of freezing on the biomechanical properties of rabbit muscle-tendon units (extensor digitorum longus) was investigated (Leitschuh, et al., 1996). Two groups of sixteen specimens were tested in failure fresh and after frozen storage (at -80 °C for 28 days). Frozen/thawed specimens had significantly lower values for ultimate load, failure energy and ultimate strain. The mode of failure was also altered by freezing. Fresh specimens failed at the musculotendinous junction compared to the frozen specimens which failed at the fascia-muscle interface.

2.6 VARIATIONS IN STRES S-STRAIN RESPONSE

Other studies have quantified the longitudinal variation in tissue specimens and found that strain appears to be concentrated at the grips or insertion sites (Butler, et al., 1984; Stouffer, et al., 1985; Butler, et al., 1990). Study of the longitudinal variations in specimen strain may be useful in understanding the effects of tissue clamping on mechanical property measurements or the differences between the structural properties of bone-tissue-bone preparations and the mechanical properties of the tissue mid-substance. Also of interest is the quantification of transverse variation in tissue response, particularly in studying the characteristics of PT autograft reconstructions (Noyes, et al., 1984).

Previously, Yamamoto, et al. (1992) investigated the mechanical properties of the lateral, central and medial thirds of the rabbit PT. The elastic modulus, ultimate tensile stress and ultimate tensile strain of the tissue specimens were quantified. The ultimate tensile stress of the lateral third was significantly higher than the that of the central portion. No other significant differences were found. Butler et al. (1984) found no significant differences in failure properties of isolated preparations of the central and medial portions of human PT specimens. Strain variation of whole cat PT specimens in cyclic loading was reported by Archambault (1995). No significant differences were found between the lateral, central and medial strains but a trend of decreasing strain was reported in the lateral to medial direction.

3 METHODS

First, a description of the methods used for the *in vitro* investigation of left-right differences in PT properties is presented. Second, the methodology of the *in situ* experiment is described. (It should be understood that this experiment was conducted to obtain knee joint kinematic data *in addition* to PT force-elongation data. The methodology and results of the kinematic analysis are not presented in this study). Third, the technique developed to quantify tendon surface strain is described in detail. Finally, the methods used to quantify the stress-strain behaviour of PT are presented. An experiment was conducted in order to develop a technique for quantifying PT stress and strain in the intact knee joint of an anesthetised animal model.

3.1 *IN VITRO* STUDY

3.1.1 Specimen preparation

All procedures received ethical review and approval from the University of Calgary Animal Research and Ethics Committee. Specimens were obtained from the hind limbs of skeletally mature male and female cats (Table 3-1). Maturity was indicated by closure of the epiphyseal growth plates of the proximal tibia verified in X-rays of the specimens. Left-right pairs of hind limbs were sealed in plastic bags and frozen (-20° C) for a period not exceeding six months. Pairs were removed from storage 12 hours prior to testing and thawed at room temperature (23° C). Patella-PT-tibia complexes (PPTCs) consisting of the proximal tibia, including the tibial tuberosity, patellar tendon and patella were dissected from the hind limbs. All knee joint soft tissues were dissected from the joint leaving the patella and PT intact. The tibia was cut 5 cm distal to the joint line. The proximal tibia was positioned and secured in a steel mounting pot using acrylic cement (PMMA). When the cement had set, the cast was removed from the mounting pot and a 0.125 inch hole was drilled through the cast. A steel pin was inserted into the hole to prevent slipping between the bone and cast. The cast was replaced in the pot. The pot was then attached to the actuator of the materials testing device (MTS Systems Corporation, Minneapolis, Minnesota). The patella was inserted into a custom steel box clamp that was fixed to the device's loading table (Figure 3–1). The clamp held the specimen by gripping the anterior

and posterior faces of the distal end of the patella. The tibial pot was positioned such that the angle between the anterior face of the patella, the patellar tendon (PT) and the tibial insertion in the sagittal plane was approximately 0 (±5)°. The pot was aligned with the clamp such that there was no visible twist about the long axis of the PT. Tests were conducted at room temperature. Specimen hydration was maintained by spraying with phosphate buffered saline (PBS) solution every two minutes during preparation and testing.

Specimen Pair	*1*	*2*	*3*	*4*	*5*	*6*
Sex	F	F	F	F	F	F
Weight (kg)[1]	3	3	3	3.5	3	2.75
Skeletal Maturity	M	M	M	M	M	M
Specimen Pair	*7*	*8*	*9*	*10*	*11*	*12*
Sex	F	M	M	F	F	F
Weight (kg)[1]	4	4	4	3.5	3	2.75
Skeletal Maturity	M	M	M	M	M	M

Table 3–1 Specimen data. [1]Whole number indicates best estimate of animal's mass.

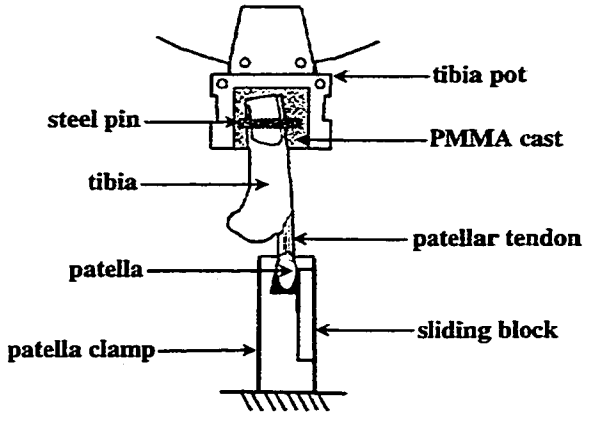

Figure 3–1 Lateral view of mounted specimen with potting and clamping details.

3.1.2 Loading protocol

Structural and mechanical properties for each specimen were determined with a four phase loading protocol (Table 3–2). In the first phase, two cycles of loading to 10 N (ramp rate of 1 mm min^{-1}) were applied to the PT specimen. At the end of the second cycle, the force level in the specimen was at 0.1 N, and the specimen elongation (displacement transducer signal from the MTS) was set to 0.00 (±0.05) mm. The purpose of this phase was to provide consistent initial conditions of length and tension for all specimens. In the second phase, the PT was loaded to 10 N (ramp rate of 1 mm min^{-1}) and held at a constant length. The specimen was allowed to relax for one minute prior to making cross-sectional area (*CSA*) measurements. The *CSA* measurements were made in 3 to 5 minutes. After this test, the specimen's length (*L*) was measured. Techniques used to measure specimen *CSA* and L_0 are described in Section 3.1.3. In phase three, the specimen was subjected to a cyclic loading test. A cyclic loading test consisted of 30 or 60 cycles of loading to 250 N (ramp rate of 10 mm min^{-1}) (Table 3-3). The purpose of this test was to condition the specimen prior to failure testing. Specimen length was measured, again, after the cyclic test. A final failure test was conducted at one of three loading rates, 100, 750 or 1000 mm·min^{-1} (Table 3-3).

Procedure Name	Description	End State	Sampling Rate
TZERO	2 cycles to 10 N at 1 mm min^{-1} (0.89 MPa; 0.1 % sec^{-1})	0.1 N at 0 mm. (0.09 MPa)	2.5 Hz
TXAREA	Load to 10 N at 1 mm min^{-1}. Hold at constant length for *CSA* measurements. (0.89 MPa; 0.1 % sec^{-1})	0.1 N at 0 mm. (0.09 MPa)	50 Hz
TCYCL	30 cycles to 250 N at 10 mm min^{-1} or 60 cycles to 250 N at 10 mm min^{-1} (22 MPa; 1.0 % sec^{-1})	0.5 N at a constant length. (0.45 MPa)	20 Hz
TFAIL	Load to failure at 100, 750 or 1000 mm min^{-1} (10 , 75 or 100 % sec^{-1})		1000 Hz

Table 3–2 Four phase loading protocol. Stress and strain equivalents (based on mean specimen *CSA* and grip-to-grip L_0) are shown in brackets.

Specimen Pair	Number of cycles		Actuator speed (mm min^{-1})		
	30 Cycles	60 Cycles	100	750	1000
1		*		*	
2		*		*	
3		*		*	
4	*			*	
5	*			*	
6	*		*		
7	*				*
8	*				*
9	*				*
10	*				*
11	*				*
12	*				*

Table 3–3 Details of the testing protocol for each pair.

3.1.3 Cross-sectional area and initial length

PT specimen length (L_0) was defined as the distance from the PT insertion on the tibia to the top of the patellar clamp. This distance was measured to the nearest 0.5 mm using vernier callipers carefully held against the mounted specimen. An average of three measurements was used to quantify specimen L_0 from clamp-to-bone. *CSA* measurements were taken on the PT approximately 3 to 5 mm distal to the apex of the patella. *CSA*s were obtained with tissue area callipers (Shrive, et al., 1988). When the callipers passed across the tendon, strain gauges on the calliper arms and an LVDT produced voltage outputs corresponding to tendon thickness and width respectively. Bridge output (thickness voltage) was calibrated using gauge blocks. LVDT output (width voltage) was calibrated with a dial gauge. These voltage signals were recorded by the data acquisition system (DAQS) of the MTS, sampling at 50 Hz. *CSA*s were calculated, after testing, as the area prescribed by width and thickness data based on three repeat measurements for each PT (Figure 3–2).

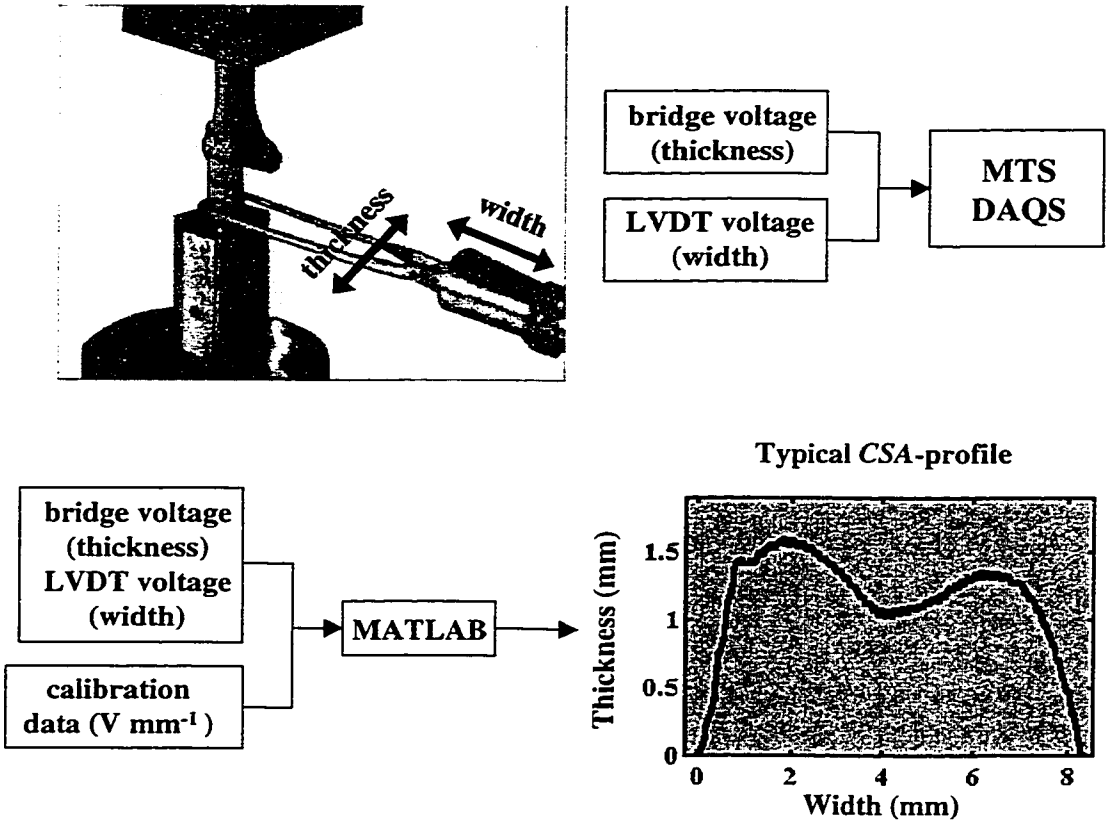

Figure 3–2 Details of the PT *CSA* measurements. Tissue area callipers calibrated for thickness and width (Shrive, et al., 1988) were used to measure tendon cross-sections (top); voltage data and calibration data were processed in Matlab5.1 (The Mathworks, Inc., Natick, MA) and tendon *CSA*s were estimated from numerical integration of thickness-width curves (bottom).

3.1.4 Cyclic properties

Both specimen stiffness and elastic modulus were estimated from analysis of the force-elongation data collected in cyclic loading tests. Data from the loading portion of each cycle were isolated. The loading portion was that part of a cycle in which the force increased from 0 N to 250 N. Thirty sets of force-elongation data were obtained from each cyclic test. The data sets to provide estimates of the instantaneous stiffness, $dF/d\Delta L$, were resampled with a GCV spline program (Woltring, 1986). The linear stiffness in each cycle was calculated as the average of twenty-one samples of $d(F)/d(\Delta L)$ centred on a point corresponding to 60% of the elongation from 0 N to 250 N of force. At a sampling rate of 20 Hz (Table 3–2), these twenty-one points represented a time period of approximately 1 s. This approach produced one stiffness estimate per cycle and a total of 30 estimates for each specimen.

Final values of K_{CYC} for each specimen were taken as the average of the stiffness estimates from the last five cycles (from $n = 26$ to $n = 30$). Estimates of modulus (E_{CYC}) were obtained by multiplying K_{CYC} values by the ratio of L to CSA for that specimen.

3.1.5 Failure properties

Force-elongation curves were plotted for each specimen using the data collected during failure tests. Estimates of specimen failure stiffness (K_{FAIL}) values were estimated as the slope between two points on the approximately linear portion of the curve from a point beyond the toe-region to the proportional limit. Points were selected by visual inspection of force-elongation plots.

The ultimate tensile properties (F_{UT} and ΔL_{UT}) of specimens were obtained by isolating the maximum values of force and elongation from the failure test data. Estimates of PT modulus (E_{FAIL}) were obtained by multiplying the stiffness estimates with the ratio of L to CSA for that specimen.

3.1.6 Assessment of left-right differences

Left-right pairs of property estimates were assessed in terms of the *absolute* and *relative* difference. Given a pair of property values from a single specimen, for example left

stiffness, K_L, and right stiffness, K_R, it is possible to describe the left-right difference in two ways: as the absolute magnitude of the difference $| K_L - K_R |$ or as the arithmetic difference $(K_L - K_R)$. For the purpose of this analysis, we define the former quantity as the *absolute difference* and the latter quantity as the *relative difference*. The difference, $| K_L - K_R |$, will always be a positive number whereas the sign of the quantity, $(K_L - K_R)$, indicates whether the difference is *biased* in favour of the left or right limb. If $(K_L - K_R)$ is a negative number, then K_R is larger than K_L and the bias is said to favour the right limb (Altman, 1995). The distinction between the absolute and relative difference is not particularly meaningful when a single left-right pair is considered. These two descriptions of left-right difference were chosen in order to provide more information about the average differences between property values in the entire set of eleven left-right pairs.

Each set of left-right pairs of structural property estimates were assessed statistically with the linear correlation coefficient (r) and the paired t-test (equal variance, two tailed). The hypothesis test was formulated as follows. Let P stand for a structural property (e.g., stiffness, K). Then μ_P^L and μ_P^R are the mean values of the left and right groups in the set of estimates of P. The null hypothesis H_0, was:

$$H_0 : \mu_P^L - \mu_P^R = 0 ,$$

The alternative hypothesis, H_α, was:

$$H_\alpha : \mu_P^L - \mu_P^R \neq 0 , (\alpha = 0.05).$$

The statistical analysis was carried out using Excel 8.0 Analysis ToolPak (Microsoft Corporation). The statistical power, $1-\beta$, of each t-test was tested with a *nomogram* (Altman, 1995). Statistical power depends on two factors: the *relevant difference* and the observed *SD* in the differences. In the present study, the magnitude of the relevant difference was chosen, *a priori*, to be 10% of the overall mean value in each set of structural properties. For example, if the overall mean failure stiffness, K_{FAIL}, was 350 N mm^{-1}, then the relevant left-right difference for failure stiffness estimates was set at 35 N mm^{-1}.

One of the primary objectives of the study was to determine whether the properties of a contralateral PT could be substituted for those of the PT of interest, given a matched

pair of PT specimens. This objective was formulated within the context of PT properties as inputs to an analytical model of the cat PF joint. An experimentally observed absolute left-right difference on the order of 10% of the observed mean value was felt to be a reasonable level of agreement between pairs of property estimates in terms of quantifying model inputs.

3.2 *IN SITU* EXPERIMENT

3.2.1 Preparation

All procedures received ethical review and approval from the University of Calgary Animal Research and Ethics Committee. The experiment to study the *in situ* mechanical behaviour of the PT was conducted on a skeletally mature male cat (5.5 kg). The right knee joint of the animal was X-rayed prior to the experiment. Skeletal maturity was indicated by closure of the epiphyseal growth plates of the distal femur and proximal tibia as observed in the X-rays. The experimental set-up was based on that described by Ronsky et al. (1995).

The animal was kept under deep anaesthesia during the entire experiment. A nerve cuff was surgically implanted on the femoral nerve of the right hind limb (Hoffer, et al., 1990; Herzog, et al., 1995). After the nerve cuff was in position the animal was placed in a hammock. The ilium was fixed between two pins in a rigid steel frame. The femur was also fixed rigidly in the frame between two pins, set laterally and medially, roughly 20 mm proximal to the knee joint. This arrangement allowed for free extension of the tibia. An instrumented restraining bar was put in place to limit the extension of the tibia to a fixed angle of was 75(±10)° with respect to the femur (Figure 3–3).

After the ilium and femur of the animal were secured, the tibial tuberosity, anterior surface of the PT and the patella were surgically exposed. The anterior aspect of the distal pole of the patella and the PT insertion at the tibia were marked with black tissue stain. Three lines were marked on the PT mid-substance with the stain. The most distal and most proximal lines were roughly 15 mm apart. Prior to initiating the stimulation protocol, hydration of exposed knee joint tissues was maintained by covering the knee joint with a gauze pad soaked in PBS solution.

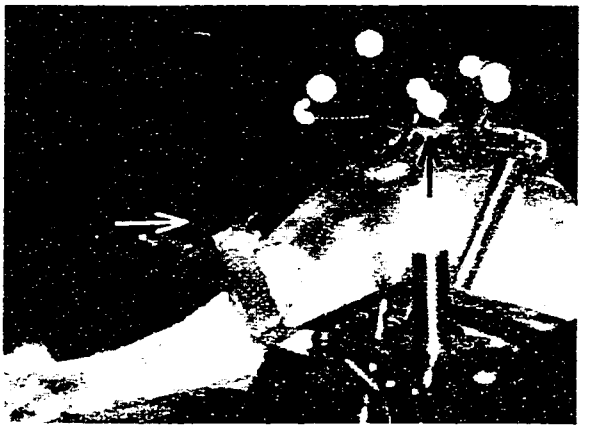

Figure 3–3 Photograph of the right hindlimb prepared for the *in situ* protocol. The restraining bar (white arrow) is positioned to restrict extension of the tibia to 75°. Also visible is the exposed PT (black arrow). The white balls are part of the kinematic marker sets on the tibia and the patella.

3.2.2 Stimulation protocol

Quadriceps contractions were produced by electrical stimulation of the femoral nerve via the implanted nerve cuff. The stimulations were applied in a 500 ms train of 0.1 ms pulses at 100 Hz (Herzog et al., 1992).The stimulation signal was produced by a Grass S8800 Stimulator (Astro-Med Inc., Longueuil, Quebec). The restraining bar was instrumented with strain gauges (half-bridge arrangement measuring bending strain). During contractions of the *quadriceps*, the strength of contractions was determined by monitoring the restraining force voltage signal as the tibia extended against the bar. The stimulation voltage and bridge output signals were recorded using AT-CODAS (Dataq Instruments, Akron, Ohio) sampling at 1000 Hz.

Voltage levels corresponding to a threshold and a maximal *quadriceps* force were determined. The threshold voltage was the lowest voltage which produced a visually detectable response from the *quadriceps* muscles. The maximum voltage was the voltage which produced a maximal tetanic contraction of the *quadriceps* muscles. Voltage levels ranged from roughly 0.1 V (threshold) to 0.9 V (maximum). After these levels were established, the PT was loaded under the action of the *quadriceps* in a series of stimulation

trials over a range of *quadriceps* forces. For purposes of data collection and analysis, each loading condition of the stimulation protocol was designated according the level of *quadriceps* stimulation voltage. Loading condition *one* consisted of stimulation trials at < 10% of maximum level. At this voltage level, the tibia barely extended against the bar producing a weak restraining force signal. Loading conditions *two, three, four* and *five* corresponded to stimulation levels at 20%, 50%, 70% and 100% of the voltage corresponding to the maximum *quadriceps* force.

Throughout the course of the whole stimulation protocol, the exposed tissues of the knee joint were regularly irrigated with PBS solution at two minute intervals. The solution was dripped onto the knee joint, in 1 ml amounts, through a plastic tube attached to a syringe. Muscle stimulation and tissue irrigation were conducted according to a carefully timed procedure. The sequence of these events during each loading condition are summarised in Table 3–4. The *quadriceps* muscles were allowed one minute to recover between successive stimulation trials. The knee joint was irrigated every two minutes immediately following a stimulation.

EVENT	**t = T - 1 min**	**t = T min**	**t = T + 1 min**	**t = T + 2 min**
Irrigate the tissue	no	yes	no	yes
Trigger quadriceps stimulation	yes	yes	yes	yes
Record timing pulse	yes	yes	yes	yes
Record stimulation voltage	yes	yes	yes	yes
Record restraining bar voltage	yes	yes	yes	yes
Collect 2D video	yes	yes	no	no
Collect 3D motion	no	no	yes	yes

Table 3–4 Sequence of events during each loading condition of the stimulation protocol.

3.2.3 Voltage signal acquisition

The muscle stimulator was configured to produce two synchronised signals when it was triggered. The first signal, S1, was a timing pulse (square wave, amplitude 5 V, duration 500 msec). This signal was recorded on Channel 1 of the AT-CODAS system. The second signal, S2, was the stimulation voltage (described above) whose amplitude depended on the loading condition. The stimulation voltage was sent to both Channel 2 of the DAQS and the nerve cuff. The bridge output voltage from the restraining bar was recorded on Channel 3. All of the signals were sampled at 1000 Hz.

3.2.4 PT force and moment arm estimation

At the end of the experiments, the strain gage on the restraining bar was calibrated by suspending weights statically from the bending member. A range of weights was used which duplicated the range of bridge output voltages recorded during stimulation protocol. A calibration curve of voltage (V) versus force (N) was obtained from this procedure. This calibration curve was used to convert the voltage-time data from the bridge on the restraining bar into force-time data.

Following the completion of the stimulation protocol, the 3D motion of the tibia with respect to the femur was measured. It was intended that these data be used to determine the PT moment arm (r_T) and the restraining force moment arm (r_R) about the knee joint centre as quantified by the instantaneous helical axis (IHA) of knee joint motion (Boyd and Ronsky, 1998). The results of this analysis were unavailable at the time of writing. Therefore, the magnitude of the PT moment arm with respect to the knee joint centre of rotation (r_T) was estimated at 10(±1.5) mm (Boyd and Ronsky, 1998). The moment arm of the restraining force (r_R) was measured as the distance from the apex of the patella to the point of application of the restraining force on the tibia. This measurement was made from marker position data collected for the IHA analysis. The restraining force moment arm was found to be to be 100 mm. An uncertainty of ±2.5 mm in r_R was assumed. The tensile force in the PT was calculated from a moment balance using the values of r_T and r_R. (Figure 3–4). If F_T is the force in the PT and F_R is the restraining force, then the relation between F_T and F_R is:

$$r_T \cdot F_T = r_R \cdot F_R . \qquad [7]$$

PT force data were normalised by PT *CSA* estimates (determined from subsequent in vitro tests) to produce estimates of PT stress during *quadriceps* stimulation. This section should explain the analysis (averaging) of the stress-time data.

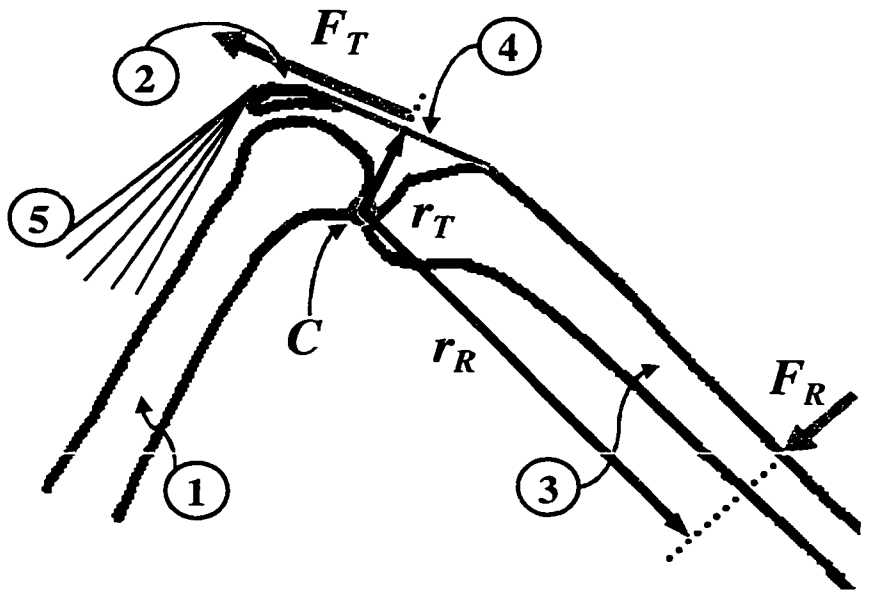

Figure 3–4 Schematic of the 2D model used to estimate PT force.Forces are indicated with grey arrows: PT force (F_T); restraining force (F_R). Moment arms are indicated with black arrows: PT force moment arm (r_T); restraining force moment arm (r_R). Knee joint centre (C); femur (1); patella (2); tibia (3); PT (4); quadriceps (5).

3.3 2D STRAIN ANALYSIS

3.3.1 Video recording and image acquisition

The technique used to quantify surface strain in the PT mid-substance was essentially the same for both the *in vitro* and *in situ* experiments. PT specimens were filmed with a high-speed (200 Hz) video camera and high-speed video recorder (NAC Inc., Japan). Interlacing of the recorded video resulted in an effective frame rate of 100 Hz. The resolution of the camera's image sensor was 320×244 pixels. The camera recorded motion

of the stain lines during the *in vitro* failure tests and during each of the stimulation trials in the *in situ* experiments.

After the completion of the *in vitro* (or *in situ*) force-elongation experiments, video recordings of tissue elongation were captured as digital movie files. Each frame of the digital movie was converted to a TIFF image (320×240, 8-bit, uncompressed PC grayscale). This video data processing was performed using Adobe Premiere 4.2 (Adobe Systems Incorporated, City, State) on a Power MAC (Macintosh Corporation). The digital image files were stored on a CDROM disc.

3.3.2 Collection of edge location data

The relative motions of stain line edges in sequential frames of the video recordings were tracked by analysing the digital images (Figure 3–5). Every second frame was analysed resulting in a sampling rate of 50 fps (20 ms between points). In each frame processed, the centroids of the stains marking the PT insertion at the tibia and the distal pole of the patella were identified. The direction of strain was assumed to be parallel to the line joining the two centroids. This direction was close to the orientation of fibres visible on the tendon surface. Strain was determined over a region between the stain line closest to the tibia and the stain line closest to the patella (Figure 3–5a). The pixel coordinates of the distal edges of these two lines were determined by the application of a 1D edge-detection algorithm (Tabatabai and Mitchell, 1984). Five target-points on the edge of a stain line were manually selected (Figure 3–5b). A fourth order polynomial was fit to the pixel coordinates of this set of target-points. The polynomial was used to define a band or region 15 pixels wide, centred about the target-points, containing the edge of a stain line. The edge detection algorithm was applied to each row of pixels in this band to determine the pixel coordinates of the stain line edge (Figure 3–5c).

3.3.3 Tissue surface strain

The surface of the PT between the edge of the tibial line and the edge of the patellar line was divided into three longitudinal zones corresponding to the lateral, central or medial zones of the PT mid-substance (Figure 3–5d). The mean distance (in pixels) between stain line edges across each zone was used to calculate tissue strain. Each set of images (from a

failure test or a stimulation trial) produced three sets of strain-time data for each failure test. This analysis was carried out with the Image Analysis Toolbox in Matlab5.1 (The MathWorks, Inc., Natick, MA) on an Indigo2 Workstation (Silicon Graphics Inc., Mountain View, CA).

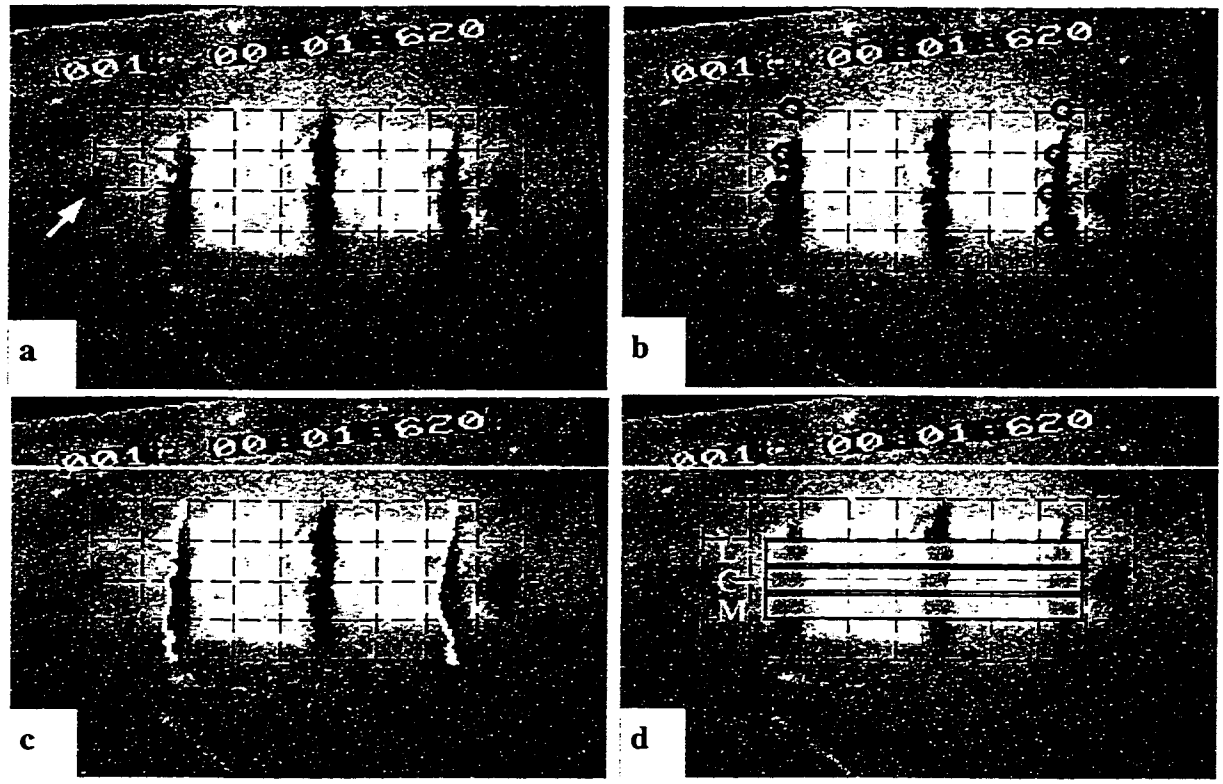

Figure 3–5 Image of PT surface from the *in situ* experiment. This figure illustrates the strain analysis technique applied to one frame of a video recording of a stimulation trial. (a) The PT insertion on the tibia (arrow) and the apex of the patella were marked with tissue stain. A grid centred on these markers was projected on the image. The purpose of the grid was to provide a consistent reference for the selection of target points. (b) Five target points across the stain lines of interest were selected to define the region of the image analysed by the edge-detection algorithm. (c) Calculated edges of the stain lines mapped onto the image of the PT. (d) Lateral (L), central (C) and medial (M) zones of the PT surface.

The tracking of stain line edges produced length values L and L_0 in terms of mean distance in pixels rather than absolute units. For the determination of mid-substance strain in the *in vitro* tests, gauge length, L_0, was taken to be the mean distance between stain line

edges corresponding to a tensile force of 5.5(±1.6) N. In the *in situ* experiments, L_0 was determined from analysis of video recordings of the minimal-force trials. The *quadriceps* force in these trials was less than 10% of the maximal *quadriceps* force. This stimulation level corresponded to a tensile force in the PT of 39(±9) N.

3.4 PT MECHANICAL BEHAVIOUR

3.4.1 Modeling of strain-time data

3.4.1.1 *In vitro* strain-time data

The strain analysis produced three sets of strain-time data for each video recording of a failure test. Data sets were smoothed using a moving average technique to remove outliers. A strain value was considered an outlier if the magnitude of the difference between this value and the mean strain was greater than 1 *SD*. Following the removal of outliers, strain-time data were fit to a cubic spline to produce strain-values as a continuous function of time. The spline fit data were also used to produce estimates of strain-rate in the PT mid-substance. Strain rates were estimated from the slope of a line between the end-points of the strain-time data from the central zone. Analysis was carried out using Matlab 5.1 on a PC (Pentium 133).

3.4.1.2 *In situ* strain-time data

Analysis of strain for the *in situ* experiment produced three sets of strain-time data for each *stimulation trial*. A timing light (LED) was placed in field of view of the high speed video camera. This LED was triggered by the S1 output from the muscle stimulator. Each point in the strain-time record could be matched to a point in the stress-time record to within ±10 ms. Three sets of strain-time data corresponding to the lateral, central and medial zones were grouped by load condition and then averaged. This approach produced three sets of strain-time data for each *load condition* from 20% to 100% of maximum. For each of these load conditions, averaged strain-time data were resampled and smoothed using a GCV-spline routine (Woltring, 1986) running on an Indigo2 Workstation. The purpose of averaging and resampling the strain-time data was to produce a smooth, continuous model of the strain response of the PT tissue. The spline fit data were also used

to produce estimates of strain-rate in the PT mid-substance. Strain rates were estimated by calculating the slope of the linear portion of the ramp region from the resampled strain-time data, using the central zone. Analysis of strain rates was carried out using Matlab 5.1 on a PC (Pentium 133).

3.4.2 Stress-strain response

3.4.2.1 *In vitro* stress-strain analysis

In order to determine the mechanical response of the *in vitro* specimens, the stress-time (load cell output) and mid-substance strain-time (high speed video) data had to be synchronised. The time $t = 0$ s for the strain-time data in each test was determined by identifying the onset of actuator motion from force-elongation data during *in vitro* failure tests. The initial stress in PT specimens was calculated from the force levels at time $t = 0$ s. It was possible to detect the onset of actuator motion in the video recordings to the nearest 10 ms. The time code on the first frame of actuator motion was used to set time zero for the strain-time data. Three sets of stress-strain data were obtained for each *in vitro* failure test. Each set corresponded to one of the designated zones in the PT mid-substance.

The stress-strain response was evaluated from the onset of actuator motion ($t = 0$ s) to the point at which failure of tendon fibres could be observed in the digital images from video recordings. It was assumed that the tensile stress in the PT specimens was uniformly distributed throughout their *CSA*s until this point. Elastic modulus values based on mid-substance strain measurements (E_{MS}) were approximated from the slope of the stress-strain curve. Stress-strain analysis was carried out using Matlab 5.1 on a PC (Pentium 133).

3.4.2.2 *In situ* stress-strain analysis

Averaging of the stress data produced four sets representing the stress response of the PT in each of the four load conditions from 20% to 100% of maximum. These were combined with the resampled mean strain-time responses from the central zone to produce a model of the *in situ* stress-strain behaviour of the PT. Stress-strain data from the ramp region was used to characterise the linear elastic modulus of the PT mid-substance. Stress-strain analysis was carried out using Matlab 5.1 on a PC (Pentium 133).

4 RESULTS

4.1 *IN VITRO EXPERIMENTS*

4.1.1 Biomechanical properties of the PPTC

4.1.1.1 Cross sectional area and initial length

Measurements of tendon *CSA*s were highly repeatable (Table 4–1). The mean standard deviation (*SD*) of three successive measurements of a single specimen was 0.30 mm^2. This represents approximately 3% of the left and right mean *CSA* values of 11.1 mm^2 and 11.4 mm^2. Estimates of tendon initial length were measured with an accuracy of ±0.5 mm (Table 4–1). This represents 3% of the left and right mean *L* values of 16.9 mm and 17.3 mm.

	CSA (mm^2)		*L* (mm)	
Pair	**Left**	**Right**	**Left**	**Right**
1	13.5	15.7	21.5	23.7
2	16.5	17.7	21.2	21.1
3	13.2	11.0	17.8	17.6
4	9.6	10.4	14.0	15.5
5	10.9	9.3	13.0	14.2
6	10.7	8.9	14.5	14.5
7	11.4	9.0	15.2	15.0
8	8.9	9.6	15.7	15.3
9	13.7	16.6	17.0	17.0
10	9.3	9.4	17.5	19.0
11	9.6	9.8	18.0	17.0
12	8.5	9.0	17.0	18.0

Table 4–1 Specimen cross-sectional area and initial length measurements.

4.1.1.2 Characteristics of cyclic response

The response of a single specimen can be used to illustrate the characteristic features of the cyclic force-elongation behaviour. Specimens exhibited a creep response to cyclic loading typical of soft connective tissues (Figure 4–1). The total cyclic creep (difference in elongation at peak load between cycle $n = 1$ and $n = 30$) was 0.42 mm for the selected specimen. More than half of the creep, 0.28 mm, occurred within the first ten cycles. During the loading portion of cycle $n = 1$, the specimen appeared to stretch from 0 mm (at 0 N of force) to approximately 2.4 mm (at 250 N of force). In cycle $n = 2$, the elongation from 0 N to 250 N was 1.2 mm. The amount of elongation in subsequent cycles was consistent with the elongation in the second cycle. Values of loading-energy, U, for each cycle exhibited a pattern that is consistent with the observed behaviour of PT specimens in cyclic loading. There was a large difference (121.1 J) in the values of U between cycles $n = 1$ and $n = 2$. The loading energy response of the specimen became more repeatable as the number of cycles increased. In the last five cycles of the test ($n = 26$ to 30), the mean loading-energy value is 108.9 (±0.9) J (Figure 4–2).

Observations of specimens made during the experiments can explain the large amount of elongation of the first cycle. During the first cycle of loading to 250 N, the patellae of mounted specimens were observed to slip upwards in the clamp until becoming firmly seated against the sliding block (Figure 3–1). It is speculated that this "self-adjustment" in position of the mounted PPTC specimens results in the lower force-rate and excessive elongation seen in the first cycle (Figures 4–1 and 4–2).

This stability, characterised by a repeatable response between consecutive cycles as n approaches 30, was not quantified statistically. However, analyses of the loading-energy data for each specimen demonstrated extremely consistent results. Calculation of specimen K_{CYC} values (as the average of the stiffness estimates from cycles $n = 26$ to $n = 30$) was based on the observed stability of the PPTCs' responses.

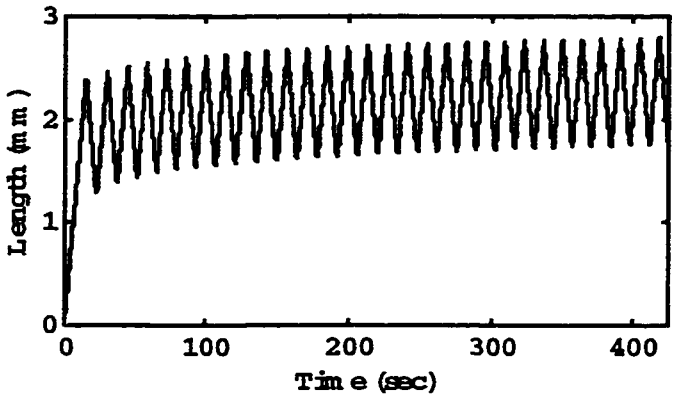

Figure 4–1 Typical specimen creep response in cyclic loading.

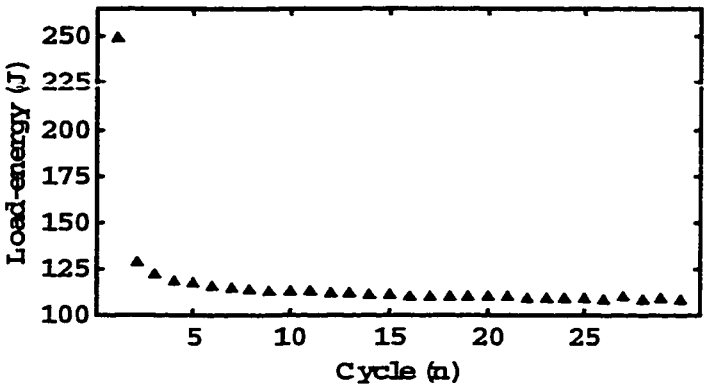

Figure 4–2 Loading-energy versus cycle number for a typical specimen.

4.1.1.3 Characteristics of failure response

Specimen 9 (Table 3–1) was excluded from the analysis because the right patella slipped out of the clamp during the failure test. Specimens exhibited a non-linear response which could be divided into the four regions that characterise the behaviour of soft connective tissue specimens (Figure 4–3). For the specimen shown, the limits of the toe-region, elastic-region, and inelastic-regions have been marked. These points were identified by visual inspection of the force-elongation curves. The mean force values for

the toe-region and elastic-region limits (left specimens) were 41(±15) N and 452(±77) N, respectively (Table 4–2). For the right specimens, force values were 45(±14) N (toe-region limit) and 449(±108) N (elastic-region limit) (Table 4–2a). The range of stress in the elastic region, for the left specimens, based on a *CSA* of 11.1(±2.4) mm^2, was from 4(±2) MPa to 40(±11) MPa (Table 4–2b). The equivalent range for the right specimens was 4(±2) MPa to 40(±15) MPa, based on a *CSA* of 11.4 mm^2. The mean elongation values for the toe-region and elastic-region limits (left specimens) were 0.32(±0.14) mm and 1.68(±0.16) mm, respectively (Table 4–3). For the right specimens, elongation values were 0.34(±0.07) mm (toe-region limit) and 1.69(±0.44) mm (linear-region limit) (Table 4–3). The mean elongation over the inelastic region was 3.00(±1.58) mm (lefts) and 3.06(±1.59) mm (rights).

No mid-substance failures were observed. All of the failures were characterised as tendon avulsions from the patella. Examination of ruptured specimens after each test, revealed varying amounts of patellar tissue torn away from the ruptured specimens, from small pieces of the insertion tissue to larger pieces of bone.

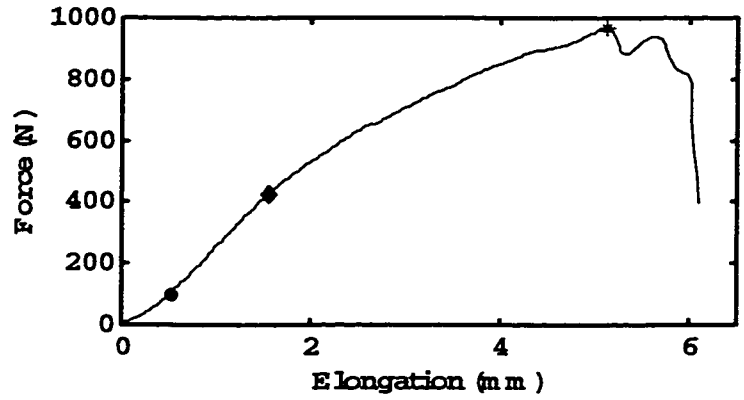

Figure 4–3 Force-elongation response of a typical specimen in failure. Toe-region limit (•); elastic-region limit (♦); ultimate force and elongation (*).

a	Force (N)					
Pair	Lefts			Rights		
	Toe	Elastic	Inelastic	Toe	Elastic	Inelastic
1	61	303	657	18	405	678
2	32	474	1174	39	709	1000
3	33	447	707	32	371	835
4	47	558	871	47	508	828
5	10	393	695	47	313	770
6	37	566	811	34	518	802
7	50	523	907	47	453	828
8	49	425	1189	57	401	1219
10	42	413	813	45	455	821
11	29	421	969	61	337	892
12	63	450	871	66	468	805
Mean	41	452	878	45	449	862
SD	15	77	177	14	108	142

b	Mean stress (MPa)					
	Lefts			Rights		
	Toe	Elastic	Inelastic	Toe	Elastic	Inelastic
Stress	4	40	78	4	40	76
Error	2	11	23	2	15	25

Table 4–2 Boundary points of the failure response. (a) Force values shown mark the limits of the toe-region, elastic-region and inelastic-region. (b) Stresses listed are based on mean force and *CSA*.

Elongation (mm)						
Pair	Lefts			Rights		
	Toe	Elastic	Inelastic	Toe	Elastic	Inelastic
1	0.59	1.73	4.85	0.29	1.99	8.72
2	0.31	1.80	8.25	0.35	2.78	5.48
3	0.30	1.81	4.68	0.30	1.49	4.29
4	0.36	1.87	3.49	0.35	1.80	3.48
5	0.04	1.52	3.66	0.21	1.12	4.49
6	0.24	1.88	4.02	0.27	1.69	3.87
7	0.40	1.60	3.01	0.36	1.52	3.23
8	0.34	1.47	6.75	0.36	1.35	5.94
10	0.30	1.48	3.47	0.38	1.86	4.49
11	0.21	1.56	5.15	0.43	1.32	4.33
12	0.48	1.71	4.21	0.42	1.73	3.98
Mean	0.32	1.68	4.68	0.34	1.69	4.75
SD	0.14	0.16	1.57	0.07	0.44	1.53

Table 4–3 Boundary points of the failure response. (a) Elongation values shown mark the limits of the toe-region, elastic-region and inelastic-region.

4.1.1.4 Range and variation in structural properties

It was found that the range and variation in property value estimates of the left specimens was representative of the property value estimates of the right specimens (Table 4–4a,b). For the left-specimens, the mean K_{CYC} was estimated to be 306 (±45) N·mm^{-1} with a range of values from 221 to 370 N·mm^{-1}. The mean value for K_{FAIL} was 322 (±42) N·mm^{-1}, with values ranging from 235 to 384 N·mm^{-1}. E_{CYC} was estimated to be 473 (±94) MPa with a range of values from 353 to 627 MPa. The mean value for E_{FAIL} was 500 (±114) MPa, with values ranging from 375 to 672 MPa. Considering the ultimate tensile property value estimates of the left specimens, F_{UT} was estimated to be 878 (±117) N with

a range of values from 657 to 1189 N. The mean value for ΔL_{UT} was 4.7 (±1.6) mm, with values ranging from 3.0 to 8.3 mm (Table 4–4a,b).

By expressing the standard deviations as a percentage of the means, it was possible to compare the relative amount of variation in property value estimates (Table 4–4a). For the left K_{CYC} estimates, the *SD* of 45 N·mm^{-1} represents 15% of the mean. The corresponding proportion for the K_{FAIL} estimates is 13%. The elastic modulus values show a trend toward slightly higher levels of variability. The ultimate tensile properties of the specimens showed larger amounts of variation than the linear elastic properties. For F_{UT} estimates, the *SD* of 177 N represented 20% of the mean. The corresponding proportion for ΔL_{UT} estimates was 34% (Table 4–4a).

a

PROPERTY		MEAN (Lefts)	SD (Lefts)	SD : Mean (%)	MEAN (Rights)	SD (Rights)	SD : Mean (%)
K_{CYC}	(N/mm)	306	45	15	294	36	12
K_{FAIL}	(N/mm)	322	42	13	319	44	14
F_{UT}	(N)	878	177	20	862	142	16
ΔL_{UT}	(mm)	4.7	1.6	34	4.8	1.5	31

b

PROPERTY		MIN (Lefts)	MAX (Lefts)	Range	MIN (Rights)	MAX (Rights)	Range
K_{CYC}	(N/mm)	221	370	148	219	348	129
K_{FAIL}	(N/mm)	235	384	150	236	377	141
F_{UT}	(N)	657	1189	532	678	1219	540
ΔL_{UT}	(mm)	3.0	8.3	5.2	3.2	8.7	5.5

Table 4–4 Structural properties of the PPTC. (a) Mean and *SD* for left and right groups (*SD* also reported as % of the mean). (b) Range of structural property estimates for left and right groups.

4.1.2 Left-right variability

4.1.2.1 Qualitative assessment of left-right differences

Mean values from the left and right groups of structural property estimates were found to be remarkably similar (Table 4–4). When the results were compared on the basis of individual pairs, larger variations in left-right differences were apparent. Absolute left-right differences in K_{CYC} values ranged from 3 N mm^{-1} to 45 N mm^{-1} (Figure 4–4a). The range in K_{FAIL} differences was slightly larger, from 2 N mm^{-1} to 50 N mm^{-1} (Figure 4–4b). Left-right differences in F_{UT} estimates ranged from 8 N to 174 N (Figure 4–4c). Left-right differences in ΔL_{UT} estimates ranged from 0 mm to 3.9 mm (Figure 4–4d). ΔL_{UT} estimates demonstrated the largest amount left-right variation relative to the overall range in those values.

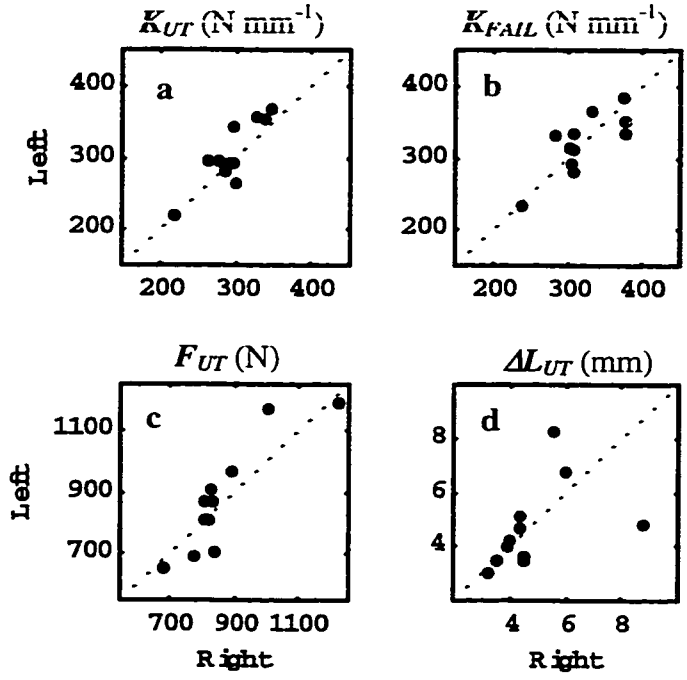

Figure 4–4 Distribution of left and right structural property estimates. Each point represents a specimen pair with the property estimates plotted left versus right. A solid line represents the equality, *left* = *right*: (a) stiffness in failure; (b) stiffness in cycling; (c) ultimated tensile force; (d) ultimate elongation.

Mean absolute left-right differences in linear elastic properties were 20 (±15) N·mm^{-1} for K_{CYC} and 22 (±16) N·mm^{-1} for K_{FAIL}. Mean absolute left-right differences in ultimate tensile properties were 64 (±51) N for F_{UT} and 1.0 (±1.2) mm for ΔL_{UT} (Table 4–5a). Differences in K_{CYC}, K_{FAIL}, F_{UT}, ΔL_{UT}, represented 7 %, 7 %, 7 %, and 21 % of their mean structural property estimates (Table 4–5a).

The average left to right biases in PPTC property values was consistently low for all of the structural properties of interest (Table 4–5b). Mean relative differences in linear elastic properties were 12 (±22) N·mm^{-1} for K_{CYC} and 3 (±28) N·mm^{-1} for K_{FAIL}. Mean (*SD*) relative differences in ultimate tensile properties were 17 (±83) N for F_{UT} and -0.1 (±1.6) mm for ΔL_{UT}. As a proportion of the mean structural property estimates for left specimens, relative differences represented 4 %, 1 %, 2 % and 2 % for K_{CYC}, K_{FAIL}, F_{UT}, and ΔL_{UT}, respectively (Table 4–5b).

a

PROPERTY		Mean Absolute Difference	*SD* in Relative Difference	Proportional Difference (%)
K_{CYC}	(N mm^{-1})	20	15	6
K_{FAIL}	(N mm^{-1})	22	16	7
F_{UT}	(N)	64	51	7
ΔL_{UT}	(mm)	1.0	1.2	22

b

PROPERTY		Mean Relative Difference	*SD* in Relative Difference	Proportional Difference (%)
K_{CYC}	(N mm^{-1})	12	22	4
K_{FAIL}	(N mm^{-1})	3	28	1
F_{UT}	(N)	17	83	2
ΔL_{UT}	(mm)	-0.1	1.6	-1

Table 4–5 (a) Mean (and *SD*) in absolute left-right differences for structural property values. (b) Mean (and *SD*) in relative differences and for structural property values.

4.1.2.2 Statistical assessment of left-right differences

The correlation coefficients obtained for the linear elastic properties were high, with $r = 0.87$ for K_{CYC} and $r = 0.81$ for K_{FAIL}. Comparison of left-right pairs of F_{UT} and stress showed a high correlation with $r = 0.89$. Ultimate elongation data demonstrated lower overall correlation between left and right groups, with $r = 0.45$ (Table 4–6).

The results from the two sample T-tests applied to the left-right data sets revealed no significant differences for any of the structural properties of interest (Table 4–6). For the three structural properties, K_{CYC}, K_{FAIL} and F_{UT}, the power ($1-\beta$) was larger than 0.8. For the set of left-right ΔL_{UT} estimates, the power was low at 0.15. This was due to the large *SD* in the relative difference (1.6 mm) compared to the relevant difference (0.48 mm) (Table 4–7).

Property	**Correlation coefficient, *r***	**T-Test (*P-value*)**
K_{CYC}	0.87	0.48
K_{FAIL}	0.81	0.88
F_{UT}	0.89	0.81
Δ_{UT}	0.45	0.92

Table 4–6 Results of the statistical comparison. Correlation coefficients, *r*, between left and right groups of structural property estimates. P-values from the paired *t*-tests.

Property	**Mean absolute left-right diff.**	***SD* in relative left-right diff.**	$1-\beta$	**Relevant difference**
K_{CYC}	20 N mm^{-1}	22 N mm^{-1}	>0.80	30 N mm^{-1}
K_{FAIL}	22 N mm^{-1}	28 N mm^{-1}	>0.80	32 N mm^{-1}
F_{UT}	64 N	83 N	>0.80	87 N
ΔL_{UT}	1.0 mm	1.6 mm	0.15	0.48 mm

Table 4–7 Evaluation of the paired *t*-tests applied to left and right groups of structural property estimates.

4.1.3 Mechanical response in high rate failure tests

4.1.3.1 Precision and accuracy

A repeatability analysis of the edge detection technique was performed in order to estimate the precision in the measurements of distance between stain line edges. A single operator conducted four repeated analyses of two frames from one failure test. The *SD*s in the distance measurements were 0.47 pxl, 0.24 pxl and 0.13 pxl for the lateral, central and medial zones, respectively. The mean *SD* was 0.28 pxl. The resolution of the images used in the repeatability test was 16.6 pxl mm^{-1}. The resolution of images was not constant from test to test due to differences in camera position. The average resolution was roughly 15.6 pxl mm^{-1}.

As with resolution, the L_0 values in the lateral, central and medial zones, determined in the strain analysis, varied from test to test. The mean L_0 values for the three zones were 116.93(±15.71) pxl, 116.96(±15.24) pxl and 116.31(±14.46) pxl, respectively. The average L_0 in pixels was 116.74 corresponding to a distance of 7.5 mm. The accuracy of the *in vitro* surface strain measurements based on a precision of 0.28 pxl and a gauge length of 116.74 pxl was estimated at 0.24%. This is base level accuracy and does not include systematic sources of error discussed in Section 2.4.5.

4.1.3.2 PT strain response

Of the twenty-two specimens (eleven pairs) for which property data were collected in the *in vitro* study, only ten specimens provided a video record which was suitable for analysis with the strain measurement technique. There were four main reasons why less than half of the video records could be analysed: smudging of stain lines; excessive glare; poor visibility of stain lines and poor resolution. One recorded specimen failure was accidentally erased. Two records were eliminated due to smudging of stain lines. In the application of the stain lines to specimens, the ideal is to produce straight, even bands of stain. The edge detection algorithm responded poorly to images in which the stain lines were discontinuous or very irregular. One record was eliminated due to excessive glare from the specimen's surface. The intense lighting required combined with the moisture on the tendon resulted in light being reflected from the surface of PT specimens. This glare

interfered with the ability of the edge detection algorithm to identify the edges of the stain lines in images from some of the video recordings. Two records were eliminated because stain lines were obscured by the time display. Six records were eliminated because of insufficient resolution. These tests were performed without adequate magnification of the specimen image. The resolution of the images was too low for the strain analysis to detect deformation in the surface fibres of the specimens.

The ten specimens analysed with the strain measurement technique were divided into two groups. A specimen was assigned to Group 1 if it demonstrated a uniform strain response across the three zones. A specimen was assigned to Group 2 if it demonstrated a non-uniform strain response across the three zones or a lack of measurable response in at least one of the zones. For example, Specimen 8–L was assigned to Group 1 (Table 4–8). As the stress increased to 40 MPa, the strain in all three zones of the PT mid-substance rose from 0 % strain to 3 % strain (Figure 4–5). Specimen 7–L was assigned to Group 2 (Table–8). As the stress rose to 40 MPa, the lateral region exhibited a linear strain response similar to that seen in Specimen 8–L (roughly 2.5% strain at 40 MPa). The strain response in the central zone was barely detectable (0.5% strain at 40 MPa). In the medial zone the strain response was very irregular, with a final strain of roughly 1.6% strain (Figure 4–6).

The results of the *in vitro* study suggested that 40 N (toe-region limit) and 450 N (elastic-region limit) bound the elastic region of the structural response of PPTC specimens. These force levels were equivalent to stresses of roughly 4 MPa and 40 MPa (Table 4–2). Therefore, the zonal variation in the PT strain response was examined at stress levels in the elastic-region, corresponding to 5 MPa and 30 MPa (Table 4–8).

In both Group 1 and Group 2, the inter-specimen variation in strain was relatively high compared to the average lateral to medial variation in strain. Specimens from Group 2 demonstrated particularly high inter-specimen variation. This is reflected in the non-uniform lateral to medial strain response of Group 2 specimens.

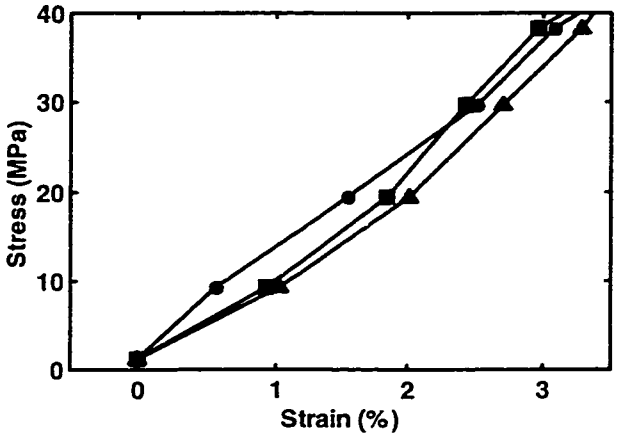

Figure 4–5 Stress versus strain. The uniform stress-strain response of Specimen 8–L is shown. Lateral zone (●); central zone (▲); medial zone (■).

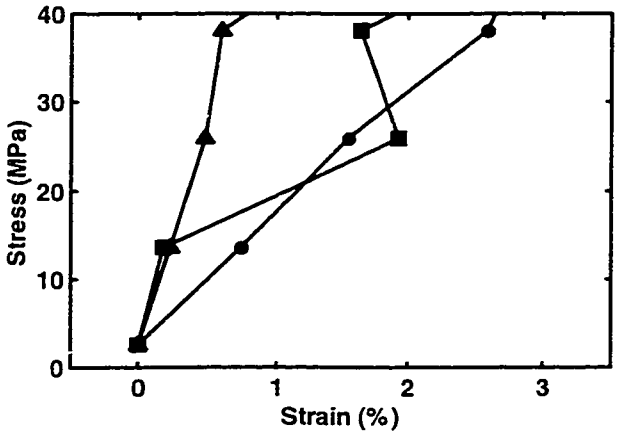

Figure 4–6 Stress versus strain. The non-uniform stress-strain response of Specimen 7–L is shown. Lateral zone (●); central zone (▲); medial zone (■).

GROUP 1

	Strain at 5 MPa				Strain at 30 MPa			
Spec.	**Lateral**	**Central**	**Medial**	**SD**	**Lateral**	**Central**	**Medial**	**SD**
2L	1.21	0.09	1.13	0.62	2.38	2.15	2.66	0.26
5L	0.39	0.27	0.33	0.06	1.93	1.74	2.09	0.17
8L	0.23	0.51	0.46	0.15	2.53	2.72	2.44	0.14
11L	0.21	0.21	0.22	0.01	2.65	2.37	2.09	0.28
12L	0.29	0.24	0.19	0.05	2.27	2.31	2.36	0.05
AV	*0.47*	*0.27*	*0.47*		*2.35*	*2.26*	*2.33*	
SD	*0.42*	*0.15*	*0.39*		*0.28*	*0.36*	*0.24*	

GROUP 2

	Strain at 5 MPa				Strain at 30 MPa			
Spec.	**Lateral**	**Central**	**Medial**	**SD**	**Lateral**	**Central**	**Medial**	**SD**
7L	0.20	0.02	-0.32	0.27	1.90	0.45	1.86	0.82
7R	0.67	0.08	-0.14	0.42	2.93	1.24	0.24	1.36
10L	0.09	-0.11	1.72	1.00	0.91	0.24	2.94	1.40
10R	0.61	0.08	1.52	0.73	2.57	0.58	3.09	1.33
11R	0.06	0.69	1.31	0.63	1.80	1.84	1.53	0.17
AV	*0.32*	*0.15*	*0.82*		*2.02*	*0.87*	*1.93*	
SD	*0.29*	*0.31*	*0.97*		*0.78*	*0.66*	*1.16*	

Table 4–8 Strain variation in the elastic region. The table is divided into Group 1 and Group 2 specimens. The *lateral to medial* variation in strain is presented for each specimen by row at 5 MPa and 30 MPa. The mean inter-specimen strain and the inter-specimen variation are presented by column at 5 MPa and 30 MPa.

4.1.3.3 Elastic modulus

Elastic modulus estimates are based on the average strain-time record of three zones combined (Table 4–8). For Group 1, the mid-substance modulus values were 2.5 times larger than the grip-to-grip to modulus values. For Group 2, the mid-substance modulus values were 3.9 times larger than the grip-to-grip to modulus values.

GROUP 1 Spec.	Average Strain 5 MPa	Average Strain 30 MPa	E_{MS} (MPa)	E_{G2G} (MPa)
2L	0.81	2.40	1577	405
5L	0.33	1.92	1575	398
8L	0.40	2.56	1157	619
11L	0.21	2.37	1160	586
12L	0.24	2.31	1207	672
GROUP 2 Spec.	**Average Strain 5 MPa**	**Average Strain 30 MPa**	E_{MS} (MPa)	E_{G2G} (MPa)
7L	-0.03	1.40	1739	513
7R	0.20	1.47	1972	627
10L	0.56	1.36	3126	626
10R	0.74	2.08	1858	571
11R	0.69	1.72	2414	536

Table 4–9 Average mid-substance strain at 5 and 30 MPa and elastic modulus estimates.

4.2 *IN SITU* EXPERIMENT

4.2.1 Stress response

4.2.1.1 PT stress-time response *in situ*

The recorded voltage signal from the instrumented restraining bar was divided into two regions: a *ramp* region and a *plateau* region (Figure 4–7). The plateau region of the restraining force signal was assumed to correspond to an isometric contraction of the quadriceps muscles. Restraining voltage data were converted to force-time data and the mean plateau region force (peak force) was determined.

For each of the five loading conditions, the mean plateau region restraining force values were highly repeatable in subsequent trials. Values ranged from 3.9(±0.9) N to 53.0(±0.1) N. The highest variation occurred in the 70 % load condition, with a mean and *SD* of 28.31 (±1.82).

Throughout the protocol, the stimulation voltage levels were adjusted in an attempt to maintain a constant restraining voltage output for each loading condition. Variations in the mean peak restraining force measurements were observed, in spite of this "tuning" of the stimulation voltage. In particular, trends in mean peak force measurements for the 20 % and 70 % loading conditions were observed (Figure 4–8). At 20 % of maximal, an increase in restraining force from 21.2 N to 24.2 N was observed over 12 trials. For the loading condition corresponding to 70 % of maximal, a decrease in restraining force from 44.5 N to 34.3 N over 20 stimulation trials was observed. These patterns of change in restraining force were due to the changing response of the *quadriceps* to the applied stimulation voltage.

Mean peak stress values ranged from 2.93(±0.69) MPa to 39.55(±0.07) MPa (Table 4–10). Data from all of the stimulation trials for which strain measurements were made were averaged to produce single stress-time curves for each of the five loading conditions (Figure 4–9).

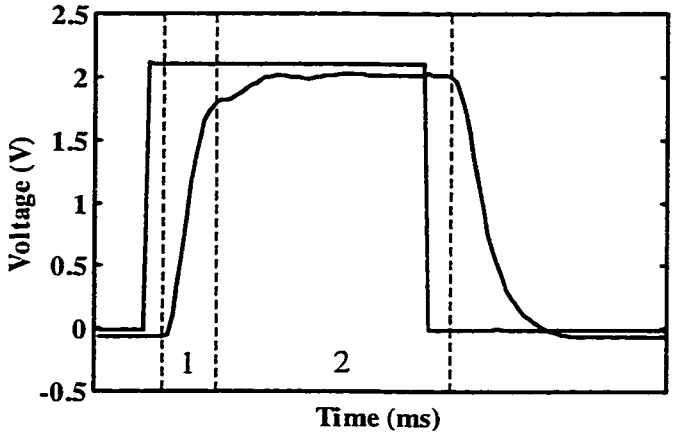

Figure 4–7 Voltage data.. Data shown are from a stimulation trial at the 50% loading condition. The synchronisation pulse (square wave) and the voltage output from the restraining bar are shown. The duration of the synch-pulse is 500 ms. Ramp region (1); plateau region (2).

Stimulation level (% of max)	n	Stress [MPa] Mean (SD)
<10%	8	2.93(0.69)
20%	12	16.74 (0.89)
50%	17	24.55 (0.86)
70%	20	28.31 (1.82)
100%	2	39.55 (0.07)

Table 4–10 Mean plateau region stress corresponding to each loading condition.

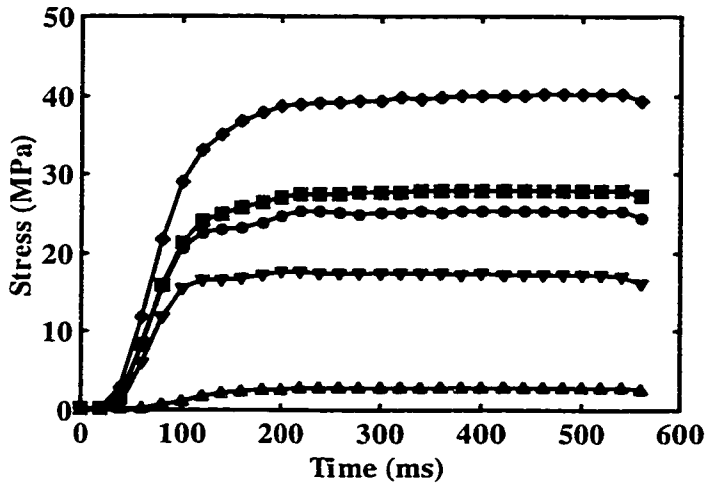

Figure 4–8 The mean stress-time response for each of the five loading conditions. Features of the stress response that were described in the previous section can be observed, i.e., the ramp region and peak (or plateau) region. <10% loading condition (▲); 20% loading condition (▼); 50% loading condition (◆); 70% loading condition (■); 100% loading condition (●).

4.2.2 Strain response

4.2.2.1 Characteristics of the strain-time data

Tissue gauge lengths were taken from the stain line distance data from eight trials (Table 4–11). The mean gauge lengths (L_0 values) in the lateral, central and medial zones were 141.32(±0.97) pxl, 140.28(±0.66) pxl and 133.93(±0.67) pxl, respectively. The variability in L_0 measurements within each trial was less than the inter-trial variability with the exception of the medial zone measurements. The configuration of the stain lines applied to the tissue was such that the medial zone L_0 values were the shortest and had the least precision. The highest precision was obtained in the central zone measurements. Precision estimates (based on the largest per trial *SD*) were 0.34 %, 0.25 % and 0.55 % of the lateral, central and medial L_0 values, respectively (Table 4–11).

The precision values were used to obtain estimates of the minimum error in elongation (ΔL) and strain (ε) measurements during the experiment. Estimated errors in strain values in the lateral, central and medial zones, based on precision estimates were 0.4 % strain, 0.3 % strain and 0.6 % strain, respectively (Table 4–12). The combination of magnification and object distance (lens to tissue) during the experiment was such that a resolution of approximately 10 pxl·mm^{-1} was obtained.

	Lateral zone	**Central zone**	**Medial zone**
Mean (SD) L_0 [pxl] (n = 8)	141.32 (0.97)	140.28 (0.66)	133.93 (0.67)
Largest SD (n = 20)	0.52	0.35	0.74
Approx. length [mm]	14	14	13

Table 4–11 Mean value of tissue gauge lengths (L_0) in each zone. Lengths are shown in units of pixels and approximate lengths in mm.

	Lateral zone	Central zone	Medial zone
Error in ΔL [pxl]	0.52	0.35	0.74
Error in ε [%] *	0.4	0.3	0.6

Table 4–12 Estimated error in strain measurements in each zone. These are base errors and do not include systematic sources of error discussed in Section 2.4.5.

4.2.2.2 PT strain-time response *in situ*

Mean peak strain estimates were calculated from the plateau regions of the averaged strain-time responses. Two distinctive features were observed in the mean peak strain estimates. First, the strain increased with increasing stress. Second, the strain response in the medial zone was low compared to the lateral and central zones. The strain

in the lateral region increased 2.2 times and the strain in the central region increased 2.7 times as the stress in the PT increased from 16.74 to 39.55 MPa (2.3 times). Medial region strain was less responsive to the increase in PT stress. Strain in the medial zone was consistently less than 40 % of the lateral and central zone values across the four load conditions from 20 to 100 % of maximum. The variation in mean peak strains was high compared to the magnitude of the measurements. For example, at the third loading condition (50 % of maximum) strain estimates were 1.4±0.6 %, 1.4±0.5 % and 0.3±0.6 % in the lateral, central and medial regions, respectively. The largest amount of variation was observed in the medial region in the second loading condition, at ±1.2 %. Values of mean peak strain in the central zone had the smallest amounts of variation in each of the four load conditions from 20 % to 100 % (Table 4–13).

Stimulation level (% of max)	n	Stress [MPa] Mean (SD)	Lateral zone strain [%] Mean (SD)	Central zone strain [%] Mean (SD)	Medial zone strain [%] Mean (SD)
<10%	8	2.93(0.69)			
20%	12	16.74 (0.89)	1.0 (0.7)	1.0 (0.5)	0.2 (1.2)
50%	17	24.55 (0.86)	1.4 (0.6)	1.4 (0.5)	0.3 (0.6)
70%	20	28.31 (1.82)	1.4 (0.7)	1.8 (0.6)	0.3 (0.7)
100%	2	39.55 (0.07)	2.2 (0.2)	2.7 (0.2)	0.8 (0.3)

Table 4–13 Mean peak stress and corresponding mean peak strain in the lateral, central and medial regions.

In examining the mean peak strain values versus trial number, it is more difficult to extract a consistent pattern (Figure 4–10a,b). There was no trend relating mean peak strain to trial number for any of the four loading conditions from 20 to 100 % of maximal. The range of zonal strain values across trials was large relative to mean peak values (Table 4–13). The largest range in peak strain estimates was obtained in the medial region at 20 % load condition. This is reflected in the large scatter in the strain values (Figure 4–10a) and

the large *SD* in mean peak strains (Table 4–13). The central zone strain consistently demonstrated the smallest range from minimum to maximum values for all of the loading conditions. For example, at the 70 % loading condition, the central zone strain ranged from

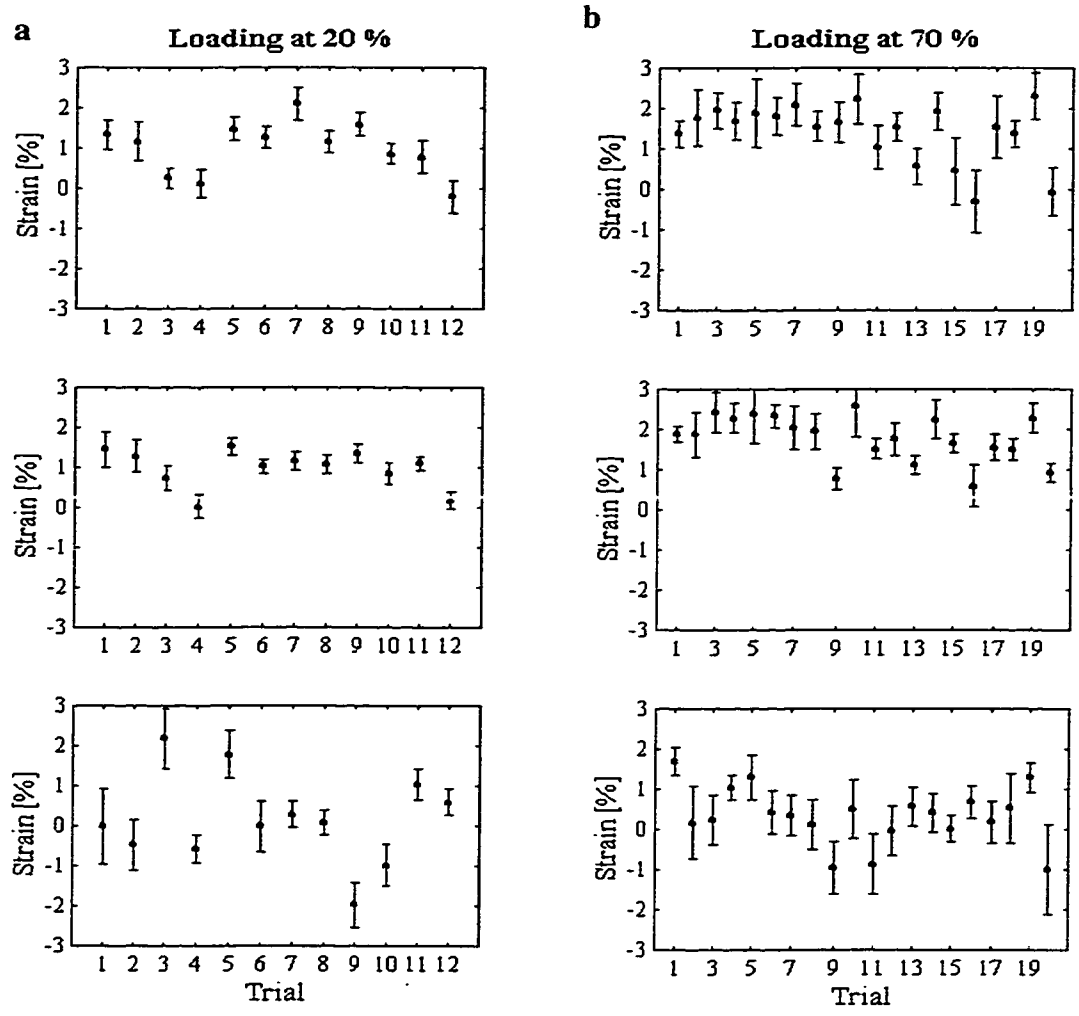

0.6 to 2.6 % compared to –0.3 to 2.3 % and –1.0 to 1.7 % in the lateral and medial zones.

Figure 4–9 Mean peak strain versus trial number. Data for the lateral, central and medial zones are shown from top to bottom. (a) 20% loading condition; (b) 70% loading condition.

Averaging the strain-time responses was found to smooth the large variability observed in the responses from individual trials (Figure 4–11a). Sets of averaged

strain-time data were modelled well with the spline-fitting program that was used (Figure 4–11b). The peak region strains in the spline-modelled data were consistent with the values of mean peak strain obtained from the "raw" strain-time data sets (Table 4–13). The smoothed sets of strain-time data were used to estimate the average of the strain-rate of the PT tissue. Strain rates were found to increase as the stimulation level was increased during the experiment (Table 4–14).

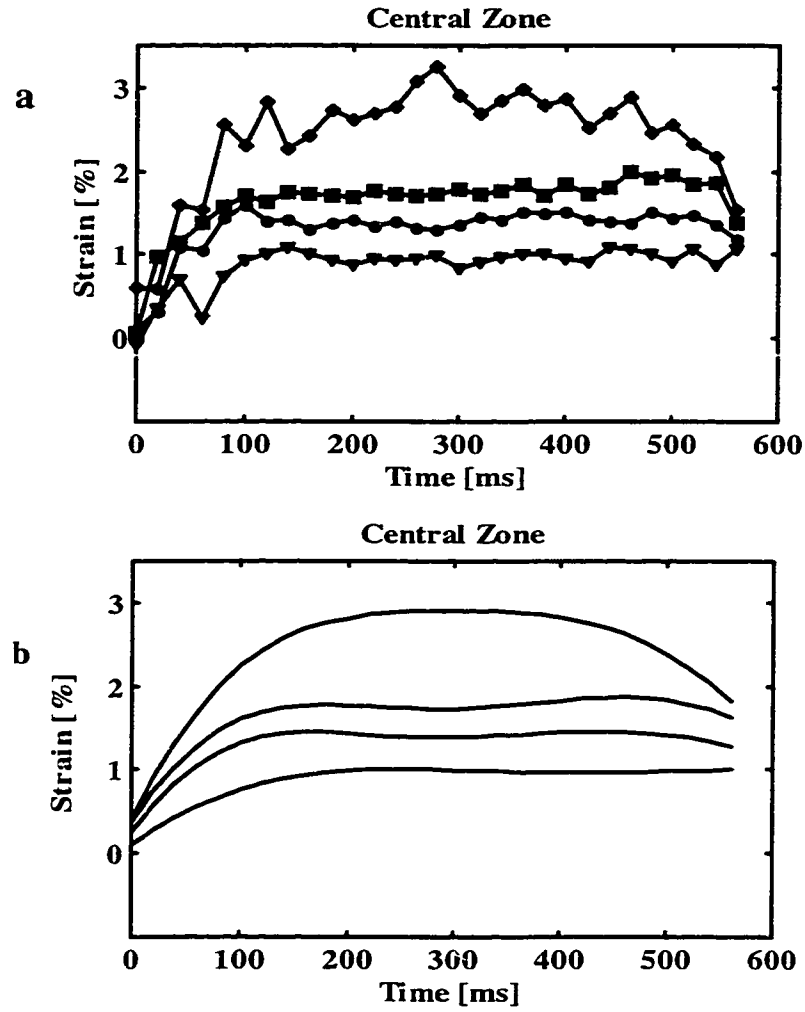

Figure 4–10 Strain response in the central zone. (a) Strain-time response averaged from all stimulation trials; (b) average strain-time response following smoothing with the spline fitting program.

Strain rate	
Load condition (% of max)	**$\%\cdot s^{-1}$**
20 %	5
50 %	10
70 %	13
100 %	19

Table 4–14 Estimated strain rates in the four highest loading conditions from the central zone strain response.

4.2.3 The stress-strain response

The *in situ* elastic modulus of the PT was calculated based on mean peak values of stress and strain (Table 4–13). Six modulus estimates were calculated over six different ranges of stress and strain values. The mean *in situ* modulus based on the <10% loading condition was less than the *in situ* modulus based on the 20% loading condition. The difference was within the variability observed in the modulus estimates (Table 4–15).

Range	*E* (MPa)	Range	*E* (MPa)
<10% to 50%	1544	*20% to 50%*	1953
<10% to 70%	1410	*20% to 70%*	1446
<10% to 100%	1356	*20% to 100%*	1342
Mean	1437	*Mean*	1580
SD	97	*SD*	327

Table 4–15 Elastic modulus results based on mean peak stress and mean peak strain in the central zone. The ranges over which the modulus estimates were calculated corresponded to the four loading conditions of the *in situ* experiment.

5 DISCUSSION

5.1 *IN VITRO* STUDY

5.1.1 Introduction

This study was motivated by the need to determine PT mechanical properties as inputs for a mathematical model of *in vivo* PF joint mechanics in the cat. There was also a practical need to quantify the left-right variability in PT properties. Experimental methods developed for determining PF joint kinematics, joint surface geometries and contact characteristics are invasive and destructive, precluding the use of the experimental limb for mechanical testing. It was necessary to establish whether PT properties of the contralateral limb could represent the properties from the PT in the experimental limb. A study quantifying PT properties and left-right differences in PT properties is deserving of wider attention in the area of tissue biomechanics. The PT of several species have been studied, including rabbit, dog, goat, monkey and human but little attention has been given to the cat PT. Recent investigations have used the cat knee as a model of injury related OA and PF joint contact. Therefore, a need exists to quantify the properties of the soft tissue structures of the cat knee joint, particularly the PT. Furthermore, the question of variability in contralateral tissue structures has seldom been the subject of systematic study. This is surprising considering the importance of the contralateral control in many investigations in orthopaedic biomechanics.

5.1.2 The *in vitro* technique

The *in vitro* study was based on established techniques for quantifying tissue biomechanical properties. The structural response of a PT specimen was directly obtained through measurements of force during a prescribed elongation. Specimen stress and strain were required for the determination of the specimen's mechanical response. Tissue stress and strain was obtained by normalising force and elongation data with *CSA* and L_0, respectively. Estimates of specimen mechanical response were therefore subject to the inaccuracies and limitations that constitute the basis of the *CSA* and L_0 measurements.

In the present investigation, *CSA* measurements were made with tissue area callipers. The accuracy of this technique has been established to be within ±5% (Shrive, et al., 1988). A high degree of repeatability was demonstrated in the *CSA* measurements, with an average *SD* of ±0.3 mm^2 (2.7% of the mean *CSA*).

The overall mean *CSA* was 11.4 (±2.8) mm^2. There were four out of eleven pairs where the difference in *CSA* was 2.0 mm^2 or greater, a difference comparable to the inter-specimen variability in *CSA* measurements as quantified by the *SD*. These large differences may be attributed to a true, anatomical difference, or artefacts related to experimental factors.

Experimental factors such as alignment, pre-load and hydration may change the specimen cross-section. The *area calliper* technique has been shown to be sensitive to tissue pre-load (Shrive, et al., 1988). It is speculated that changes in specimen alignment between tests may have altered the distribution of pre-load tension in PT specimens and that this factor was largely responsible for the large left-right variations in *CSA* observed. An analysis of the sensitivity of *CSA* measurements to these experimental factors is required in order to determine if observed left-right differences reflect real variability in left-right differences or are related to measurement artefacts.

The procedure for determining grip-to-grip strain was based on established methods. L_0 was defined to be the length from the top of the patella clamp to the tendon insertion on the tibia. Zero elongation ($\Delta L = 0$) was set at an arbitrarily chosen force level. For the strain measurements in the cyclic tests, $\Delta L = 0$ was set at 0.1 N. For the failure tests, $\Delta L = 0$ corresponded to the onset of actuator motion as indicated by the MTS length signal transducer. The force level in this case was 5.5 (±1.6) N. Methods for setting the zero elongation force levels were chosen to allow for a repeatable basis of comparison within the cyclic stiffness (modulus) and failure stiffness (modulus). There was a difference in zero elongation levels between the cyclic loading and failure tests. This difference may have affected the comparisons of the cyclic properties versus the failure properties in the toe region of the structural and mechanical response. It is felt that the effect of the force offset in the failure force response was minimal in comparisons of the cyclic properties versus failure properties in the linear elastic region.

Structural property estimates were also subject to the limitations of the accuracy of the measurement technique. The accuracy in the stiffness estimates is based on the repeatability of the K_{CYC} measurements. This was determined to be ±9 N mm^{-1} and was used as the base accuracy of the K values determined from the force-elongation data. The method described for determining K_{FAIL} values was less objective and less repeatable. An error of ±10 N mm^{-1} was found to be a reasonable estimate for the repeatability in K_{FAIL} estimates. The total accuracy of the K_{FAIL} estimates was then ±19 N mm^{-1}. For the purposes of this study, ±5 N was used for the accuracy of the MTS force measurements. Finally, the accuracy of the MTS elongation measurements was estimated at ±0.25 mm.

5.1.3 Results

5.1.3.1 Failure modes

No failures of the PT mid-substance were observed in tests of the PPTC specimens. Failures were classified as avulsion failures at the patella. In order to describe the failure properties of tendon tissue rather than the behaviour of the PPTC, it is desirable to achieve mid-substance failures of the PT substance. It has been suggested that failure mode can be driven by strain rate, but the studies of the rabbit FMTC by Woo, et al. (1986) suggest that maturity is a more important factor. This tendency may not hold true for the cat PPTC, but the results of this investigation suggest that mid-substance failures do not occur for the specific loading protocol that was adopted. Alignment is closely linked to failure mode for other bone-tissue-bone specimens (Momersteeg et al., 1995). It is speculated that attaining an alignment between the patella and the PT that more closely approximates the functional or physiological alignment would result in a structurally stronger attachment between the PT and the patella. This could lead to higher ultimate strength and possibly to mid-substance failures of the PT.

While all of the failure modes were classified as patellar avulsions, examination of the specimens after each test revealed a considerable variation in the amount and shape of the insertion material and bone attached to the PT after each test. At the extremes was either a very small amount of hard tissue attached to the tendon to what appeared to be the

whole apex of the patella broken away. It is speculated that these observations indicate variations in the exact mode of failure across specimens.

5.1.3.2 Strain rate sensitivity

Sensitivity of failure properties to strain rate was investigated by conducting the failure tests at three actuator head speeds corresponding to 10, 75, and 100 % strain (grip-to-grip measurement). A qualitative analysis based on mean and *SD* in estimates of failure properties did not reveal any distinct trends. Consequently, further quantitative statistical analyses were not applied to this data.

5.1.3.3 Comparisons with previous studies

PT biomechanical properties of several species have been studied in earlier investigations. Human PTs have been studied in the context of understanding tendon injury mechanisms and characteristics of PT autograft replacement of the injured ACL (Butler, et al., 1984; Johnson, et al., 1994). PT properties of the dog, and rabbit have also been studied. These investigations have been motivated by the development of models of PT autograft replacement and joint immobilisation studies (Burks, et al., 1990; Haut, et al., 1992; Yamamoto, et al., 1992). Methods used for deriving PT biomechanical properties are fairly standard and are similar to the techniques applied in this study. In some studies, however, there are often important differences in the approach. Variations in the experimental technique include: testing of portions of the PT, typically the central third fascicles, as opposed to the whole PT tissue structure; differences in the *CSA* measurement technique and definitions of tissue L_o; and differences in pre-conditioning and applied strain rates. Failure modes are typically characterised as (patellar) avulsions or (mid-) substance failures. Comparison of the ultimate structural and mechanical property measurements should be made carefully if failure modes differ across studies.

Only one investigation of the biomechanical properties of the cat PT was found in the scientific literature reviewed (Archambault, 1995). This study focussed primarily on the sub-maximal behaviour of cat PT specimens at low strain rates. The sub-maximal loading protocol consisted of three cyclic load-relaxation tests at 10, 100, and 500 mm min^{-1}. Peak loads were from 250 N to 400 N. Elastic modulus values obtained from the cyclic protocol were 437 MPa, 477 MPa and 467 MPa for the low, medium and high loading rates

respectively. These values are close to the average E_{CYC} and E_{FAIL} estimates of 473 MPa and 500 MPa observed in this study (Table 5–1). One failure specimen was extended to complete failure. The failure stiffness (K_{FAIL}) of the specimen in the study by Archambault (1995) was higher than the average K_{FAIL} value in the present study, but not outside the range of values observed. The ultimate load attained was 578 N which was low compared to the present study (Table 5–1). High levels of force (80%) in the series of cyclic load relaxation tests performed in Archambault's study (1995) may have weakened the tendon at the patellar insertion, resulting in the low ultimate tensile force.

Yamamoto et al., (1992) reported the structural properties of the rabbit PPTC and mechanical properties of the PT tissue. In this study, the lateral, central and medial third sections of the tissue were tested in bone-tissue-bone preparations. The structural properties of the whole tissue were estimated from the properties of the central third. The results for the rabbit were close to those obtained in the present study (Table 5–1). Both the stiffness and modulus estimates were similar. An important difference in failure modes was noted between the present study and that of Yamamoto, et al., (1992). The rabbit PT specimens all failed in the tendon substance rather than at the patella, as was the case in the present study. It is therefore difficult to make direct comparisons of ultimate tensile properties. Mean values of F_{UT} and ΔL_{UT} were higher for the cat than for the rabbit. It is speculated that the difference in testing protocols i.e., whole tissue in the present study compared to sections in Yamamoto (1992) was responsible for the difference in failure modes.

Previous studies have presented the results of the biomechanical testing of whole PPTC specimens harvested from the knees of dogs (Burks, et al., 1990; Haut, et al., 1992). In these investigations, estimates of specimen failure stiffness were roughly 80% and 95% of the 332 N mm^{-1} obtained in the present study (Table 5–1). While the stiffness estimates were lower, estimates of average ultimate tensile force of the dog were substantially higher than those of the cat (Table 5–1). Values obtained in the earlier study (Burks, et al., 1990) were 2.6 times larger than those for the cat.

Species	Cat	Cat	Rabbit	Dog	Dog	Human
n	22	1	14	6	27	7 7
	mean (sd)	-	mean (sem)	mean (sem)	mean (sd)	mean (sem)
K_{FAIL} *(N mm-1)*	322 (42)	506	347 (13)	260 (19)	308 (66)	-
F_{UT} *(N)*	878 (177)	578	799 (40)	2300 (210)	2080 (620) 3250 (700)	-
ΔL_{UT} *(mm)*	4.7 (1.6)	-	2.9 (0.1)	9.3 (0.5)	-	-
E_{FAIL} *(MPa)*	500 (114)	-	549 (13)	360 (36)	457 (28)	305.5 (59.0) 361.3 (34.4)
σ_{UT} *(MPa)*	82 (24)	-	-	-	-	58.3 (6.1) 56.7 (4.4)
ε_{UT} *(%)*	28 (7)	-	-	-	-	26.5 (2.9) 24.2 (2.5)
Preparation	whole tendon	whole tendon	central third	whole tendon	whole tendon	central third medial third
Failure Mode	avulsion	avulsion	substance	avulsion	avulsion substance	substance
Study	Present study	Archambault, 1995	Yamamoto, et al., 1992	Burks, et al., 1990	Haut, et al., 1992	Butler, et al., 1984

Table 5–1 Structural and mechanical properties of PT specimens.

The mean masses of the dogs in the two studies were 29.9 (±1.9) kg and 26.7(±8.4) kg (Burk, et al., 1990; Haut, et al., 1992). These values are roughly eight times larger than the mean mass of the animals used in the present study. Because they were larger animals, it is assumed that tissue structures in the dog knee were subjected to higher loads in comparison to tissues of the cat knee. It is possible that the PPTC in the dog specimens had adapted and were stronger to accommodate these higher loads. The elongation, ΔL_{UT}, observed by Burks et al., (1990) was roughly twice the average elongation for the cat specimens. Specimen lengths for the dog PTs were roughly 35 mm (Burks, et al., 1990) and 17 mm for the cat (present study). The dog PTs were more that twice as long as the cat PTs, on average.

5.1.3.4 Left-right variation in structural properties

The first objective of the present study was to quantify the magnitude of left-right differences in structural property values relative to experimentally observed mean values in those properties. The boundary of 10% was arbitrarily chosen as an acceptable level for which properties of the contralateral PT could be said to represent properties of PT of interest in a left-right pair. In relation to observed mean structural properties, 10% represents 30 N mm^{-1}, 32 N mm^{-1}, 87 N, and 0.48 mm for K_{CYC}, K_{FAIL}, F_{UT} and ΔL_{UT}, respectively. No *significant differences* were found between left and right groups of any of these structural property values. However, the power, $1-\beta$, of the statistical tests was acceptable for the paired sets of K_{CYC}, K_{FAIL}, and F_{UT} values only. The high variability in the ΔL_{UT} estimates resulted in a low power for the chosen relevant difference.

It is felt that the techniques used were capable of correctly measuring structural property values to a level of ±10% of the overall mean values. In the structural properties of interest (excluding ΔL_{UT} values), the mean absolute left-right difference was less than 10% of overall mean values. For ΔL_{UT} values, the difference was larger at 21%. Despite the relatively low mean absolute differences, individual pairs of specimens demonstrated larger amounts of variation. For example, 2 pairs of K_{FAIL} estimates had differences larger than 15%. K_{CYC} and F_{UT} differences were similarly distributed and the ΔL_{UT} values showed a

much larger range of differences with the largest being 80% of the mean value. Inter-limb (left-right) differences in may be attributed to experimental or biological factors.

For the purpose of the present study *apparent differences* are those arising from experimental factors. *Real differences* will be defined as those arising from biological factors. Experimental and biological factors that influence the biomechanical properties of tissue have been reviewed in Section 2.4.

Through the mechanisms which were described, any experimental conditions that are not precisely duplicated in the testing of two tissue specimens could produce apparent differences in property estimates. It was felt that a standard protocol was applied to left-right pairs of specimens. The preparation of pairs for frozen storage, storage time, PT hydration during testing and testing temperature were consistent. It is speculated that variations in specimen alignment across tests contributed to larger left-right differences in structural property values. The most difficult part of the procedure to apply precisely was the specimen alignment during the mounting protocol. A repeatable, neutral alignment was sought for each of the tests as described in Section 3.1.1. Due to inaccuracy in positioning the patella there may have been variation in the relative alignment of the patellar and tibial insertion sites from test to test. It is estimated that this variation was less than ±5°.

During the experiments, it was observed that following the first part of the protocol in which the initial length was set, some specimens demonstrated differences in the amount of tension in the tendon fibres latero-medially, across the specimen. This may have resulted in differences in the distribution of tension across the fibres of PT specimens. It is speculated that differences in alignment and distribution of pre-tension contributed to the variations in the failure mode and the measurement of PPTC properties. The ultimate properties appeared to be affected the most by this mechanism and this is reflected in the larger left-right variation particularly in the ΔL_{UT} values.

The effect of injury on tissue properties has been demonstrated in studies based on animal models (Frank, et al., 1983; Burks, et al., 1990; LaPrade, et al., 1997). In the models of injury and healing presented, tissue structures that healed after an injury did not regain normal levels of biomechanical response. Based on these studies, it is speculated that differences in biomechanical properties between contralateral tissue structures due to a

previous injury that may cause variations in estimates of left and right PT properties. When the specimens were prepared for testing, no visible evidence of disease or injury were noted.

The connection between activity level and the mechanical properties of ligament and tendon has been well demonstrated (Tipton, et al., 1970; Amiel, et al., 1982; Woo, et al., 1987; Yamamoto, et al., 1993). These studies demonstrate that immobilisation and inactivity will have an adverse affect on the biomechanical properties of tissue structures as characterised, for example, by ultimate tensile stress, ultimate tensile strain and elastic modulus. It is possible to speculate that favoured use of one hind limb over the other will result in stronger tissue structures in the preferred hind limb. Paw preference, has been reported in cats (Tan and Kutlu; 1991) and could contribute to left-right differences in measured biomechanical properties. However, the history of animal activity levels in the present study is unknown and there is no evidence for relating any of the left-right biases with preferred use of one hind limb.

The results of the present study have for the first time established boundaries on the magnitude of contralateral variations in normal cat PT. The results support the first hypothesis that contralateral differences in structural properties are not significant for K_{CYC}, K_{FAIL} and F_{UT}. These findings are important in the context of providing PT biomechanical property inputs to a model of PF joint contact. Depending on the accuracy required for model inputs it would appear that using the properties of the contralateral PT is justified. In addition it is believed that, allowing for limitations in *CSA* and strain measurement techniques, the results could be extended to include the mechanical response of PT tissue.

These results may also provide an additional basis for interpreting the results of earlier studies including animal models of changes in PT autograft strength over time or the effect of immobilisation on PT properties.

5.1.4 Recommendations

In future experiments to quantify aspects of the PT biomechanical behaviour, a critical change in the testing technique would be the addition of a specimen mounting apparatus that allowed for precise and controlled alignment of tissue specimen. It is believed that this addition would reduce the variability in biomechanical property

estimates. Improvements in the method of mounting and aligning the specimen may lower the measured left-right variation in PT properties. The analysis of experimental results focussed on the structural and mechanical properties in failure. Given the speculated functional importance of tissue creep response, it will be of interest to quantify in more detail the *submaximal* response of cat PT. The results of the present study could aid in estimating functional stress levels for testing specimens in cyclic loading protocols.

The quantification of tissue *CSA* is critical for deriving specimen stress response. Previous studies have examined the relation between specimen alignment and tissue biomechanical properties. Future investigations of cat PT properties could include an examination of the sensitivity of tissue *CSA* measurements to specimen alignment.

5.1.5 PT tissue strain response

The literature reviewed for the present study has established the basic characteristics of the biomechanical response of soft tissues (e.g., Butler, 1978). Previous studies have also established characteristics of mid-substance strain measurements of tissue properties (Woo, et al., 1983; Butler, et al, 1984). The following aspects of tissue strain response were expected from the results of the strain analysis of the present study:

1. The tissue strain will increase as the stress in the specimen increases;
2. Grip-to-grip strain is larger than mid-substance strain; and
3. Lateral to medial strain distribution of PT specimens will be uniform.

In fact, the strain analysis of the present study revealed a mixed response in PT surface strain. In a given zone, corresponding to a lateral, central or medial third of the PT surface, the strain response was assigned to one of three groups: i) linear response with a measurable increase in strain; ii) linear response with no measurable increase in strain; and iii) non-linear (erratic) response. These three types of responses were illustrated in the Chapter 4. The first type of response is the expected response. The second type of response is characteristic of a very stiff material and not typical of soft tissue structures. It was speculated that observed responses of this type arose from slipping of surface fibres of the PT or even of the whole specimen in the patellar clamp. There were two speculated sources for the non-linear (erratic) response. First, specific features of the image record such as glare, shadow and/or blurred or crooked stain lines on the surface of PT specimens.

Second, errors in stain line edge position could have arisen from the limitations of the precision achievable and inaccuracies affecting the repeatability of the technique.

Observations of the video tests revealed that close to failure, tendon fibres had a tendency to slip with respect to the patellar clamp. It is possible to speculate that slipping of fibres occurred at earlier stages in the test but this is not known. Tissue fibres of the patellar insertion were not tracked with the strain analysis technique. Specimens exhibiting a lack of measurable strain response were placed into Group 2 under the assumption that strain measurement were affected by slipping of PT fibres.

5.1.5.1 Comparisons with previous studies

For Group 1 at 30 MPa, the average strain across the three zones of the PT was found to be 2.35(±0.28) %, 2.26(±0.36) % and 2.33(±0.24) % in the lateral, central and medial zones respectively. For Group 2 at 30 MPa, strains in the corresponding zones were 2.02(±0.78) %, 0.87(±0.66) % and 1.93(±1.16) %, respectively. The lowest strains measured by Archambault (1995) at 20 MPa were, 2.55(±0.22) %, 2.59(±0.25) % and 2.67(±0.24) % in the medial, central and lateral zones. At a stress that was higher by 50%, the average strains of the present study were 14%, 15% and 11% less than the average strains of Archambault (1992). Archambault's strain data were obtained from low rate cyclic loading of PT specimens tested in a saline bath.

The grip-to-grip and mid-substance elastic modulus of rabbit has been reported (Yamamoto, et al., 1992). In the rabbit study, PT were tested in sections with each section being roughly one third of the entire tissue. Modulus estimates for the central portion of the rabbit PT were 549(±13) MPa and 1390(±53) MPa based on grip-to-grip and mid-substance measurements. In the present study, the whole tissue modulus was 536(±127) MPa (grip-to-grip) and 1335(±221) MPa (mid-substance). These values (for cat PT) were in excellent agreement with the results of Yamamoto (for the rabbit).

5.1.5.2 Conclusion

The second hypothesis of the study was that the lateral-to-medial strain distribution in PT tissue specimens would be uniform. The strain response data from the Group 1 specimens clearly supports this hypothesis. However, as there were only five specimens in

this group, a formal statistical test was not applied to the data. The response of the Group 2 specimens was highly non-uniform. It was speculated that this type of response was due to the specimen slipping in the clamp and poor image quality.

The third hypothesis was that elastic modulus estimates based on mid-substance strain would be higher than elastic modulus estimates base on grip-to-grip strain. The hypothesis test was not tested formally.

5.2 THE *IN SITU* STUDY

5.2.1 Introduction

In the first and second parts of the present study, the biomechanical response of the cat PT was quantified. The results can be used to characterise the linear elastic behaviour of the PT in a model of *in vivo* PF joint contact. Many previous tissue property investigations have sought to quantify tissue mechanical properties in order to characterise their *in vivo* behaviour. An important question in tissue biomechanics is how realistically do tissue properties derived *in vitro* repeat the *in vivo* behaviour of the tissue. In a living animal, a tissue structure such as the PT functions in a complex physiological environment. Some components of this environment that influence the mechanical properties include tissue alignment, the presence of other connective tissue structures and muscles, the presence of bony structures and a functional level of stress and strain brought about by muscle forces as well as the passive forces in tissues and bony structures. Some biological aspects of the physiological environment include: temperature, sources of hydration such as synovial fluid and blood supply, and the biological response of the tissue to its stress-strain environment. The *in vitro* mechanical test is an extreme departure from the physiological environment. Furthermore, *in vitro* testing may add confounding factors such as specimen storage and the influence of measurement techniques on the biomechanical response of tissues.

The motivation for conducting the *in situ* experiment described in the present study was to develop a technique to measure the force-elongation behaviour of the cat PT in the intact knee joint. Knowledge of the *in situ* biomechanical behaviour of the PT may aid in understanding the differences between the *in vitro* standard and the true *in vivo* condition. The technique presented was a new method that combined strain measurement techniques

based on previous investigations together with an approach for estimating PT forces in a live, anaesthetised animal model.

5.2.2 Methodological considerations

Previous investigations that attempted to quantify the force and strain in tissues *in vivo*, have employed transducers that attach directly to the connective tissue structures. Herzog, et al., (1992) used *buckle transducers* on the extensor muscles of the cat ankle joint to measure muscle forces in cat walking on a treadmill. Hasler, et al., (1998) measured *in vivo* PT forces in cats walking on a treadmill using an *implantable force transducer* (IFT). Beynnon and co-workers (1994) used *Hall effect transducers* (HET) to measure strain in new PT autograft reconstructions Beynnon, et al. (1994). It is acknowledged that attaching such devices to a connective tissue structure may alter its structural and mechanical response. In addition, impingement of bony structures and other tissues may affect the measurements made from an implanted transducer. The relative magnitude of these effects is not known. In experiments involving the use of implantable transducers, such as those mentioned, are capable of providing direct estimates of either the force or strain in an instrumented tissue. It is not possible to quantify the structural or mechanical behaviour of tissues, as characterised by the force-elongation or stress-strain response.

5.2.2.1 *CSA*, stress and strain measurements

Estimates of tissue stress and strain were limited by measurements of *CSA* and tissue elongation in relation to a gauge length, L_0. These limitations were outlined in section 5.1.

PT stress during stimulation trials in each of the loading conditions was determined by normalising the PT force-time response by tissue *CSA*. It is important to note that the *CSA* value used to calculate tissue stress was obtained in an *in vitro* experiment as described in Section 3.1.3. It is not clear if and how the *CSA* of the PT would change in the *in vitro* testing environment compared to the *in situ* intact environment. As it is likely that the alignment and hydration of the tissue was altered in the *in vitro* test then it is speculated that the *CSA* measured *in vitro* was different from the *in situ* value. The magnitude and direction of the change in *CSA* is uncertain and may be a source of uncertainty in the stress measurements.

The definition of "tendon zero strain" presented a problem in the application of *in situ* experiment, as it does in the implementation of standard *in vitro* tissue testing protocols. In the *in situ* experiment, the undeformed gauge or base length, L_0, was set at a stimulation level where both force and elongation could be measured (Section 3.2.4). Tendon zero strain was determined to correspond to a calculated PT force of 39(±9) N or 2.93(±0.69) MPa. Results of the *in vitro* quantification of PT biomechanical properties would seem to suggest that stresses of these magnitudes are well into the toe region of the mechanical response of the cat PT. Compared the *in vitro* "tendon zero strain" forces (roughly 5 N in failure tests) the *in situ* levels were high. As a result, the estimates of *in situ* strain may be affected by an offset. Since the *in situ* gauge lengths were only measured at the <10% loading condition, the amount of offset in the strain compared to a lower force level is not known. The results of previous studies demonstrate that the toe region of soft tissue structures may run from 0 % to approximately 3 % strain (Butler, et al., 1978). Therefore, it is speculated that the *in situ* strains may be underestimated by as much as 1 % strain. Any direct comparison of the *in vitro* and *in situ* strain should be made in view of this offset.

In situ estimates of elastic moduli, E, were made at stress levels that were assumed to correspond to the elastic region of the tissue's response. As values of E were based on a change in strain it was felt that the effect of an offset in strain due to "tendon zero" force estimates was negligible.

5.2.2.2 Sources of errors in PT force estimates

Experimental measurements of the restraining force on the tibia, F_R, and the restraining force moment arm, r_R, were combined with a 2D model of the knee joint in order to estimate PT forces. F_R values included in the PT force model were assumed to reflect an accurate force-voltage calibration of the bridge output from the restraining bar. It is acknowledged that this model was over-simplification of the complexities of the knee joint 3D kinetics and that the model places limitations on the accuracy of the PT force estimates. The 2D model was based on four underlying assumptions. The purpose of this section is to state the assumptions and outline the sensitivity of the PT force estimates to errors in the assumptions.

Assumption 1. The tibia contacted the restraining bar such that the line of action of F_R was perpendicular to the long axis of the tibia, in a plane defined by the long axes of the tibia and femur.

The bar was instrumented to measure force along a single axis. If the true restraining force had components that were not parallel to the axis of measurement, then the magnitude of the measured restraining force, F_R, was underestimated. Components of F_R that were i) out of the plane of flexion and ii) not perpendicular to the tibial axis could have contributed to the error in the PT force (F_T) estimates.

Rolling of the tibia on the restraining bar would have resulted in components of F_R that were out of the plane of flexion. It is felt that passive resistance of the cruciate and collateral ligaments of the knee joint would have limited the possibility of lateral-medial rotation of the tibia with respect to a fixed femur (Maitland, et al., 1998). It is estimated that the rolling of the tibia with respect to the restraining bar was limited to ±2.5°.

During the experiment, an attempt was made to position the restraining bar such that the direction of force measurement was perpendicular to the tibial axis. It is estimated that the restraining bar was accurately positioned with respect to the tibia to within ±10°. Rolling of the tibia and a non-perpendicular restraining force acting together at their estimated limits could reduce the measured value of F_R by a factor of 0.98 ($cos2.5° \cdot cos10°$) from its true value. The moment balance of the 2D model implies that F_T and F_R are directly related. Therefore this direction error will also reduce the F_T estimates by a factor of 0.98.

Assumption 2. The restraining force, F_R, and PT force, F_T , were in the same plane.

It was felt that the second assumption was reasonable given that the primary function of the PT is to transmit tensile force from the *quadriceps* to the tibia in knee extension. Therefore, it was unlikely that the PT contributed significantly to in-eversion moments about the knee. This type of action is the domain of other structures, notably the collateral ligaments. Any component of the tensile force in the PT that did not contribute to an extension moment was thought to be insignificant.

Assumption 3. The magnitude of the restraining force moment arm, r_R, with respect to the knee joint centre was 100.0 mm. The magnitude of the

PT moment arm, r_T, with respect to the knee joint centre at 75° was 10.0 mm.

If the PT force, F_T, is given by the simple balance of moments:

$$r_T \cdot F_T = r_R \cdot F_R, \quad [8]$$

then the sensitivity of FT estimates with respect to changes in the rR is given as:

$$\frac{dF_T}{dr_R} = \frac{F_R}{r_T}. \quad [9]$$

The accuracy of the restraining force moment arm measurement was ±2.5 mm. With a restraining force of $F_R = 55$ N, the sensitivity of the PT force values to changes in the restraining force moment arm is ±5.5 N mm^{-1} (for a PT moment arm of 10 mm). An uncertainty of ±2.5 mm in r_R results in an error of ±14 N. This is equivalent to 2.5% of a 550 N of PT force.

The sensitivity of F_T values to changes in the PT moment arm, r_T, is given as:

$$\frac{dF_T}{dr_T} = -\frac{R_R \cdot F_R}{r_T^2}. \quad [10]$$

A value of $r_T = 10.0 \pm 1.5$ mm was chosen from the literature. For a PT moment arm of $r_T = 10$ mm, a restraining force moment arm of $r_R = 100$ mm and a restraining force of $F_R = 55$ N, the sensitivity of the PT force values to changes in the PT moment arm is ±55 N mm^{-1}. An uncertainty of ±1.5 mm in r_T results in an error of ±85 N, or 15 % of 550 N of PT force.

Assumption 5. There was no hamstring co-contraction, and the actions of other soft tissue structures were neglected.

Finally, there was the possibility of co-contraction from the hamstring muscles. No measurements were made of muscle activity during stimulated contractions of the *quadriceps*. The possibility of hamstrings activity at the knee was ruled out as the femoral nerve alone was stimulated.

Uncertainties in the magnitudes of r_R and r_T (±2.5 mm and ±1.5 mm, respectively) were the most important sources of error in F_T estimates, according to this analysis. The resulting errors were large relative to the magnitude of peak PT force measurements (Table 5–2). It is important to note that neither the restraining force moment arm nor the PT

moment arm estimates were very reliable (Section 3.2.4). The uncertainties in these 2D knee joint model inputs were chosen to reflect a conservative level of accuracy in r_R and r_T values. The implementation of the IHA approach to identifying the joint centre of rotation would provide more accurate measurements (within ±1.0 mm or less) of both moment arms (Boyd and Ronsky, 1998). This would increase the confidence in estimates of PT force obtained from the 2D knee joint model.

Load Condition	F_T (N)	r_R error (N)	r_T error (N)
20%	224	± 6	± 34
70%	379	± 9	± 57
100%	530	± 13	± 80

Table 5–2 Errors in PT tensile force estimates. Three loading conditions: 20%, 70% and 100%. Mean peak PT force, F_T. The third and fourth columns show the range of uncertainty in F_T due to the uncertainty in r_R and r_T, respectively.

5.2.3 *In situ* strain response

The capabilities and limitations of the *in vitro* strain analysis technique were demonstrated in the second part of the study. Observations of differences between grip-to-grip strain and mid-substance strain were in agreement with the findings of previous investigations involving tissue surface strain measurements. The elastic response of the PT mid-substance was similar to that observed in rabbit PT specimens (Yamamoto, et al., 1992). The strain measurement system was incorporated into the *in situ* experiment in an attempt to quantify tissue surface strain in the intact PT. It was expected that the measurements would demonstrate a direct relationship between stress and strain. Furthermore, it was anticipated that the strain response across the PT would be uniform.

Two trends were observed in the strain data as represented by the mean peak strain response. First, at each load condition, the lateral and central zone strain levels were similar and increased with increasing stress. Second, strain in the medial zone was appreciably less than the strain in either of the other two zones at each load condition and did not appear to

correlate with stress. These results were not expected, and the cause of the non-uniform strain response iss not known. It is speculated that the results may be attributed to either:

i) **variations in the mechanical properties** of the medial zone compared to the other two zones or,

ii) a **non-uniform stress distribution** throughout the tissue cross section.

5.2.3.1 Variation in PT mechanical properties

The implication of the first situation is that the modulus of the medial zone was roughly twice the lateral or central zone moduli. Studies have found differences in strain or mechanical properties in longitudinal sections of the PT. Yamamoto, et al., (1992) reported a ratio of 1.00:0.94:0.98 in the elastic modulus of the lateral, central and medial third sections of rabbit PT specimens. Archambault (1995) reported a ratio of 1.00:1.03:1.08 in the mid-substance strain in the lateral, central and medial zones of whole cat PT specimens at 20 MPa. Based on the results of these studies, differences a large as 100% in the mechanical properties of zones of the cat PT were felt to be unlikely. Therefore, it was concluded that the medial zone strain response was not related to a difference in tissue mechanical properties.

5.2.3.2 Possible mechanisms for a non-uniform stress distribution

The second explanation for lateral to medial variation in strain response was that the stress was non-uniformly distributed throughout the fibres of PT cross-section. It is speculated that a non-uniform stress distribution may be related to two factors: the alignment of the tibia with respect to the patella and the direction of *quadriceps* muscle force relative to the PT fibre direction.

In vitro specimen alignment has been shown to alter the measured biomechanical response of knee joint ligaments (Woo, et al., 1987; Momersteeg, et al., 1995). Investigators have speculated that patterns of fibre recruitment in loaded tissue structures may depend in part on the relative alignment of the insertion sites of a bone-tissue-bone specimen. Analysis of the relative motion of the tibia with respect to the patella during the stimulation trials at the 70% load condition showed a consistent varus rotation of 3.1(±0.4)° and a lateral rotation of 11.0(±0.8)° in the plateau region of the stress response. This

rotation was relative to a neutral position and indicates a change in the patellar-tibial alignment with respect to the neutral position when the PT stress was at peak values. A quantification of the influence of patellar-tibial alignment on PT surface strain variation is required in order to estimate the effects of changes in alignment. However, it is felt that this mechanism could be partially responsible for the observed variation in PT surface strain.

The relative orientation of applied force with respect to the fibre direction of tissues has been shown to influence the biomechanical response of knee joint ligament specimens (Woo, et al., 1987). It is speculated that the direction of *quadriceps* muscle force may also have been a factor affecting the *in situ* strain response. Qualitatively, the position of the immobilised femur did not appear abnormal when the animal was secured in the surgical frame. However, it is possible that the femur orientation was not physiological. Assuming that the PT fibres are oriented in the direction of the *quadriceps* muscle force during physiological loading of the knee it is possible that immobilisation of the femur may have altered its position relative to its functional position in gait. This may have changed the functional direction of the *quadriceps* muscle force relative the PT fibre orientation. It is important to note that this is speculation and the direction of *quadriceps* muscle force was not measured during the experiment. Furthermore, the influence of muscle force direction on PT surface strain in must be quantified experimentally before making strong conclusions regarding this effect.

5.2.4 Systematic errors in strain measurement

Two important types of error affecting strain measurement techniques were relevant to both the *in vitro* and *in situ* experiments. The first type of error is associated with strains calculated from the measurement of a change in length with respect to a gauge length (Section 2.4.1). Strain measurements based on this approach will be affected by large errors at low strain levels (Shrive 1994). The results from the *in vitro* study and the *in situ* experiment demonstrate this effect. In high rate failure tests, the variation in strain measurements was high relative to calculated strains at the 5 MPa level (Table 4–8). At each of the four loading conditions from 20% to 100%, the measured variation (*SD*) was high compared to the mean peak strain values (Table 4–13). These levels of error were inherent in the strain measurement technique used in the present study. It is speculated that

increasing the resolution of captured images through the use of better quality video monitoring and recording equipment would improve the presicion of the length change calculations and therefore increase the accuracy of the method.

The second type of error, associated with 2D optical methods, arises from motion (translation or rotation) of the specimen with respect to the plane of measurement (Section 2.4.5). Derwin and co-workers (1994) reported negligible apparent strains arising from translation along the optical axis. The largest apparent strains were associated with rotation about the in-plane axis perpendicular to the direction of strain measurement, i.e., the x-axis of Figure 2–6. Rotations of ±5° resulted in apparent strains on the order of –0.1 % strain and rotations of ±10° resulted in apparent strains on the order of –1.0 % strain (Derwin, et al., 1994). Note that regardless of the direction of rotation, the effect was to underestimate the actual strain in the specimen.

The controlled loading of the *in vitro* experiments was maintained by the fixation of PT insertion points in the mounting apparatus. Therefore, it was felt that rotations of this magnitude were unlikely. No rotations greater than ±5° were detected in repeated observations of *in vitro* specimens during the cyclic loading protocol.

However, in the *in situ* experiment, any x-axis rotation of the PT would have been roughly coincident with the plane of knee flexion-extension. When the video camera was set up at the beginning of the experiment, care was taken to ensure that the anterior surface of the PT was perpendicular to the optical axis of the camera as the tibia was lifted manually to contact the restraining bar. Motion of the tibia, and consequently of the PT tibial insertion, was restricted by the instrumented bar. Therefore, it was felt that extension of the tibia during *quadriceps* contractions would not be responsible for out of plane rotation of the PT. In the case of the PT insertion on the patella, motion of the patella with respect to the femur was not restrained. It is possible that motion of the patella during *quadriceps* contractions could have produced out of plane rotations of the PT. The magnitude of such rotations was assumed to be small (less than 5°) and this effect was not incorporated into the strain analysis. Large out of plane motions may have been indicated by the image of the PT surface coming out of focus during *quadriceps* contractions. No out of focus images were observed in the strain analysis.

5.2.5 *In situ* force measurements

Ronsky, et al. (1995) presented a method of measuring the PF joint contact areas, stresses and patellar displacements. The method employed stimulated contractions of the *quadriceps* muscles and PT tensile force measurement with an IFT. Measurements were made in experiments on four adult male cats (5.2±1.2 kg). The patella tendon forces measured were 183 N, 408 N and 476 N for the low (20 %), medium (60 %) and high (100 %) level stimulations respectively. In the current study, the mean peak PT force estimates were found to be 224 N, 379 N, 530 N for the 20 %, 70 % and 100 % loading conditions, respectively. Force values predicted in the present study matched those from the previous study within 20%. The values from the series of experiments compared well to the values from the single experiment carried out in this study on a skeletally mature male cat of 5.5 kg. The results indicate that, the method developed in this study is capable of reproducing the force measurements obtained using a similar technique.

The results of the *in vitro* study identified the stress levels of the linear elastic region of PT tissue. The linear elastic region was found to be from 4(±2) MPa to 40(±15) MPa. Mean peak stress values ranged from 2.93(±0.69) MPa to 39.55(±0.07) MPa. The lowest stress was during the during the <10% load condition and the highest at 100%. Stress at <10% was roughly 75% of the average *in vitro* toe region stress. Stress at the 100% load condition was roughly 100% of the *in vitro* stress at the proportional limit. The intermediate range of stimulation (where the strain data were collected) was from 16.74(±0.89) MPa to 28.31(±1.82) MPa at 20% and 70% respectively. The stresses at 50 and 70% were similar. From smallest to largest the intermediate, *in situ* mean peak stresses were at roughly 40% and 70% of the average *in vitro* stress at their proportional limit. This comparison suggests that the *quadriceps* muscles are capable of inducing stresses in the PT at the limit of its elastic response gauged from *in vitro* failure tests. At this level of stress, there will be micro damage to tissue substructures according to the model of soft tissue failure presented earlier (Chapter 2). It was not possible to determine the ultimate tensile stress of the PT tissue from *in vitro* failure tests because no true mid-substance failures of the tendon were observed. It is interesting to note, however, that the maximum mean peak

PT *in situ* force (530 N) was substantially lower than the average ultimate tensile force (roughly 870 N).

Inaccuracies in the PT force measurements and the *CSA* measurement technique contribute to substantial errors in the *in situ* PT stress estimates. Furthermore, the results represent the findings of one experiment only. Additional experiments need to be conducted in order to determine if the *in situ* stress estimates are repeatable. At best the results represent an order of magnitude estimate of the *in situ* stress magnitude. Comparison with the *in vitro* results indicates that these magnitudes correspond to the linear elastic region of the tissue stress-strain response.

5.2.6 Comparison of *in vitro* and *in situ* elastic modulus

The motivation for developing an *in situ* technique was to determine the mechanical behaviour of PT tissue in an environment closer to the *in vivo* situation than the *in vitro* experiment. Modulus values were calculated over a range of stress levels in what was speculated to be the elastic region of the PT response (Table 4–15). A value of PT elastic modulus on the order of 1509 (±229) MPa was estimated from the results of the *in situ* experiment. From the *in vitro* study, the mean elastic modulus was 1335 (±221) MPa (Group 1 specimens). The difference between the *in situ* and *in vitro* modulus estimates was within the observed standard deviations. The present findings may indicate that *in vitro* tests are able to provide a reasonable estimate of the *in situ* PT properties. However, it was not possible to determine whether the apparent agreement between modulus estimates was statistically significant with the results from only one *in situ* experiment. Results from additional *in situ* experiments are required before making strong conclusions.

5.3 RECOMMENDATIONS

Four important limitations were associated with the new *in situ* technique: high variation in strain measurements, definition of tissue L_0, uncertainty in PT moment arm estimates and uncertainty in patello-tibial movement. Applying some improvements to the technique may aid in addressing these limitations.

1. A high-resolution video recording system and more reliable image analysis techniques would improve the precision of the tissue strain measurement method.

2. Analysis of the force-time data demonstrated that the force levels corresponding to the L_0 measurements were high relative to force levels in the *in vitro* study. It may be preferable to measure the "unloaded," L_0 length of the tissue with the knee joint in passive flexion.
3. Analysis of kinematic data will provide a more reliable estimate of the knee joint centre. Additionally, knowledge of the relative motion of the patella and the tibia may provide insight into the causes of variations in the strain response of the PT.

The experimental method presented was successfully used to quantify the stress-strain response of an intact PT. With further experiments, the *in situ* response of the cat PT may be characterised with greater confidence. This will allow for a quantitative statistical comparison between the *in vitro* and *in situ* PT mechanical behaviour. Additionally, a technique that combines tissue stress and strain measurements with kinematic data has the potential to be used as a tool for studying the relation between PT strain variation and knee joint alignment.

REFERENCES

Allard, P., Thiry, P.S., Bourgault, A. and Drouin, G. (1979) Pressure dependence of 'the area micrometer' method in evaluation of cruciate ligament cross-section. *J. Biomed. Engng.* **1**, 265-267.

Altman, D.G. (1995) Practical Statistics for Medical Research, Chapman and Hall.

Amiel, D., Akeson, W.H., Harwood, F.L., Frank, C.B. (1983) Stress deprivation effect on metabolic turnover of the medial collateral ligament collagen. A comparison between nine- and twelve-week immobilization. *Clin. Orthop.* **172**, 265-270.

Amiel, D., Woo, S.L., Harwood, F.L. and Akeson, W.H. (1982) The effect of immobilization on collagen turnover in connective tissue: a biochemical-biomechanical correlation. *Acta. Orthop. Scand.* **53**, 325-332.

Apter, J. (1972) Influence of composition on thermal properties of tissues. In *Biomechanics: Its Foundation and Objectives.* (Eds. Y.C.B. Fung, N. Perone and Anliker), 217, Prentice-Hall, Englewood Cliffs, N.J.

Archambault, J.M. (1995) Clinical Aspects of Overuse Tendon Injury and Experimental Aspects of Tendon Properties. MSc Thesis.University of Calgary Press, University of Calgary.

Arms, S., Boyle., J., Johnson, R. and Pope, M. (1983) Strain measurement in the medial collateral ligament of the human knee: an autopsy study. *J. Biomech.* **16**, 491-496.

Bach, J.M., Hull, M.L. and H.A. Patterson (1997) Direct measurement of strain in the posterolateral bundle of the anterior cruciate ligament. *J. Biomech.* **30**, 281-283.

Barad, S., Cabaud, H.E. and Rodrigo, J.J. (1982) Effects of storage at –80°C as compared to 4°C on the strength of rhesus monkey anterior cruciate ligaments. *Trans. Orthop. Res.* **7**, 378.

Beer, F.P. and Johnston, E.R. Jr. (1985) Mechanics of Materials. McGraw-Hill Ryerson Ltd.

Betsch, D.F. and Baer, E. (1980) Structure and mechanical properties of rat tail tendon. *Biorheology* **17**, 83-94.

Beynnon, B.D., Johnson, R.J., Fleming, B.C., Renstrom, P.A., Nicols, C.E., Pope, M.H. and Haugh, L.D. (1994) The measurement of elongation of anterior cruciate-ligament grafts in vivo. *J.Bone Joint Surg.* **76**, 520-531.

Blankevoort, L., Kuiper, J.H., Huiskes, R. and Grootenboer, H.J. (1991) Articular contact in a three-dimensional model of the knee. *J. Biomech.* b, 1019-1031.

Bosch, U. and Kasperczyk, W.J. (1992) Healing of the patellar tendon autograft after posterior cruciate ligament reconstruction—a process of ligamentization? An experimental study in a sheep model. *Am. J. Sports Med.* **20** (5), 558-566.

Boyd, S.K. (1997) A 3D in-situ model for patellofemoral joint contact analysis in the normal and anterior cruciate ligament deficient knee. MSc. Thesis, University of Calgary Press, Calgary.

Boyd, S.K. and Ronsky, J.L. (1998) Instantaneous moment arm determination of the cat knee. *J. Biomech.* **31**, 279-283.

Burks R.T., Haut R.C. and Lancaster R.L. (1990) Biomechanical and histological observations of the dog patellar tendon after removal of its central one-third. *Am. J. Sports Med* **18** (2), 146-153.

Butler, D.L., Grood, E.S., Noyes, F.R. and Zernicke, R.F. (1978) Biomechanics of ligments and tendons. *Exerc. Sport Sci. Rev.* **6**, 125-181.

Butler, D.L., Grood, E.S., Noyes, F.R., Zernicke, R.F. and Brackett, K. (1984) Effects of structure and strain measurement technique on the material properties of young human tendons and fascia. *J. Biomech.*, **17**(8), 579-596.

Butler, D.L., Kay, M.D., Stouffer, D.C. (1986) Comparison of material properties in fascicle-bone units from human patellar tendon and knee ligaments. *J. Biomech.* **19**(6), 425-432.

Butler, D.L., Sheh, M.Y., Stouffer, D.C., Samaranayake, V.A. and Levy, M.S. (1990) J. Biomech. Eng. 112, 38-45.

Chan, S.S., Livesay, G.A., Morrow, D.A. and Woo, S.L.-Y. (1995) The development of a low-cost laser reflectance system to determine the cross-sectional shape and area of soft tissues. *ASME Adv. Bioeng.*, **BED-31**, 124-124.

Chimich, D., Shrive, N., Frank, C., Marchuk, L. and Bray, R. (1992) Water content alters the viscoelastic behaviour of the normal adolescent rabbit medial collateral ligament. *J. Biomech.* **25**, 831-837.

Clayton ML and Weir, GJ., Jr. (1959) Experimental effects of ligamentous healing. *Am. J. Surg.* **98**, 373-378.

Cooper R.R. and Misol S. (1970) Tendon insertion and ligament insertion: a light and electron microscopy study. *J. Bone Joint Surg.* **52-A**(1), 1-20.

Curwin, S.L. and Stanish, W.D. (1984) *Tendinitis: Its Etiology and Treatment.* Collamore Press, Toronto.

Danto, M.I. and Woo, S.L.-Y. (1993) The mechanical properties of skeletally mature rabbit anterior cruciate ligament and patellar tendon over a range of strain rates. *J. Orthop. Res.* **11**, 58-67.

Derwin, K.A., Soslowsky L.J., Green, W.D. and Elder, S.H. (1994) A new optical system for the determination of deformations and strains: calibration characteristics and experimental results. *J. Biomech.* **27** (10), 1277-1285.

Ellis, D.G. (1969) Cross-sectional area measurements for tendon specimens: comparison of several methods. *J. Biomech.* **2**, 175-186.

Figgie, H.E., Bahnuik, E.H., Heiple, G.K. and Davy D.T. (1986) The effects of tibial-femoral angle on the failure mechanics of the canine anterior cruciate ligament. *J. Biomech.* **19**, 89-91.

Frank, C., Woo, S-L., Amiel, D., Harwood, F., Gomez, M., and Akeson, W. (1983) Medial collateral ligament healing: a multidisciplinary assessment in rabbits. *Am. J. Sports Med.* **11** (6), 379-389.

Frank, C.B. and Shrive N.G. (1994) Ligament. In *Biomechanics of the Musculoskeletal System* (Eds. B.. Nigg and W. Herzog), pp. 106-132. Chischester, England: John Wiley & Sons.

Frank, C.B., Loitz, B., Bray, R., Chimich, D., King, G. and Shrive N. (1994) Abnormality of the contralateral ligament after injuries of the medial collateral ligament. *J. Bone Joint Surg.* **76-A** (3), 403-412.

Garrett, W.E., Jr., and Tidball, J., (1988) Myotendinous junction: structure, function, and failure. In *Injury and Repair of the Musculoskeletal Soft Tissues* (Eds. S.L-Y. Woo and J.A. Buckwalter), pp.171-207. Park Ridge: AAOS.

Hasler, E.M., Herzog, W., Leonard, T.R., Stano, A. and Nguyen, H. (1998) In vivo knee joint loading and kinematics before and after ACL transection in an animal model. *J. Biomech.* **31** (3), 253-262.

Haut RC (1983) Age-dependent influence of strain rate on the tensile failure of rat-tail tendon. *J. Biomech. Engng.* **105,** 296-299.

Haut, R.C. and DeCou, J.M. (1984) The influence of water content on the strength characteristic of tendon-a first study. GM research Report BI-272, 1-16. Warren, Michigan.

Haut, R.C. and Little, R.W. (1969) Rheological properties of canine anterior cruciate ligaments. *J. Biomech.*, **5**, 423-430.

Haut, R.C. and Powlison, A.C. (1990) The effects of test environment and cyclic stretching on the failure properties of human patellar tendons. *J. Orthop. Res.* **8**, 532-540.

Haut, R.C., Lancaster, R.L. and Decamp, C.E. (1992) Mechanical properties of the canine patellar tendon: some correlations with age and the content of collagen. *J. Biomech.* **25**(2), 163-173.

Haut, T.L. and Haut, R.C. (1997) The state of tissue hydration determines the strain-rate-sensitive stiffness of human patellar tendon. *J. Biomech.* **30**, 79-81.

Hay and Reid (1988) *Anatomy, mechanics and human motion.* Prentice-Hall, New Jersey.

Herzog, W. and Loitz, B. (1994) Tendon. In *Biomechanics of the Musculoskeletal System* (Eds. B.. Nigg and W. Herzog), pp. 133-153. Chichester, England: John Wiley & Sons.

Herzog, W., Adams, M.E., Matyas, J.R. and Brooks, J.G. (1993) Hindlimb loading, morpology and biochemistry of articular cartilage in the ACL-deficient cat knee. *Osteoarthritis and Cartilage* **1**, 243-251.

Herzog, W., Leonard, T.R. and Stano, A. (1995) A system for studying the mechanical properties of muscles and the sensiomotor control of muscle forces during unrestrained locomotion in the cat. *J. Biomech.* **28**(2), 211-218.

Herzog, W., Leonard, T.R., Renaud, J.M., Wallace, J., Chaki, G. and Bornemisza, S. (1992) Force-length properties and functional demands of cat gastrocnemius, soleus and plantaris muscles. *J. Biomech.* **25**, 1329-1335.

Hoffer, J.A., Leonard, T.R., Cleland, C.L. and Sinkjaer T. (1990) Segmental reflex action in normal and decerebrate cats. *J. Neurophysiol.* **64**, 1611-1624.

Hunter, J. and Williams, M.G. (1951) A study of the effect of cold on joint temperature and mobility. *Can. J. Med. Sci.*, **29**, 255.

Ianconis, F., Steindler, R. and Marinozzi, G. (1987) Measurements of cross-sectional area of collagen structures (knee ligaments) by means of an optical method. *J. Biomech.* **20**, 1003-1010.

Jansen, M.O. and Savelberg, H.H. (1994) Stress and strain of equine tendons of the forelimb at failure. *Equine Vet. J. Suppl.*, **17**, 57-60.

Johnson, G.A., Tramaglini, D.M., Levine, R.E., Ohno, K., Choi, N-Y. and Woo, S. L-Y (1994) Tensile and viscoelastic properties of human patellar tendon. *J. Orthop. Res.*, **12 (6)**, 796-803.

Johnson, R., Beynnon, B., Nichols, C. and Renstron, A. (1992) The treatment of injuries of the anterior cruciate ligament. *J. Bone Joint Surg.* **74** , 140-151.

Kuei, S., Woo, S.L-Y., Gomez, M.A., and Akeson, W.H. (1979) The viscoelastic, thermoelastic, and time dependent properties of the knee ligaments. *Trans. Orthop. Res. Soc.*, **4**, 25.

Lam, T.C., Frank, C.B. and Shrive, N.G. (1992) Calibration characteristics of a video dimension analyser (VDA) system. *J. Biomech.* **25** (10), 1227-1231.

LaPrade, R.F., Hamilton, C.D., Montgomery, R.D., Wentorf, F. and Hawkins, H.D. (1997) The reharvested central third of the patellar tendon. A histologic and biomechanical analysis. Am. J. Sports Med. 25, 779-785.

Laros, G.S., Tipton, C.M. and Cooper, R.R. (1971) Influence of physical activity on ligament insertions in the knees of dogs. *J. Bone Joint Surg.* [Am] **53**, 275-286.

Lee, T.Q. and Woo, S.L.-Y. (1988) A new method for determining cross-sectional shape and area of soft tissues. *J. Biomech. Engng.* **110**, 110-114.

Leitschuh, P.H., Doherty, T.J., Taylor, D.C., Brooks, D.E. and Ryan JB (1996) Effects of postmortem freezing on tensile failure properties of rabbit extensor digitorum longus muscle tendon complex. *J. Orthop. Res.* **14** (5), 830-833.

Ma, C.B., Ikeda, K., Inoue, N., McFarland, E.G. and Chao E.Y.S. (1996) Biomechanical analysis of the effect of the loading angle on the failure mechanism of canine patellar tendon-tibia unit. 42nd Annual Meeting, ORS.

Maitland, M.E., Leonard, T., Frank, C.B., Shrive, N.G. and Herzog, W. (1998) Longitudinal measurement of tibial motion relative to the femur during passive displacements in the cat before and after anterior cruciate ligament transection. *J. Orthop. Res.* **16**, 448-454.

Martini, F. and Welch, K. (1998) *Fundamentals of Anatomy and Physiology*. Prentice-Hall, New Jersey.

Matthews, L.S. and Ellis, D. (1968) Viscoelastic properties of cat tendon: effects of time after death and preservation by freezing. *J. Biomech.* **1**, 65-71.

Momersteeg, T.J., Blankevoort, L., Huiskes, R., Kooloos, J.G., Kauer, J.M. and Hendriks, J.C. (1995) The effect of variable relative insertion orientation of human knee bone-ligament-bone complexes on the tensile stiffness. *J. Biomech.* **28** (6), 745-752.

Monahan, J.J., Grigg, P., Pappas, A.M., Leclair, W.J., Marks, T., Fowler, D.P. and Sullivan, T.J. (1984) *In vivo* strain patterns in the four major canine knee ligaments. *J. Orthop. Res.*, **2**, 408-418.

Ng, G.Y., Oakes, B.W., Deacon, O.W., McLean, I.D. and Lampard, D. (1995) Biomechanics of patellar tendon autograft for reconstruction of the anterior cruciate ligament in the goat: three-year study. *J. Orthop. Res.* **13**(4), 602-608.

Nigg, BM and Cole GK (1994) Optical Methods. In *Biomechanics of the Musculo-Skeletal System* (Eds. B.M. Nigg and W. Herzog), John Wiley and Sons, pp. 254-285.

Njus, G.O.and Njus, N.M. (1986) A non-contact method for measuring cross-sectional area of soft tissues. *Trans. 32nd Meet. ORS,* **11**, 126.

Noyes, F.R. and Grood, E.S. (1976) The strength of the anterior cruciate ligaments in humans and rhesus monkeys: age-related and species-related changes. *J. Bone Joint Surg.* **58A** , 1074-1082.

Noyes, F.R., DeLucas, J.L. and Torvik, P.J. (1974) Biomechanics of anterior cruciate ligament failure: an analysis of strain-rate sensitivity and mechanisms of failure in primates. *J. Bone Joint Surg.* [Am] **56**(2), 236-253.

Panagiotacopulos, N.D., Knauss, W.G. and Bloch, R. (1979) On the mechanical properties of human intervertebral disc material. *Biorheology.* **16**(4-5):317-330.

Panagiotacopulos, N.D., Pope, M.H., Bloch, R. and Krag, M.H. (1987) Water content in human intervertebral discs. Part II. Viscoelastic behavior. *Spine.* **12**(9), 918-924.

Peterson, R.H., Gomez, M.A. and Woo, S.L.-Y. (1987) The effects of strain rate on the biomechanical properties of the medial collateral ligament: a study of immature and mature rabbits. *Trans. Orthop. Res. Soc.* **12**, 127.

Rigby, B., Hirai, N. Spikes, J. and Eyring, H. (1958) The mechanical properties of rat tail tendon. *J. Gen. Physiol.*, **43**, 265.

Ronsky, J.L. (1994) In-vivo quantification of patellofemoral joint contact characteristics. PhD. Thesis, University of Calgary Press, Calgary.

Ronsky, J.L., Herzog, W., Brown, T.D., Pedersen, D.R., Grood, E.S. and Butler, D.L. (1995) In vivo quantification of the cat patellofemoral joint contact stresses and areas. *J. Biomech.* **28**(8), 977-984.

Shrive, N.G. (1994) Strain Measurement. In *Biomechanics of the Musculo-Skeletal System* (Eds. B.M. Nigg and W. Herzog), John Wiley and Sons, pp. 287-307.

Shrive, N.G., et al. (1988) A new method for measuring the cross-sectional area of soft tissues. *J. Biomech. Engng.* **110**, 104-109.

Shrive, N.G., Lam, T.C., Damson, E. and Frank C.B. (1988) A new method for measuring the cross-sectional area of soft tissues. *J. Biomech. Engng.* **110**, 104-109.

Shrive, NG, Damson, EL, and Frank, CB. (1992) Technology transfer regarding the measurement of strain on flexible materials with special reference to soft tissues. In *Experimental Mechanics: Technology Transfer Between High-tech Engineering and Biomechanics* (ed. E.G. Little) Elsevier, New York, 121-130.

Sikoryn, T.A. and Hukins, D.W. (1990) Mechanism of failure of the ligamentum flavum of the spine during *in vitro* tensile tests. *J. Orthop. Res.* **8**(4), 586-591.

Stouffer, DC, Butler, DL and Hosny D. (1985) The relationship between crimp pattern and mechanical response of human patellar tendon-bone units. *J. Biomech. Eng.* **107**(2), 158-165.

Tabatabai and Mitchell (1984) Edge location to subpixel values in digital imagery. *IEEE Transactions on Pattern Analysis and Machine Intelligence* **6**(2), 188-201.

Tan, U. and Kutlu, N. (1991) The distribution of paw preference in right-, left-, and mixed pawed male and female cats: the role of a female right-shift factor in handedness. *Int. J. Neurosci.* **59** (4), 219-229.

Tipton, C.M., James, S.L., Mergner, W. and Tcheng, T.K. (1970) Influence of exercise on the strength of the medial collateral ligaments of dogs. *Am. J. Physiol.* **218**, 758-761.

Turner, W.D., Vasseur, P., Gorek, J.E., Rodrigo, J.J. and Wedell, J.R. (1988) An in vitro study of the structural properties of deep-frozen versus freeze-dried, ethylene oxide-sterilized canine anterior cruciate ligament bone-ligament-bone preparations. *Clin. Orthop.* **230**, 251-256 .

Viidik, A. (1990) Structure and function of normal and healing tendons and ligaments. In *Biomechanics of Diarthroidal Joints* (Volume 1) (Eds. V.C. Mow, A. Ratcliffe and S. L-Y. Woo), pp. 3-38. New York: Springer-Verlag.

Viidik, A. and Lewin, T. (1966) Changes in tensile strength characteristics and histology of rabbit ligaments induced by different modes of postmortal storage. *Acta. Orthop. Scand.* **37**, 141-155.

Walker L.B., Harris, E.H. and Benedict, J.V. (1964) Stress-strain relationship in human cadaveric plantaris tendon: a preliminary study. *Medical Electronics and Biological Engineering.* **2**, 31-38.

Woltring, H.J. (1986) A FORTRAN package for generalized cross-validatory spline smoothing and differentiation. *Advances in Engineering Software* **8**(2), 104-113.

Woo, S. L-Y. and Young, E. P. (1997) Structure and Function of Tendons and Ligaments. In *Basic Orthopaedic Biomechanics* (Eds. V.C. Mow and W. C. Hayes), pp. 209-251. New York:, Raven Press, Ltd.

Woo, S. Y-L., Gomez, M.A., Seguchi, Y., Endo, C.M. and Akeson, W.H. (1983a) Measurement of mechanical properties of ligament substance from a bone-ligament-bone preparation. *J. Orthop. Res.* **1**, 22-29.

Woo, S. Y-L., Gomez, M.A., Woo, Y.K. and Akeson, W.H. (1982) Mechanical properties of tendons and ligaments. I. Quasi-static and non-linear viscoelastic properties. *Biorheology* **19**, 385-396.

Woo, S.L.-Y., Hollis, J.M., Adams, D.J., Lyon, R.M. and Takai, S. (1991) Tensile properties of the human femur-anterior cruciate ligament-tibia complex: the effect of specimen age and orientation. *Am. J. Sports Med.* **19**, 217-225.

Woo, S.L.-Y., Hollis, J.M., Roux, R.D., Gomez, M.A., Inoue, M., Kleiner, J.B. and Akeson, W.H. (1987) Effects of knee flexion on the structural properties of the rabbit femur-anterior cruciate ligament-tibia complex (FATC). *J. Biomech.* **20**, 557-563.

Woo, S.L-Y. and Sites, T.J. (1988) Current advances on the study of the biomechanical properties of tendons and ligaments. In *Collagen (Volume II)* (Ed. M.E. Nimni), 223-241. Boca Raton: CRC Press.

Woo, S.L-Y., Gomez, M.A., Sites, T.J., Newton, P.O., Orlando, C.A., and Akeson, W.H. (1987a) The biomechanical and morphological changes in the medial collateral ligament of the rabbit after immobilisation and remobilisation. *J. Bone Joint Surg.* **69A**, 1200-1211.

Woo, S.L-Y., Maynard, J., Butler, D.L., Lyon, R., Torzilli, P.A.,Akeson, W.H., Cooper, R.R. and Oaes, B. (1988) Ligament, Tendon, and Joint Capsule Insertions into Bone. In *Injury and Repair of the Musculoskeletal Soft Tissues* (Eds. S.L-Y. Woo and J.A. Buckwalter), pp. 133-166. Park Ridge: AAOS.

Woo, S.L-Y., Orlando, C.A., Camp, J.F., Gomez, M.A., and Akeson, W.H. (1984) The effects of aging, temperature and postmortem storage on ligament tensile behaviour. Am. Soc. Mech. Eng. Winter Annu. Meet., 337.

Woo, S-L.Y., Orlando, C.A., Camp, J.F. and Akeson, W.H. (1986) Effects of postmortem storage by freezing on ligament tensile behaviour. *J. Biomech.* **19,** 399-404.

Yahia, L.H. and Drouin, G. (1989) Microscopical investigation of canine anterior cruciate ligament and patellar tendon: Collagen fascicle morphology and architecture. *J. Orthop. Res.* **7**, 243-251.

Yamamoto, N., Hayashi, K., Kuriyama, H., Ohno, K., Yasuda, K. and Kaneda, K. (1992) Mechanical properties of the rabbit patellar tendon. *J. Biomech. Engng.* **114**, 332-337.

Yamamoto, N., Hayashi, K., Kuriyama, H., Ohno, K., Yasuda, K. and Kaneda, K. (1996) Effects of restressing on the mechanical properties of stress-shielded patellar tendons in rabbits. *J. Biomech. Engng.* **216**, 118-220.

Yamamoto, N., Ohno, K., Hayashi, K., Kuriyama, H., Yasuda, K. and Kaneda, K. (1993) Effects of stress shielding on the mechanical properties of rabbit patellar tendon. *J. Biomech. Engng.* **115**, 23-28.

Yin, F.C.P., Tompkins, W.R., Peterson, K.L. and Intaglietta, M. (1972) A video-dimension analyzer. *IEEE Trans. Biomed. Engng.* **BME-19**(5), 376-381.

Zernicke, R.F., Butler, D.L., Grood, E.S., Hefzy and M.S. (1984) Strain topography of human tendon and fascia. *J. Biomech. Eng.* **106** (2), 177-180.